Title

A Comprehensive Review on Food Applications of Terahertz Spectroscopy and Imaging

Journal

Comprehensive Reviews in Food Science and Food Safety, 18(5)

ISSN

1541-4337

Authors

Afsah-Hejri, Leili
Hajeb, Parvaneh
Ara, Parsa
et al.

Publication Date

2019-09-01

DOI

10.1111/1541-4337.12490

Peer reviewed

Comprehensive REVIEWS in Food Science and Food Safety

A Comprehensive Review on Food Applications of Terahertz Spectroscopy and Imaging

Leili Afsah-Hejri, Parvaneh Hajeb, Parsa Ara, and Reza J. Ehsani

Abstract: Food product safety is a public health concern. Most of the food safety analytical and detection methods are expensive, labor intensive, and time consuming. A safe, rapid, reliable, and nondestructive detection method is needed to assure consumers that food products are safe to consume. Terahertz (THz) radiation, which has properties of both microwave and infrared, can penetrate and interact with many commonly used materials. Owing to the technological developments in sources and detectors, THz spectroscopic imaging has transitioned from a laboratory-scale technique into a versatile imaging tool with many practical applications. In recent years, THz imaging has been shown to have great potential as an emerging nondestructive tool for food inspection. THz spectroscopy provides qualitative and quantitative information about food samples. The main applications of THz in food industries include detection of moisture, foreign bodies, inspection, and quality control. Other applications of THz technology in the food industry include detection of harmful compounds, antibiotics, and microorganisms. THz spectroscopy is a great tool for characterization of carbohydrates, amino acids, fatty acids, and vitamins. Despite its potential applications, THz technology has some limitations, such as limited penetration, scattering effect, limited sensitivity, and low limit of detection. THz technology is still expensive, and there is no available THz database library for food compounds. The scanning speed needs to be improved in the future generations of THz systems. Although many technological aspects need to be improved, THz technology has already been established in the food industry as a powerful tool with great detection and quantification ability. This paper reviews various applications of THz spectroscopy and imaging in the food industry.

Keywords: food inspection, imaging, quality control, spectroscopy, terahertz

Introduction

The far-infrared or terahertz (THz) region refers to a very small gap between the microwave (MW) and infrared (IR) regions of the electromagnetic spectrum. THz waves with a frequency range of 0.1 to 10 THz (3.3 cm^{-1} to 333.6 cm^{-1}) have unique properties, making them suitable for both fundamental research and industrial applications (Xie, Yang, & Ying, 2014). There have been great advances in THz spectroscopy technology since its emergence in the early 1990s. While they share some properties with MW and IR radiation, THz waves have distinct properties. THz spectroscopy provides an informative link between MW spectroscopy and IR spectroscopy as well as reflects the interface of these techniques (Figure 1) (Kawano & Ishibashi, 2008; Mcintosh, Yang, Goldup, & Donnan, 2012). Due to the energy of photons in the THz region, THz spectroscopy can be used to study the vibrational activities of molecules. Torsional and rotational modes of molecules can also be observed in the low frequency THz region. THz radiation is an excellent non-ionizing alternative to the use of X-rays in generating high resolution images from the inner parts of a solid object. Many molecules exhibit unique dispersion or absorption in the THz range (Blanchard et al., 2007). Nonmetallic, nonpolar, and dry materials are transparent to THz waves while polar molecules absorb THz waves due to their intermolecular activities (Mathanker, Weckler, & Wang, 2013). Water is a strong THz wave absorber, and the presence of water is a nuisance when performing measurements in the THz region (Jin, Williams, Dai, & Zhang, 2017). Measurements made from THz images or spectroscopy can be performed in the two following forms: a) frequency-domain measurements that use continuous-wave (CW) THz sources and detectors or b) time-domain measurements (THz-time-domain spectroscopy (TDS)).

THz applications include security screening (García-rial et al., 2018; Kaltenecker et al., 2018; (Liu, Zhong, Karpowicz, Chen, & Zhang, 2007), astronomical studies (Leisawitz et al., 2000), communication (Akyildiz, Miquel, & Han, 2014; Ergün & Sönmez, 2015, nondestructive testing (Probst, Scheller, & Koch, 2011; Rutz, Koch, Khare, & Moneke, 2006), medical imaging (Bowman et al., 2018; Chavez, Bowman, Wu, Bailey, & El-Shenawee, 2018; Dougherty et al., 2007; Fitzgerald et al., 2006; Sun et al., 2017; Truong, Fitzgerald, Fan, & Wallace, 2018), imaging of dental caries (Karagoz, Altan, & Kamburoglu, 2015; Ripoche, Reynard,

CRF3-2019-0116 Submitted 5/8/2019, Accepted 7/11/2019. *Authors Afsah-Hejri and Ehsani are with Mechanical Engineering Dept., School of Engineering, Univ. of California, Merced, 5200 N. Lake Rd., Merced, CA 95343. Author Hajeb is with Dept. of Environmental Science, Aarhus Univ., Frederiksborgvej 399, 4000 Roskilde, Denmark. Author Ara is with College of Letters and Sciences, Univ. of California, Santa Barbara, Santa Barbara, CA 93106. Direct inquiries to authors Afsah-Hejri and Ehsani (E-mail: lafsahhejri@ucmerced.edu; rehsani@ucmerced.edu).*

doi: 10.1111/1541-4337.12490

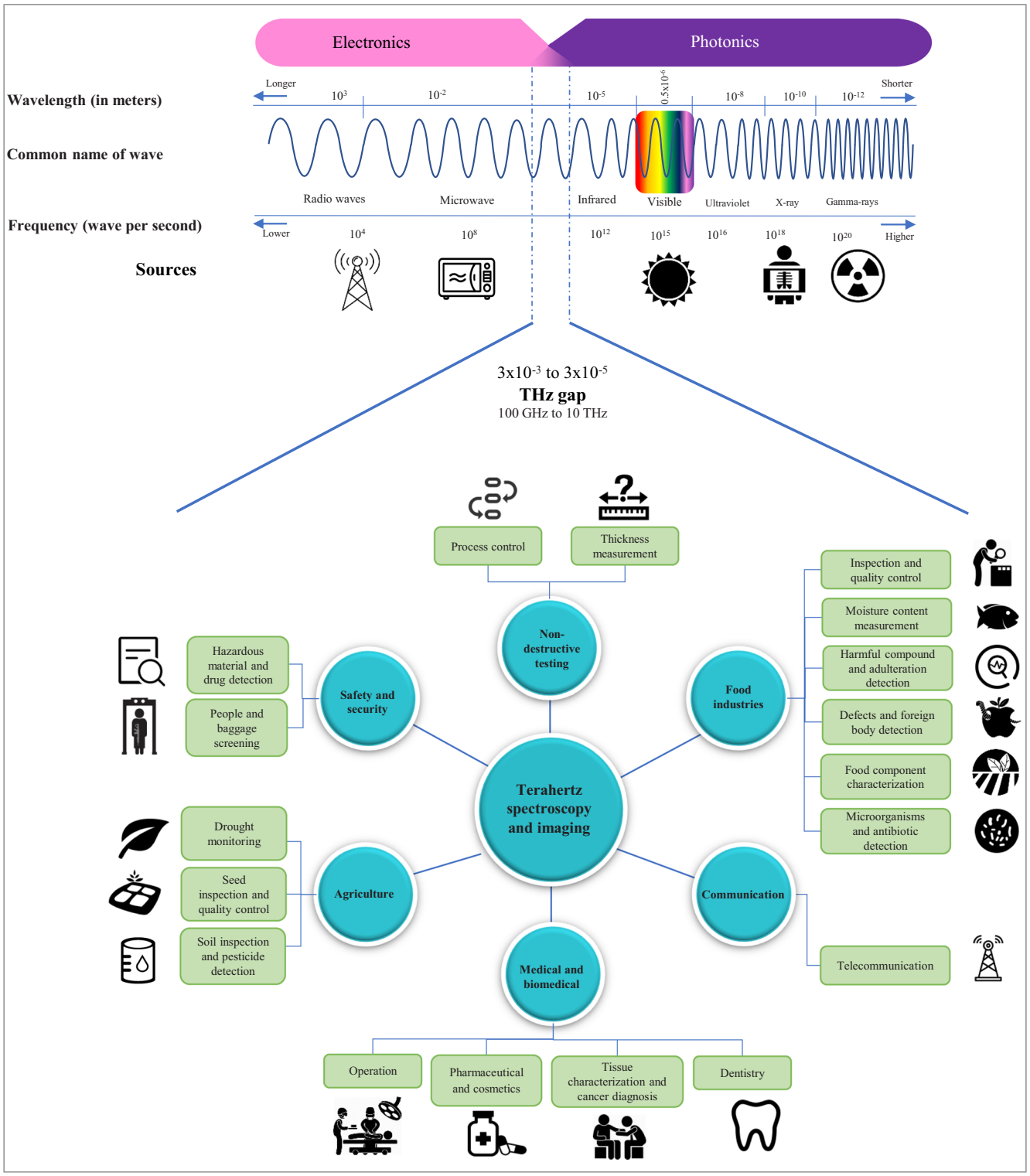

Figure 1–Location of THz region in the Electromagnetic Spectrum and some applications of THz spectroscopy and imaging.

Narcisse, & Roberts, 2018), pharmaceuticals (Markl, Dong, Li, & Zeitler, 2018; Pei et al., 2018; Sibik & Zeitler, 2015; Warnecke et al., 2019, agricultural products (Liu et al., 2018; Liu, Liu, Hu, Yang, & Zheng, 2016; Luo, Zhu, Xu, & Cui, 2019; Nie, Qu, Lin, Dong, & He, 2017; Ogawa et al., 2006; Qin, Li, Chen, & Chen, 2017), food inspection and quality control (Ge, Jiang, Lian, & Zhang, 2016; Huang et al., 2015, Shin, Choi, & Ok, 2018; Ok, Park, Kim, Chun, & Choi, 2014; Ok, Park, Lim, Jang, & Choi, 2018; Wang, Sun, & Pu, 2017; Yan, Liu, Qu, & Liu, 2018), environmental monitoring (Bigourd et al., 2006), and biosensing and label-free monitoring of various biological processes (Yang et al., 2016). Full body THz scanners are installed in many airport checkpoints for detection of concealed objects and explosives. THz waves are considered as data carriers for wireless communications. The insulation of the space shuttle is nondestructively inspected using THz imaging (Redo-Sanchez, Laman, Schulkin, & Tongue,

2013). Some defects are not optically detectable but are clearly visible in THz images. THz systems are being used as noncontact corrosion detection and thickness measurement devices in pipe and cable production lines. THz imaging can differentiate between the normal and cancerous organs and tissues. Cancerous tissue accumulates more water and consequently absorbs THz waves more than the normal tissue (Sun et al., 2017). THz imaging is also an excellent alternative to X-ray for detection of dental caries. One of the main applications of THz systems has been in the pharmaceutical industry for thickness determination, coating examination, and chemical characterization of tablets (Pei et al., 2018). THz imaging is a good tool for monitoring drought stress and water content of plants. THz systems are used for detection of pesticides, soil contaminants, and transgenic and insect damaged seeds (Figure 1).

Previous studies reviewed some early applications of THz technology in agriculture and food (Gowen, O'Sullivan, & O'Donnell, 2012; Qin, Ying, & Xie, 2013; Wang et al., 2017; Wang et al., 2018; Xie et al., 2014). However, there is no detailed publication available for THz-specific food applications. In this paper, we will provide a detailed review on recent THz applications in the food industry and discuss the pitfalls of THz technology as well as future research areas for THz technology.

Food Applications of THz Spectroscopy and Imaging

At present, there is an increasing demand for food, and food manufacturers are required to implement accurate food quality control techniques to deliver safe food to the public. The majority of the food quality testing methods are destructive and time consuming. Current food inspection and imaging methods are unable to detect foreign bodies, defects, and contaminants in packaged food. Moisture control is a critical factor for dried foods and also a key parameter in the weight of the final product.

There are a few non-destructive food quality control and imaging methods. Magnetic resonance imaging (MRI), Raman chemical imaging, X-ray imaging, and hyperspectral imaging are the most common nondestructive imaging techniques used in the food industry. Like any other imaging technique, these methods have advantages and limitations. Hyperspectral imaging is the most simple and rapid technique but is not suitable for in-line applications and requires a lot of data processing. Raman chemical imaging requires little sample preparation, has high spatial resolution, and provides chemical information but is an expensive method with a long mapping time. Although X-ray imaging is considered a high resolution, convenient, and less costly method, it has limited applications due to its high ionizing properties. MRI provides 3D information about the chemical structure of the food as well as detecting tiny physical changes in the food. The main limitations of MRI are its high equipment and maintenance cost, long image acquisition time, and tedious data analysis procedure (Wang et al., 2017).

THz spectroscopy and imaging is a nondestructive method that provides valuable information about the interior and intermolecular structure of a product (Jepsen, Cooke, & Koch, 2011). THz spectroscopy provides a large number of spectral data. The information about the chemical, physical, and structural properties of the sample need to be extracted from these THz spectra. Over the past decade, chemometric methods have been used for processing THz spectral data. Implementation of chemometric methods will reduce the large number of variables and facilitate the data analyzing process. The combination of chemometric methods with THz spectroscopy can be used as an analytical technique (Wang et al., 2017). Figure 2 shows the main steps involved in data acquisition and data analysis based on the combination of chemometric methods with THz imaging for identification and discrimination purposes. Spectral preprocessing methods, such as smoothing and standard normal variate, are used to remove irrelevant information from the optical parameters and increase the signal-to-noise (SNR) ratio. Multivariate analysis techniques can be used for qualitative classification.

The majority of chemical compounds show a very specific frequency-dependent absorption spectrum in the THz region (Hu & Nuss, 1995), and chemicals in food can be detected and quantified based on their THz fingerprint. The detection of toxins, antibiotics, additives, and harmful compounds are some of the important applications of THz technology in the food industry.

Nonpolar and nonmetallic substances, such as plastic, cardboard, and common packaging materials, are transparent to THz radiation and show very weak interaction with THz waves. This means that the content of a package can easily be investigated using THz (Gowen et al., 2012). The moisture content, protein, and fat content of food products can be evaluated using THz spectroscopy. Applications of THz spectroscopy and imaging in food are listed in Tables 1–13.

Foreign body detection

Foreign bodies, such as metal pieces, plastic, stones, glass, nails, and hair, might fall into food products during manufacturing or packaging processes. Compared to nonmetallic contaminants, detection of metallic contaminants in food is easy. X-ray imaging is extensively used for quality control inspection in the food industry, but is not suitable for detection of low-density contaminants hidden in an optically opaque food products (Haff & Toyofuku, 2008). Due to its non-ionizing characteristic, THz waves are safe to use in food operations. THz waves have see-through capabilities and can penetrate through many common materials, for example, paper and plastic used in the food industry (Wang et al., 2017).

Powders and lipids are transparent to THz waves. Flour, sugar, and talc powder were among the first food powders studied with THz radiation (Herrmann, Tani, Watanabe, & Sakai, 2002). Eggshell and plastic pieces with particle sizes ranging from 20 to 300 μm were detected in samples. Higher image resolution was achieved for small particle size samples.

Small stones, glass splinters, and metal screws in chocolate bars were also detected by THz-TDS (Jördens, Rutz, & Koch, 2006). Foreign bodies absorb THz waves, act as scattering objects, and consequently change the shape of the wave. Signal decreases were observed for stone and glass particles due to their high absorption and scattering loss (Table 1). Analyzing the shape and height of THz waves, Jördens and Koch (2008) differentiated between foreign bodies and nuts in chocolate.

THz-TDS can detect very fine foreign objects, such as human hair. Hiromoto, Shiba, and Yamamoto (2013) used polarization-dependent THz-TDS for detection of a single human hair through its transmittance spectra. They observed that the arrangement of human hair affected its transmittance spectra and the arranged hairs appeared like a polarization grating. Lower transmittance was observed for human hairs that were parallel or in the same direction as the THz field. They observed small standard deviations and reported their test as an accurate method for detection of tiny objects.

Li, Cao, Mathanker, Zhang, and Wang (2010) showed that nutmeat, shells, inner separators, and insect-infected pecans had different THz absorption characteristics. Using an in-house-developed THz-TDS system, they distinguished between dead and living

Table 1–Foreign body detection using THz imaging and spectroscopy techniques.

Application and Product	THz range	Mode/THz Type	Chemometrics	Experiment details	Findings	Reference
Flour, sugar, and talc powder	0.5 THz	THz-TDS	NA	Ti:sapphire femtosecond laser Scan area 20 × 20 mm^2 Image acquisition time 9–11 h Particle size 20–300 μm Ample thickness 10 mm	Eggshell and plastic were detected Higher image resolution for small particle size samples	Herrmann et al. (2002)
Chocolate	50 GHz and 2.5 THz	THz-TDS	NA	Photoconductive emitter THz spectrometer Femtosecond laser source PCA detector	Small stone, glass splinters, and metal screws were detected Spatial resolution < 1 mm 2-D images Signal decreased in stone and glass particles Better results at scanning speeds = 0.55 m/s	Jördens et al. (2006)
Chocolate	0.4 and 0.75 THz	THz-TDS	NA	Femtosecond Ti: sapphire laser Pulse duration = 20 fs Repetition rate = 75 MHz Scanning speed = 0.5 m/s Transmission mode	Single THz signal for pure chocolate Two peaks for contaminated chocolates Distinguished foreign bodies from added nuts through their different refractive indexes Sample thickness affected the transmitted signal Reduced the effect of sample thickness by operating at the scanning speed of 0.5 m/s	Jördens and Koch (2008)
Human hair	0.2 to 3 THz	THz-TDS	NA	THz emitter: LT-GaAs PC antenna	Human hair was detected Even one hair can be detected	Hiromoto et al. (2013)
Pecans	0.2 to 2 THz	THz-TDS	NA	In-house developed THz-TDS system Ti:sapphire femtosecond laser Transmission spectroscopy Particle size 1 to 2 cm	Distinguish between nutmeat, shell, inner separator, and insect infected pecans due to different THz absorption characteristics Different absorption profile for nuts and contaminants between 1.2 to 1.8 THz. Differentiation of dead and living insects based on their water content. Penetration limitation for the inshell whole pecan	Li et al. (2010)
Cracker and peanuts	0.2 THz	CW	NA	Diode-type magnetron injection gun was used to accelerate electron beams	Metallic and soft objects in a piece of cracker were detected System was used for real-time inspection of inshell peanuts to distinguish between full and empty peanut shells	Han et al. (2012)
Instant noodles	0.2 THz	CW	NA	Solid-state oscillator (0.1-THz Gunn diode) Aluminum and granite pieces particle size: 1 to 5 mm Maggots: 8 to 22 mm in length and 3 mm in thickness Crickets: 35 to 50 mm in length and 5.5 to 7 mm in thickness	Both high and low-density objects were detected Did not show fine details for high-density foreign bodies due to the wave diffraction from the edges Low-density foreign bodies (cricket and maggot pieces) were clearly detected while they were not detected by X-ray	Lee et al. (2012)

(*Continued*)

Table 1–Continued.

Application and Product	THz range	Mode/THz Type	Chemometrics	Experiment details	Findings	Reference
Flour and instant noodles	0.2 THz	CW	NA	CW source: a frequency-multiplied Gunn oscillator WR-5 horn antenna	Detected metallic cubes (1 to 4 mm^3), stones 1–5 mm^3), paper, grasshoppers (max. 7-mm thickness), and mealworms (1 to 3 mm in diameter), flour thickness (8 mm) Method increased transmitted power up to 6 times higher compared to the pinhole aperture Method had high sensitivity for detection of soft organic samples inside food Spatial resolution: up to 500 μm	Kim et al. (2012)
Noodles	210 GHz	CW	NA	Source: 210-GHz transmitter, output power of 75 mW Sub-THz quasi-Bessel beam (QBB) WR-5 conical horn antenna	Crickets (35 to 50 mm in length and 5.5 to 7 mm in thickness) were detected with high spatial resolution	Ok et al. (2013)
Milk	210 GHz	CW	NA	210-GHz transmitter Sub-THz Gaussian beam WR-5 conical horn antenna	Insects, metals, and polymers were detected	Ok et al. (2014)
Noodle and chocolate	210 GHz	CW	NA	210 GHz transmitter Sub-THz transmission imaging Gaussian beam from a conical horn (WR-5.1) Using an F-Theta lens and a polygonal mirror Beam scanning performed over a range of 150 mm	Crickets (35 to 50 mm in length, and 5.5 to 7 mm in thickness) detected Melting defects in packaged chocolates were identified A pattern with 2.83 mm line width at 210 GHz was identified with a scanning speed of 80 mm/s	Ok et al. (2015)
Chocolate	140 GHz	CW	NA	140-GHz diode Circular horn antenna Bessel-Gauss beam	Paper clip (8 to 34 mm; 1-mm thick) attached to the back side of a chocolate bar (65 mm, 26 mm, 8 mm) detected Mealworm (16-mm-long and 2-mm-thick) buried in the chocolate bar detected Dried maggot (9-mm-long and 1.4-mm-thick) attached to the chocolate bar was detected	Ok et al. (2018)

NA, not applicable.

Table 2–Detection of toxic and harmful compounds using THz imaging and spectroscopy techniques.

Application and Product	THz range	Mode/THz Type	Chemometrics	Experiment details	Findings	Reference
Aflatoxins in peanut oil	0.3 to 1.7 THz	THz-TDS	SMLR PLSR	LT-GaAs photoconductive antenna ZnTe electro-optical crystal Ti:sapphire laser	SMLR model: more stable, lower prediction precision Based on the degree of correlation, only the following frequencies were related to AFB_1 concentration: 0.34, 0.43, 0.72, 0.94, 1.11, 1.30, 1.54, and 1.66 THz Used data from 1.11 and 0.72 THz SMLR model: RMSEC = 18.2, RMSECV = 27.7 μg/mL, rc = 0.9639, and rcv = 0.9309 Accuracy of the method was slightly lower than the routine analytical methods Combination of THz-TDS + chemometric methods is a good nondestructive and rapid tool for quantification of AFB_1 in peanut oil	Chen and Xie (2014)
Aflatoxin B1 in corn	0.2 to 1.2 THz	THz-TDS	D-S method	Femtosecond pulsed Ti:sapphire laser Microstripline antenna on a GaAs crystal	AFB1 detected in all samples In 94% of the samples, the correct concentration of AFB_1 was determined Combination of information-fusion technology with THz spectroscopy successfully identified and quantified AFB_1 in corn	Zhao et al. (2015)
Aflatoxin	0.4 to 1.6 THz	THz-TDS	PLS PCR SVM PCA-SVM	Mode-locked Ti:sapphire laser	Linear regression models, such as PCR and PLS, were more precise for aflatoxin B1 range of 1 to 50 μg/mL Nonlinear-regression-based models (PCA-SVM and SVM) showed more accuracy in the range of 1 to 50 μg/L AFB_1 For PLS and PCR, the correlation coefficient was 0.985 and 0.986, respectively RMSE was 0.753 and 0.587 in aflatoxin B1 range of 1 to 50 μg/mL. PCR resulted in 87.5% prediction accuracy in the 1 to 50 μg/mL range SVM and PCA-SVM had prediction accuracy 85% and 93.75% in the 1 to 50 μg/L range, respectively. AFB_1 in maize was quantified within 5 s	Ge et al. (2016)

(*Continued*)

Table 2–Continued.

Application and Product	THz range	Mode/THz Type	Chemometrics	Experiment details	Findings	Reference
Aflatoxin B1 in soybean oil	0.1 to 5 THz	THz-TDS	RF PLS LS-SVM BPNN	Femtosecond laser Both transmission and reflection modes Polyethylene cylinder was used as sample holder Used *t*-distributed stochastic neighbor embedding (*t*-SNE) to convert the data set into matrix and visualize the similarities	THz spectroscopy combined with BPNN and t-SNE showed the best prediction results RMSEP = 0.7124 μg/kg, Rp = 0.9948, accuracy in prediction set = 93.33% LOD = 1 μg/kg for AFB_1 in soybean oil Classification performance the chemometrics methods was different (BPNN>LS-SVM>RF) RF combined with t-SNE showed the lowest accuracy in prediction set (86.66%)	
Melamine	400 to 4000 cm-1	THz-TDS	NA	Both reflection and transmission modes LT-GaAs dipole emitter and detector Ti:sapphire laser	Melamine and cyanuric acid were measured in infant milk formula	Ung et al. (2009)
Melamine	0-2.5 THz	THz-TDS	DFT	Ti:sapphire laser Polarization beam separator Half-wave plate GnAs photoconductive antenna ZnTe crystal	Pure melamine: peaks at 1.99 and 2.29 THz Linear relationship between the ratio of melamine in the mixture and the absorption coefficient Absorption peaks (at 1.99 and 2.29 THz) were detected in mixture with melamine content > 10% Sharp and distinct absorption peaks observed in high-melamine samples DFT for calculating vibration of melamine	Cui et al. (2009)
Melamine	0 to 1.3 THz	THz-TDS	NA	Fast scan mode (30 measurements in 1 s) Milk powder, chocolate powder, and flour with or without packaging materials with different thicknesses Packaging material (roll paper/polyethylene, oriented polypropylene/polyethylene or vinyl film)	Melamine peaks: at 2, 2.26, and 2.6 THz regardless of the thickness and type of the packaging Images at 2 THz were dose-dependent LOD of method <13% for melamine and R^2>0.913 THz imaging is a useful, nondestructive tool for detection of melamine in food samples	Baek et al. (2014)
Harmful food additives	0 to 3 THz	THz-TDS	NA	Measured both THz transmittance and phase difference Membrane device for holding food additive samples in solution	Saccharin both in solution and pellet had signature peaks near 1.1, 2.0, and 2.4 THz Thiabendazole (pellet and solutions) had peaks near 0.9, 1.2, 2.0, and 2.4 THz O-phenylphenol signature peak in pellet was at 2.0 THz, but peaks for sample solution appeared at 1.2 and 2.0 THz EDTA-2Na did not show any peak for the sample solution, but pellet had two signature peaks at 1.9 and 2.4 THz	Yoneyama et al. (2007)

(*Continued*)

Table 2–Continued.

Application and Product	THz range	Mode/THz Type	Chemometrics	Experiment details	Findings	Reference
Auramine O in medicinal herbs	0.2 to 1.6 THz	THz-TDS	PLSR	Two-dimensional correlation spectroscopy (2DCOS)	2DCOS: highlighted the spectral differences at specific concentrations, reduced the effects of noise, and improved the PLSR model and accuracy of the results 2DCOS-PLSR: accurate quantitative analysis of AO with Rc = 0.9978, RMSEC = 0.5544%, RMSEP = 0.7527%, Rp = 0.9962, and RPD = 15.38 Rapid, accurate, and reagent-free detection method for AO in medicinal herbs	Zhang et al. (2017)
Auramine O in medicinal herbs	0.2 to 1.6 THz	THz-TDS	PLS SPLS VIP-PLS	Femtosecond laser ZnTe crystal Conditions: system filled with dry air, at room temperature and 3% relative humidity Sample: Pollen Typhae	THz absorbance in powder samples was proportional to the concentration of AO VIP-PLS model omitted the unnecessary information VIP-PLS had the best performance in quantification of AO with Rc = 0.9958, RMSEC = 0.0921%, RMSEP = 0.3237%, and Rp = 0.9464	Zhang and Li (2018)
Harmful compounds	0 to 2.5 THz	THz-TDS	NA	THz transmitted through the sample: 30 times (corresponding to a signal-to-noise ratio of 50:1)	2,4,6-TCA in the solid phase: strong peaks at 0.6, 0.95, and 1.2 THz A weak absorption peak near 0.2 to 0.3 THz was observed for high volume fractions of TCA Chlorine placement had a significant impact on THz spectrum of other TCA isomers	Hor et al. (2008)
Talc powder in flour	0.2 to 1.6THz	THz-TDS	NA	Diode-pump mode-locked Ti:sapphire laser ZnTe crystal	Talc powder absorption peaks: 0.95 1.36, and 1.56 THz Talc powder can be detected in powder samples based on the absorption coefficient and refractive index	Xiao-li and Jiu-sheng (2011)
Harmful residues in honey	0.5 to 6THz	THz-TDS	NA	Amplified kHz Ti:sapphire laser EO crystal	Antibiotics in honey were detected at very low concentration (0.01 w/w) Mixtures of antibiotics and insecticides in honey were also detected with THz Sulfathiazole showed peaks at 1.88 and 2.04 THz Coumaphos had a peak at 1.88 THz The sulfapyridine fingerprint appeared at 1.064 THz Amitraz had a strong resonance peak at 4.4 THz Tetracycline exhibited peaks at 3.25, 3.98, 4.53, and 5.16 THz	Massaouti et al. (2013)

Abbreviations: **NA,** not applicable; **PCA,** principal component analysis; **PLS,** partial least squares; **PLSR,** partial least squares regression, **PCR,** principal component regression; **SVM,** support vector machine; **LS,** least squares; **LS-SVM,** least squares-support vector machine; **BPNN,** back propagation neural network; **RF,** random forest pattern recognition method; **D-S,** Dempster–Shafer method; **DFT,** density functional theory; **SMLR,** stepwise multiple linear regression; **RMSEC**, root mean square errors of calibration; **RMSECV,** root mean square errors of cross-validation; **RMSEP,** root mean square errors of prediction.

Table 3–Detection of antibiotics using THz imaging and spectroscopy techniques.

Application and Product	THz range	Mode/THz Type	Chemometrics	Experiment details	Findings	Reference
Milk, egg, powder and feed	0.1 to 2 THz	THz-TDS	NA	Mini-Z time-domain portable THz spectrometer Real-time spectral data acquisition at a rate of 7 Hz in transmission or reflection mode Eleven antibiotics: oxytetracycline, doxycycline, tetracycline, sulfamethizole, sulfamethoxypyridazine, sulfapyridine, sulfadiazine, sulfamethazine, norfloxacin, enrofloxacin, ciprofloxacin, and tylosin	Eight antibiotics were detected in food and feed samples Tylosin, tetracycline, and oxytetracycline did not have specific absorbance peaks in the 0.2 to 2 THz. Sulfapyridine added to egg, milk, and feed samples (at a ratio of 50%) showed a sharp absorbance peaks at 1.05 THz Doxycycline in egg and milk samples (at a ratio of 50%) had a sharp absorbance peaks at 1.37 THz	Redo-Sanchez et al. (2011)
Honey	0.5 to 6 THz	THz-TDS	NA	Amplified kHz Ti:sapphire laser system All measurements were based on a pump-probe, coherent detection approach Antibiotics: sulfapyridine, sulfathiazole, tetracycline	Sulfapyridine, sulfathiazole, and tetracycline were detected at the frequency range of 0.5 to 2.6 THz Sulfapyridine had a sharp single peak at 1.064 THz Sulfathiazole showed two peaks at 1.88 THz and 2.04 THz Tetracycline had several small peaks between 3.25 and 5.16 THz Antibiotics were detectable in concentrations down to 1% w/w	Massaouti et al. (2013)
Infant milk powder	0.3 to 1.8 THz	THz-TDS	PCA PLSR RPD PLS-DA	FemtoFiber pro NIR laser Tetracyclines hydrochlorides (TCsH): tetracycline hydrochloride (TCH), oxytetracycline hydrochloride (OTCH), doxycycline hydrochloride (DTCH), and chlortetracycline hydrochloride (CTCH) Concentration range: 1 to 50%	All tetracyclines hydrochloride (TCsH) was detected in infant milk powder TCH had a strong peak at 1.4 THz Detectable at concentrations at 1%–50% Residual predictive deviation (RPD) values of all these TCsH models >2 Method accuracy between 83.33 and 100% Models were considered good for screening purposes	Qin et al. (2014)
Food powders	0.1 to 3.5 THz	THz-TDS	PLSR RPD	Large-aperture photoconductive (PC) antenna Electro-optic (EO) ZnTe crystal was used for THz detection Tetracycline hydrochloride (TC-HCl)	TC-HCl residue in powders showed absorption at 0.75 and 1.40 THz RPD of 7.87 rcv = 0.9919 RMSEC = 1.31% RMSECV = 2.23% PLSR model was not suitable for liquid samples	Qin et al. (2015)

(*Continued*)

Table 3–Continued.

Application and Product	THz range	Mode/THz Type	Chemometrics	Experiment details	Findings	Reference
Liquid sample	0.2 to 0.8 THz	THz-TDS	PCA	Electro-optic ZnTe crystal for detection FemtoFiber pro NIR laser at 780 nm as pump source Metamaterials	Tetracycline hydrochloride (TCH) was detected in solution in trace amount LOD = 0.1 mg/L	Qin et al. (2016)
Liquid sample (water and milk)	0.2 to 0.3 THz	ATR THz-TDS	SLR	ATR prism made of silicon crystal InGaAs photoconductive antenna	Tetracycline hydrochloride (TCH) was detected in solution in trace amount Complex refractive indices of TCH in pure water and in pure milk observed	Qin et al. (2017)
Chicken breast and rice	0.4 to 1.1 THz	THz-TDS	PLSR	Femtosecond laser ZnTe crystal Conditions: system filled with dried air, temperature = 293K and 4% relative humidity Chlortetracycline hydrochloride (CCH) and tetracycline hydrochloride (TCH) Samples: chicken breast, rice	Combination of THz spectroscopy with PLSR model successfully quantification of TCH and CCH in chicken and rice For CCH in chicken: R = 0.9575, RMSEC = 0.0469%, RMSECV = 0.1581%, and RMSEP = 0.0744% For TCH in chicken: R = 0.9251, RMSEC = 0.0618%, RMSECV = 0.1415%, and RMSEP = 0.1280% For CCH in rice: R = 0.9480, RMSEC = 0.0525%, RMSECV = 0.1202%, and RMSEP = 0.0776% For TCH in rice: R = 0.9089, RMSEC = 0.0623%, RMSECV = 0.1405%, and RMSEP = 0.0954%	Wang et al. (2018)
Liquid sample (water)	0.2 to 1.2 THz	THz-TDS	PCA	Femtosecond Ti:sapphire laser GaAs photoconductive antenna Metasurfaces Kanamycin sulfate A square-shaped metallic optical transmission structure (showing an electromagnetic resonant response at 0.3 THz) was used to enhance THz transmittance	Detected kanamycin sulfate (as low as 100 picogram/L) in liquid form Method sensitivity increased about 10^{10} times compared to the sensitivity achieved by using silicon (1 g/L) Method sensitivity was increased by matching the resonance frequency of the metasurface structure with "fingerprints" of the target (kanamycin sulfate) Kanamycin sulfate showed a sharp peak at 0.3 THz	Xie et al. (2015)
Feed matrices	0.5 to 2 THz	THz-TDS	BPNN	Savitzky-Golay filter Transmission mode Fluoroquinolones (norfloxacin, enrofloxacin, and ofloxacin)	Norfloxacin: peaks at 0.825 and 1.187 THz in both pure form and mixed with feed matrices Ofloxacin: a sharp peak at 1.044 THz Enrofloxacin: a weak absorption peak at 0.8 THz Optimal classification accuracy = 80.56% The optimal correlation coefficients for norfloxacin, enrofloxacin, and ofloxacin in the prediction set were 0.867, 0.828, and 0.964, respectively	Long et al. (2018)

NA, not applicable; **PCA**, principal component analysis; **PLS**, partial least squares; **DA**, discriminant analysis; **BPNN**, back propagation neural network; **SLR**, stepwise linear regression; **RPD**, residual predictive deviation; **RMSEC**, root mean square errors of calibration; **RMSECV**, root mean square errors of cross-validation.

Table 4–Detection of microorganisms using THz imaging and spectroscopy techniques.

Application and Product	THz range	Mode/THz Type	Chemometrics	Experiment details	Findings	Reference
Bacillus subtillis	200 to 1200 GHz	CW	NA	Sub-THz region MOPA lasers Photomixing sweep oscillator Ultrafast THz photoconductive mixer GaAs ErAs nanoparticles A two-turn rectangular spiral antenna	*Bacillus subtillis*: distinct transmission signatures at 253, 418, and 1037 GHz both in dilute and concentrated samples	Brown et al. (2004)
Bacillus spores	0.2 to 2 THz	THz-TDS	NA	Far-infrared (THz)	*B. subtilis* spores: distinct absorption peak at 1.538 THz Dipicolinic acid peak at 1.54 THz	Yu et al. (2005)
Bacillus spores	10 kHz to 10THz	THz-TDS	NA	Mid-infrared and far-infrared (THz) Three THz sources (Hg lamp and Glow bar)	Even at high concentration of spores (10^8 to 10^9 CFU/mL), a very weak THz absorption spectra (28 times weaker) was observed compared to the mid-IR amide I band	Johnson et al. (2005)
Bacillus subtilis cells *E. coli* cells and spores	0.3 to 0.7 THz	CW	NA	Si-bolometer operating at 1.7K Transmission mode *E. coli* and *Bacillus subtilis* suspensions (concentrations: 0.01 to 1 mg/mL Computer modeling and simulation for the chromosomal DNA	DNA of *E. coli* and *B. subtilis* had measurable differences in their respective THz transmission spectra Both *E. coli* and *B. subtilis* cells showed stronger absorption spectrum than their DNA samples in the range 0.4 to 0.6 THz A good correlation between the chromosomal DNA signature and the corresponding cell and spore signature The first DNA computer modeling and simulation for the chromosomal DNA	Bykhovski et al. (2005)
E. coli and *B. subtilis*	0.3 to 0.7 THz	CW	Molecular dynamic simulations	Sub-terahertz (THz) Transmission mode FTIR infrared spectrometer Mercury lamp Si-bolometer	Method verified the differences between bacterial species Method revealed the response of bacterial cells and spores to environmental conditions (vacuum and heat) Method had a good sensitivity and reliability Spectral resolution = 0.25 cm^{-1}, spectral widths of 0.5 to 1 cm^{-1} THz vibrational spectroscopy: a reagent-free and label-free method for detection and quantification of bacterial cells or their genetic information	Globus et al. (2012)
.*Escherichia coli*	0.1 to 3 THz	THz-TDS	NA	A modified THz-TDS setup Frequency-doubled femtosecond fiber laser GaAs dipole antennae Mirrors mounted on translation rails (measurement of waveguides up to 45 cm in length without realignment) A 150-μm THz fiber core which was suspended by three sub-wavelength bridges in the center of a T4 bacteriophage-coated tube	*E. coli* was detected at concentrations range of 10^4 to 10^9 CFU/mL *E. coli* was detected and quantified based on the changes observed in the amplitude LOD of the method = 10^4 CFU/mL	Mazhorova et al. (2012)

(*Continued*)

Table 4–Continued.

Application and Product	THz range	Mode/THz Type	Chemometrics	Experiment details	Findings	Reference
E. coli and *B. subtilis*	0.1 to 2 THz	THz-TDS	NA	Ti:sapphire laser Silicon-based THz bowtie antennas ZnTe crystal Quarter wave plate Wollaston prism A pair of balanced silicon photodetectors	Layers of *E. coli* and *B. subtilis* were studied to determine the Gram type of bacteria A deposited layer of *E. coli* on a plasmonic chip showed a distinct absorbance peak at 0.3 THz THz plasmonic antennas can be used for rapid, low cost, and label-free detection and identification of bacteria	Berrier et al. (2012)
Bacteria (*E. coli*) Yeast (*Saccharomyces*) Fungi (*Aspergillus* and *Penicillium*)	0.5 to 3 THz	THz-TDS	NA	Femtosecond laser Photoconductive antenna Metamaterials (metamaterial patterns were prepared using a conventional photo-lithography method on a high-resistivity Si substrate) Microorganisms deposited in the gap and caused a change in the effective dielectric constants of the capacitor	Real-time THz transmission amplitudes of fungi were measured with metamaterials Observed a shift in resonant frequency which depended on 1) number of the microorganisms deposited in the gap area and 2) on the dielectric constants of the sample They verified the effect of the dielectric constant by fabricating dense and thick fungi films Low-density of E. coli was detected Dark-field microscope images were compared for metamaterials without and with *E. coli* at density of $0.019/\mu m^2$ A shift of 23 GHz was observed for metamaterials loaded with *E. coli*.	Park et al. (2014)
E. coli	8.5 to 11.5 THz	THz-TDS	NA	Nickel mesh Anti-*E. coli* antibody (0 to 0.1 mg/mL) was immobilized on the surface of nickel mesh *E. coli* (0 to 10^8/mL)	Increasing the concentration of *E. coli* increased the frequency shifts Significant frequency shift change at 9.5 THz was noticed even at low anti-*E. coli* antibody concentration (0.01 mg/mL) LOD = 10^6/mL for *E. coli* which was not sensitive enough for food inspection purposes	Kurita et al. (2014)
E. coli, *Staphylococcus aureus*, *Pseudomonas aeruginosa*, *Acinetobacter baumannii*	0.2 to 2.5 THz	THz-TDS	NA	Mini-review on studies in sub-THz range	*A. baumannii* had the highest absorption coefficient Living *S. aureus* had the lowest absorption in 0.5 to 2.5 THz range Dried powdered *S. aureus* absorbed more than *E. coli* and *P. aeruginosa* For living bacteria, the absorption coefficients were *A. baumannii* > *P. aeruginosa* > *E. coli* > *S. aureus*, Values for bacterial powder were approximately in the order: *S. aureus* > *E. coli* > *P. aeru-ginosa* > *A. baumannii*	Yang et al. (2016)

(*Continued*)

Table 4–Continued.

Application and Product	THz range	Mode/THz Type	Chemometrics	Experiment details	Findings	Reference
E. coli, Staphylococcus aureus, Pseudomonas aeruginosa, Acinetobacter baumannii	0 to 3 THz	CW	NA	Transmission mode	*E. coli, S. aureus, P. aeruginosa*, and *A. baumannii* were identified at different living states Living and dead bacteria were differentiated due to their structural changes and different hydration levels	Yang et al. (2017)
Yeast cells	7 to 300 GHz	CW	NA	GaAs-photomixers Microfluidic system based on PTFE tubes (inner diameter = 0.5 mm) 7 and 240 GHz frequency bands: important for collecting information on the permittivity of yeast cells in glucose solution At the 7 GHz band, a rat-race based characterizing system was used for measurements Monitoring yeast glucose solution for 16 h	Amplitude shift observed at 46 °C Detected trace number of samples (volume of 2 μL for 1 cm sample length) Amplitude information was a useful tool for differentiating samples Sensitivity of the method can be significantly increased by using an epoxy resin aperture covering the sidewalls of the tub	Wessel et al. (2013)
Yeast cells	0.6 to 1.4 THz	THz-TDS	NA	Femtosecond laser Photoconductive antenna Slot antennas are particularly localized and sensitive for sensing dielectric materials THz slot antenna patterns were prepared by using a conventional electron beam lithography method Slot width: 2 to 10 μm Yeast thickness: 0 to 15 μm	Sensors made of low permittivity substrate, such as quartz-based sensors, had higher sensitivity than silicon-based sensors (a high-dielectric constant substrate) Sensors are very sensitive to the size of the target materials Sensor sensitivity can be controlled by altering the antenna width The detection volume is extremely localized near the surface For a slot width of 2 μm, resonant frequency shift is saturated at 3.5 μm	Park et al. (2014)
Saccharomyces cerevisiae	0.75 to 1.1 THz	CW	NA	Horn antenna Normal sugar and artificial sweetener (aspartame and sucralose)	Artificial sweeteners: vigorous bubbling in the solution and maximum growth of yeast colony within 24 min Both normal sugar and artificial sweeteners had a huge change in their THz reflection coefficient at 1.0152 THz Splenda (sucralose): vigorous bubbling at 14 min and 21 min resulting in drastic changes in THz reflection spectrum Normal sugar solutions: changes in THz reflection spectrum observed at 14 and 28 min Splenda and normal sugar solution had changes of 60 dB and 15 dB, respectively, whereas the control sample was 8 dB	Fawole et al. (2015)

NA, not applicable.

Table 5–Moisture content measurement using THz imaging and spectroscopy techniques.

Application and Product	THz range	Mode/THz Type	Chemometrics	Experiment details	Findings	Reference
Moisture content of crushed wheat grain	0 to 5THz	THz-TDS	NA	Ti:sapphire laser, Parabolic mirrors, ZnTe detector Detection: electro-optic Pockels effect A fast Fourier transform was used for converting the time domain data into the frequency domain Crushed wheat grains with different moisture level: dry, 12%, 14%, and 18% Sample thickness = 0.5 mm Special sample holder (aluminum supports, layers of PTFE, sealing feature, and pockets for holding samples)	Absorption spectra observed for all moisture levels Absorption spectra represented data from both free water molecules in crushed grains and extended water network of the sample Samples at 18% moisture level showed the highest absorption THz spectroscopy can be used for measuring moisture content of crushed wheat during the milling process and storage Limitation: thickness of the sample (suitable for samples thickness smaller than 1 mm)	Chua et al. (2005)
Moisture content of wafer	0 to 4 THz	THz-TDS	NA	Dehydrated wafers (moisture content 1 to 30%) Dense wafers porosity (= 77 vol %) Light wafers porosity (88 vol %) A flow-cell was designed for the experiment	Almost 96% of the signal was detected between 0.2 and 0.6 THz A linear relationship (R^2 = 0.9988) was found between moisture content and amplitude	Parasoglou et al. (2009) Parasoglou et al. (2010)
Moisture content of instant coffee	0 to 0.4 THz	THz-TDS	NA	Mode-locked Ti:sapphire laser Micro-structured bowtie-type photoconductive antennas Dry instant coffee and instant coffee exposed to high humidity (>90% RH)	Non-contact, remote measurement of moisture content of coffee powder in glass bottles Transmission spectrum of instant coffee significantly changed after 3.5 h of exposure to forced humidity Water absorption spectrum was spotted at 0.07 THz LOD = 7.5 mg/cm^3	Yasui and Araki (2005), Yasui and Araki (2011)
Moisture content of glycine solution	0.5 to 12 THz	ATR THz-TDS	NA	Glycine powder and glycine solutions (0 to 20 wt%)	Dissolved glycine showed distinct absorption peaks at 2.1, 5.2, and 9.3 THz Glycine powder and glycine solution had different absorption peaks Hydrogen bonding of water molecules and glycine affects the vibrational mode in glycine molecules	Ogawa et al. (2009)

(*Continued*)

Table 5–Continued.

Application and Product	THz range	Mode/THz Type	Chemometrics	Experiment details	Findings	Reference
Moisture content & state of water in beverages and crystals	0 to 4 THz	THz-TDS	PWDF	Sucrose crystal and beverages with different ratio of alcohol/water (5 to 80% w/w) Reference mixtures: pure ethanol and pure water Temperature 10K Absorption coefficient of sucrose crystal sample was measured between 0 and 4 THz Water level in a non-crystalline system was measured between 0.3 and 1 THz.	For sucrose crystals, a good agreement between the experimental and the predicted vibrational modes in terms of the intensities and positions was observed Good agreement between the results from alcoholic beverages with the reference mixtures (pure ethanol and pure water) Accuracy depended on the stability of the sample at test temperature	Jepsen et al. (2007)
Water molecules in gas barrier films	1 to 10 THz	THz-TDS	NA	High-speed THz-TDS system using a voice-coil-driven time delay system Gas barrier materials (polycarbonate films) Signal acquisition time = 0.5 s	A linear relationship was observed between the spectral intensity and the amount of water molecules in the film Water molecules persisted as the 'free water molecules' and did not interacted with the atoms of the film THz-TDS for evaluation of gas barrier films and observation of water molecules inside a sample	Inamo et al. 2016)
Humidity sensor	210 to 275 GHz	CW	Finite-difference time-domain (FDTD)	Polymer-based guided mode resonance (GMR) device With and without polyvinyl alcohol (PVA) coating GMR devices fabricated at micrometer scales PVA-coated sensor absorbed nearly 6% of water contents at increased RH = 70% and temperature 20 °C	PVA-coated GMR sensor had a resonance peak around 247 GHz Non-coated GMR sensor had peak around 252 GHz PVA-coated GMR sensor showed 15% transmittance change at RH = 70% No transmittance change was observed in the GMR sensor without the PVA film FDTD simulated results were a good estimate for water absorbed by the PVA-coated GMR sensor PVA-coated GMR sensor: a good candidate for inexpensive and highly sensitive RH sensing	(Shin et al. (2017)

(*Continued*)

Table 5–Continued.

Application and Product	THz range	Mode/THz Type	Chemometrics	Experiment details	Findings	Reference
Aqueous salt solutions	0 to 7.5 THz (50 to 250 cm^{-1})	THz-TDS	NA	Low-frequency motions of aqueous salt solutions (0 to 4 M) $CaCl_2$, $CaBr_2$, CaI_2, $MgCl_2$, $MgBr_2$, $BaCl_2$, $SrCl_2$, $SrBr_2$	Specific cation and anion bands were found between 1.4 and 7.5 THz Bands in the THz region were related to vibrational modes of the ions and their hydration shells THz spectrum of salt solutions: a good estimate for the concentration of water and ion contributions THz absorption of salt solutions: linear and concentration-dependent	Funkner et al. (2012)
Water in butter and water-AOT-heptane systems	0 to 2 THz	THz-TDS	NA	Water in butter Mixture of water, AOT, and heptane A water-AOT-heptane (W-AOT-H) system is consisted of an inverse micelle having an aqueous core Rapeseed oil, grapeseed oil, lard To provide comparable conditions to butter, 15% water (v/v) W-AOT-H samples were prepared	An increase in the dielectric function of the real and imaginary part of confined water pool was observed for the W-AOT-H system Small micelles showed more increase in the dielectric function of real and imaginary part Large micelles showed properties similar to bulk water Dielectric function of water in butter was lesser than those of bulk water (water in butter can be considered as bound water) Butter has water pool size of 1 to 25 μm; therefore, the bound water region must be in the micrometer range Rapeseed oil, grapeseed oil, and lard each showed a unique THz spectrum between 0.1 and 1.5 THz	Møller et al. (2010)

NA, not applicable; **PWDF**, plane-wave density functional method; **FDTD**, finite difference time domain simulation.

Table 6–Application of THz imaging and spectroscopy techniques in food inspection and quality control.

Application and Product	THz range	Mode/THz Type	Chemometrics	Experiment details	Findings	Reference
Real-time inspection to detect microleak defects	0 to 6 THz	THz-TDS	NA	Real-time inspection of food packages Air-filled and water-filled channel defects in plastic packages	Difference between the absorption coefficients of water and plastic was used for detection of water-filled channels Refraction index difference between air and plastic was the basis of detection for air-filled channel defects Conveyer speed affected the detection limit Channel defects (10 to 100 μm) detected in polyethylene films	Morita et al. (2005)
Insects in noodle flour; and defects in chocolate bar	0.2 THz	CW	NA	Modified/in-house developed THz system Reflection mode A beam steering tool to increase the speed of detection F-Theta lens and a polygonal mirror Scanning speed of 80 Hz	Defects in chocolate bars and crickets in noodle flour were detected Wide-range detection (around 150 mm), high resolution (up to 2.83 mm at 210 GHz), and high-resolution imaging was achieved THz as a rapid and low-cost quality inspection method Quality of the image was improved when the beam size was minimized	Ok et al. (2014) Ok et al. (2015)
Insects and hidden defects in sugar and milk powder	0.15 to 1.3 THz	THz-TDS	NA	Mode-lock Ti:sapphire laser Ti/Au dipole antenna 2-D data map Samples pellets (diameter = 10 mm and thickness = 2 mm) Food samples: grains, seaweeds, and fish samples	Detection of embedded insects and defects in sugar and milk powder Absorption coefficients of the sample increased with an increase in THz frequency while the refractive index decreased Insects showed different characteristics from food matrices at 0.5 THz. THz time-of-flight imaging technique can be used for detection of low-density materials and soft-matter defects, such as insects and contaminants, defects in food products	Shin et al. (2018)
Foreign objects and worms in flour Defects in ginseng	0.2 THz	CW	NA	Gunn oscillator Horn antenna GaAs Schottky diode	A sensitive, non-destructive tool for inspection of soft organic objects inside food samples Higher transmitted power (up to 6 times) than of the system with pinhole aperture High spatial resolution up to 500 μm THz images were more clearly recognizable for samples containing inhomogeneous tissues, such as red ginseng	Kim et al. (2012)
Hull in the peanuts & defects in food	0.1 to 1 THz	CW	NA	In-house developed system A compact sub-terahertz gyrotron A compact cryogen-free magnet in CW mode at 408 GHz Diode-type magnetron injection gun	Non-invasive real-time imaging technique	Han et al. (2011) Han et al. (2012)

(*Continued*)

Table 6–Continued.

Application and Product	THz range	Mode/THz Type	Chemometrics	Experiment details	Findings	Reference
Defects in food	0.1 to 1 THz	CW	NA	KG1 operating at 0.2 THz A diode-type magnetron injection gun was used to accelerate the electron beams Pyroelectric array camera as detector	First version of a compact sub-terahertz gyrotron (KG1) for real-time food inspection Real-time images were reconstructed from the large-scale images scanned by 10 mm over the sample Defects in the crackers and hulls in the peanuts were detected A miniature sub-terahertz gyrotron for real-time detection of soft and non-dense fragments hidden in food Output power at the fundamental mode: 10 W Real-time detection with video rate of 48 Hz	S. Han (2013)
Quality control of confectionary products	200 to 600 GHz	CW	PCA	In-house developed system	Direct observation of phase transitions in confectionary products THz images were used to link the imaginary and real parts of the refractive index of confectionary samples to achieve a model to map consumer perception of creaminess	Hadjiloucas et al. (2010)
Stacked objects, holes, and unwanted fragments in leaves	0.14 to 0.22 THz	CW	NA	A lens-based quasi-optical set up Horn antenna Vector Network Analzser (VNA) Extenders 3-D scanning Metal squares were used to measure the resolution of the system	Active THz imaging system Defects, stacked objects, holes, and unwanted fragments were detected at 0.2 THz System resolution = 2 mm A good technique for thickness control and measuring the number of slices Stacked leaves showed blue color as the THz signal needed to go through more than one layer of leaf and subsequently double amount of water in leaves that turned the image to blue	Etayo et al. (2011)
Quality grade of green tea	0.2 to 1.5 THz	THz-TDS	LS-SVM NB BPANN	Mode-locked femtosecond laser GaAs and ZnTe crystal Sample pellets (thickness = 1.08 mm and diameter = 13 mm)	80 samples of Chinese green tea were classified based on their refractive index and absorption spectrum LS-SVM showed better classification results	Xi-Ai et al. (2011)
Measuring the particle size of powders	0.1 to 4 THz	THz-TDS	NA	Reflection mode Sample diameter (90 to 212 μm)	Rapid and highly sensitive technique for monitoring powder flows and controlling particle size	May et al. (2009)
Monitoring sugar crystallization	0.1 to 3 THz	ATR THz-TDS	NA	ATR crystal Sugar solution of final confectionary products Observation time: 58 h	To observe aqueous phase transition into a glassy state ATR spectra of the sugar solution were time dependent Sugar crystallization started after 50 h and around 58.5 h, crystalline material was formed ATR spectra showed a series of phonon bands ATR THz-TDS: an effective method for monitoring crystallization of sugar in confectionary products	May and Taday (2013)

(*Continued*)

Table 6–Continued.

Application and Product	THz range	Mode/THz Type	Chemometrics	Experiment details	Findings	Reference
Meat freshness	0.2 to 1.5 THz	THz-TDS	NA	Transmission mode Preserved meat (stored at 2 to 4 °C) Bad meat (exposed to air)	THz-TDS as a non-destructive and rapid method for detection of preserved meat and bad meat Absorption coefficient spectrum of bad meat was studied in more detail in the frequency range of 0.42 to 0.46 THz Decomposition of tissue material and reduction of water content resulted in changes in the absorption coefficient changes Changes were less significant at low temperature	Huang et al. (2015)
Quality evaluation of pecan	0 to 2 THz	THz-TDS	NA	In-house designed and built THz system with a Special sample holder Mode-locked Ti:sapphire femtosecond laser Frequency resolution = 1 GHz signal-to-noise ratio = 10000:1 Living insects (Manduca sexta, 2 weeks old) Pecan insects (Weevil) Sample thickness: 1 to 3 mm, width: 1 cm and length: 2 cm	Live and dead insects were detected in different parts of pecan (shell, nutmeat, and inner separator) Absorption coefficients of inner separator, shell and nutmeat showed significant difference at frequencies higher than 1.2 THz Living insects showed higher THz absorption than dry insects and nutmeat	Li et al. (2010)
Binary mixture of amino acids	0 to 2.5 THz	THz-TDS	iPLS PLS MCR-ALS	ZnTe-based semiconductor antenna 21 yellow foxtail millet samples with amino acid content 0 to 13.36% (w/w) Samples thicknesses 0.92 to 0.95 mm Latin partition was used to divide samples into prediction and calibration sets	iPLS had high R^2 value (>0.9904) and low RMSEP (0.39 ± 0.02) and was more effective than PLS model for both glutamine and glutamic acid For the PLS model, the interval dataset ranging from 1.2 to 1.37 THz showed the best results iPLS produced RMSEP 0.39 ± 0.02 for both glutamic acid and glutamine with 100 bootstraps Latin partition $R^2 = 0.9904$ for glutamine and $R^2 = 0.9906$ for glutamic acid Pure amino acids in food can be distinguished using MCR-ALS	Lu et al. (2016)

(*Continued*)

Table 6–Continued.

Application and Product	THz range	Mode/THz Type	Chemometrics	Experiment details	Findings	Reference
Ternary mixtures (reducing sugars and citric acid)	0–3 THz	THz-TDS	PCA PLS ANN	Mode-locked Ti-sapphire laser Transmission mode LT-GaAs semiconductor Pure and different mixtures of citric acid, D- (−) fructose, and α-lactose monohydrate Polyethylene (PE) as the binder	PLS and ANN had similar predictive ability Concentration of the constituents was predicted with RMSE <0.9% Combination of THz spectroscopy with chemometrics proved to be very efficient method for qualitative and quantitative analysis of the ternary mixtures	El Haddad et al. (2014)
Somatic cells in milk	0.6 to 13.2 THz (20 to 440 cm^{-1})	ATR THz-TDS	PLS	A modified system Fourier transform THz (FT-THz) High resistance silicon ATR prism Added a temperature controller below the ATR prism in the FT-THz spectrometer	A non-destructive and practical method for detection of somatic cells in milk and prediction of total solid and milk fat R^2 of the method for somatic cell, casein, milk protein, lactose, total solids, and milk fat were 0.67, 0.41, 0.37, 0.38, 0.8 and 0.72, respectively	Naito et al. (2011)
Preservatives in grains	0.2 to 2 THz	THz-TDS	NA	Mode-locked Ti:sapphire laser ZnTe Electro-optic crystal Time-domain signal-to-noise) ratio = 5000:1 Preservatives: benzoic acid, sorbic acid, sodium benzoate, potassium sorbate, sodium dehydroacetate, and sodium diacetate	Sodium diacetate showed absorption peaks at 1.08,1.29, and 1.58 THz Absorption peaks of potassium sorbate and sorbic acid were observed at 0.97 THz and1.49 THz, respectively THz absorption peaks at low frequencies were assigned to inter-molecular, intra-molecular collective motion or phonon modes	Ge et al. (2016)
Food additives	0.2 to 2.2 THz	THz-TDS	NA	*tert*-butylhydroquinone (TBHQ)	Different concentrations of TBHQ were detected based on their absorption spectra and refractive index	Zhang et al. (2011)
Flavonols (myricetin, quercetin, and kaempferol)	0.6 to 2.7 THz	THz-TDS	PLSR LS-SVM RF	Flavonols: myricetin (MYR), quercetin (QUE), and kaempferol (KAE) Concentration: 0.1, 0.05, and 0.025 mg/mL	RF model had correct classification rate of 100% LS-SVM model produced better results with higher RPD, higher Rp and low RMSEP for all three flavonols Accuracy of the calibration models was measured for kaempferol (RMSEP = 0.0048) myricetin (RMSEP = 0.0044), and quercetin (RMSEP = 0.0039) THz-TDS is a powerful tool for identification and quantification of flavonols with similar chemical structures	Yan et al. (2018)

NA, not applicable; **PCA**, principal component analysis; **PLS**, partial least squares; **iPLS**, interval PLS; **PLSR**, partial least squares regression; **LS**, least-squares; **ANN**, artificial neural networks; **MCR-ALS**, multivariate curve resolution alternating least squares; **SVM**, support vector machine; **NB**, naive Bayes; **BPANN**, back propagation artificial neural network; **RF**, random forest pattern recognition method; **RMSEP**, root mean square errors of prediction.

Table 7–Adulteration detection using THz imaging and spectroscopy techniques.

Application and Product	THz range	Mode/THz Type	Chemometrics	Experiment details	Findings	Reference
Melamine in milk powder	0 to 3 THz	THz-TDS	NA	GnAs photoconductive antenna ZnTe crystal Melamine (1%, 2.5%, 5%, 10%, 20%, and 30%) pellet (13-mm diameter and 1-mm thickness)	Pure melamine and its mixtures (more than 10% melamine) with milk powder and polyethylene showed absorption peaks at 1.99 and 2.29 THz Linear relationship between the ratio of the melamine in the mixture and the absorption coefficient Vibration of melamine crystal was calculated using density functional theory	Cui et al. (2009)
Melamine in milk powder, flour and chocolate powder	0.1 to 3 THz	THz-TDS	NA	Melamine concentration 0 to 10 wt% Packaging materials: oriented polypropylene/polyethylene film (vinyl film, thickness = 40 μm) and roll paper/polyethylene film (paper film, thickness = 80 μm)	Regardless of the thickness and type of the packaging material, distinct melamine peaks at 2, 2.26, and 2.6 THz were detected in all food mixtures Images at 2 THz were observed to be dose-dependent LOD <13% and R^2 of >0.913 THz imaging a useful nondestructive tool for detection of melamine in food samples	Baek et al. (2014)
Dairy products adulterated with fat powder	0.1 to 1.5 THz	THz-TDS	PCA SVM-DA	Skim milk and low-fat milk Fat powder concentration 2.5 to 50% (w/w).	Both skim milks and low-fat milks showed four clear peaks at 0.384, 1.16, 1.196, 1.343 THz The fifth peak of skim milk appeared at 1.422 THz while it appeared at 1.434 THz for low-fat samples Both low-fat and skim milk adulterated samples had extra absorption peaks at 0.745 and 1.262 THz SVM-DA had satisfactory results in classification of adulterated milk samples Method specificity = 100%, Method sensitivity = 88.62%	Liu (2017)
Acacia honey adulteration	0.5 to 3.5 THz	ATR THz-TDS	PLS	ATR prism made of silicon crystal High-fructose-syrup content were from 10% to 100%	PLS model had RMSEC = 0.0967 and RMSEP = 0.108 confirming the effectiveness and reliability of the technique in detection of inauthentic honey	Liu et al. (2016)
Discrimination of the botanical origin of honey	0.5 to 7 THz	ATR THz-TDS	PCA CA PLS-DA	Femtosecond laser ATR prism made of silicon crystal Medlar honey, vitex honey, and acacia honey	The floral sources of honeys were identified using time-domain attenuated total reflection spectroscopy (THz-TDS ATR) PLS-DA model in 0.5 to 1.5 THz proved to be suitable for quality identification of honey (method accuracy = 88.46%)	Liu et al. (2018)
Geographical discrimination of extra virgin olive oils	0.1 to 4 THz	THz-TDS	PCA RF GA BPNN LS-SVM	Femtosecond laser Transmission mode Customized sample holder Four geographical origin olive oils	Samples showed differences in their THz absorbance spectra and fatty acid compositions Combination of GA with LS-SVM method resulted in an excellent classification with a high accuracy = 96.25% in prediction set Combination of THz spectroscopy with chemometric is a simple and fast method in on-site discrimination of extra virgin olive oils	Liu et al. (2018)
Discrimination of transgenic Camellia oils	0.1 to 1.5 THz	THz-TDS	PLS WLDA SPA	Transgenic and non-transgenic camellia oils	A high classification accuracy was achieved with SPA-WLDA model (correct discrimination rate = 96.53%)	Liu et al. (2019)
Turmeric adulteration	2 to 10 THz	THz-TDS	NA	Mixture of turmeric powder and yellow chalk powder (ratio of 2:1)	Pure and adulterated samples showed completely different spectrum Absorbance value was concentration-dependent Peak at 6.3 THz was considered for yellow chalk powder adulteration	Nallappan et al. (2013)

NA, not applicable; **PCA**, principal component analysis; **PLS**, partial least squares; **CA**, cluster analysis; **DA**, discriminant analysis; **GA**, genetic algorithm; **SVM**, support vector machine; **BPNN**, back propagation neural network; **WLDA**, weighted linear discriminant analysis; **SPA**, successive projection arithmetic; **RF**, random forest pattern recognition method; **RPD**, residual predictive deviation; **RMSEC**, root mean square errors of calibration; **RMSEP**, root mean square errors of prediction.

Table 8–Detection of carbohydrates and sweeteners using THz imaging and spectroscopy techniques.

Application and Product	THz range	Mode/THz Type	Chemometrics	Experiment details	Findings	Reference
Glucose and uric acid	0.1 to 3 THz	THz-TDS	NA	Transmission mode Glucose and uric acid mixed with PET powder PET powder: sample ratio of 8:1 and Pellet thicknesses 1.2 to 1.4 mm for low temperature measurements Pure sample thicknesses 0.3 to 0.7 mm for room temperature measurements	D-Glucose had two sharp absorption peaks at 1.45 THz and 2.1 THz a minor peak at 1.26 THz L-Glucose displayed a sharp peak at 1.45 THz and noise at 2.12 THz THz absorption of L-glucose: completely temperature-dependent and the most distinct absorption peaks were detected at low temperatures Sucrose: three sharp peaks between 1.2 and 2 THz Uric acid: sharp peaks at 1.5 and 2.5 THz	Upadhya et al. (2003)
Structural isomers (glucose and fructose)	0.1 to 4.5 THz	THz-TDS	DFT HF	Ti:sapphire laser Four off-axis parabolic mirrors Glucose and fructose mixed with HDPE powder (ratio of 1:6) Glucose pellet thickness = 1.41 mm, Fructose pellet thickness = 1 mm Gaseous-state theory within the Linearity Combination of Atomic Orbital (LCAO) method was used to study the conformation and simulate the molecules	Based on the numerical results, the density function B3PW91 was applicable for the reproduction of bond length while the density function B3LYP was more suitable for the replication of bond angle Differences between THz spectrum of glucose and fructose is driven from the combination of inter-molecular (for example hydrogen bonds) and intra-molecular motions (for example covalent bonds).	Zheng et al. (2012)
Dehydration kinetics of monohydrated glucose	0.3 to 3 THz	THz-TDS	PBE	Femtosecond laser Photoconductive antenna Monohydrated glucose was mixed with PTFE powder in mass ratios of 1:2 and 1:3	Anhydrous and monohydrated glucose had different THz spectra at room temperature First report of the two new spectral features for monohydrated glucose Monohydrated glucose: five spectral features originated from the intermolecular modes of glucose-glucose and water-glucose molecules Specific peak of monohydrated glucose at 1.8 THz: related to the inter-molecular interactions of glucose-water molecules Anhydrous glucose: THz features came from the interactions of glucose molecules	Zheng et al. (2014)
Glucose hydration	0.25 to 1 THz	CW	NA	Modified system to improve signal stability and achieve a better detection by adding a double-beam CW THz system with a broadband beam splitter and compact phase modulators with a photonic circuit Temperature-controlled flow cell Glucose solution 1.462 M	Sub-THz glucose hydration sensing Fabry-Perot (FP)effect resulted in large waves in the transmission characteristics of glucose solutions and reduced the accuracy of the dielectric constant measurement Used a simple calibration procedure to reduce the FP effect in liquid cell window Sub-THz liquid sensing with high measurement stability	Tajima et al. (2016)
Pentoses	0.3 to 2 THz	THz-TDS	NA	Pellets thickness = 1.3 mm Pentoses: D-arabinose D-lyxose, D-ribose, and D-xylose Temperature: 295 K	D-Arabinose: sharp peak at 1.5 THz and a wide absorption at 1.1 THz D-Lyxose: strong peak at 1.8 THz D-Xylose: peak at 1.6 and very sharp peak at 1.8 THz D-Ribose: absorption at 0.74, 1.1,1.57, and 1.85 THz	Ge et al. (2006)

(*Continued*)

Table 8–Continued.

Application and Product	THz range	Mode/THz Type	Chemometrics	Experiment details	Findings	Reference
Crystallinity of ball-milled anhydrous β-lactose & control of milling process	0 to 3 THz	THz-TDS	PLS	Transmission mode Test period: 60 min Anhydrous β-lactose and α-lactose Differential scanning calorimetry (DSC) Quantification of crystalline content: measuring the melting of crystalline part as well as measuring the devitrification of the amorphous part	Residual crystallinity of β-lactose and α-lactose monohydrate was compared between 1.16 and 1.8 THz α-lactose monohydrate produced 20 to 30% more amorphous material than β-lactose DSC was more reliable method than THz for measuring the crystallinity of anhydrous β-lactose after milling THz was the method of choice for measuring α-lactose monohydrate	Smith et al. (2015)
Fructose-syrup in Acacia honey	0.5 to 3.5 THz	ATR THz-TDS	PLS	Fructose syrup (10% to 100%)	PLS model is a reliable and effective technique (RMSEC = 0.0967 and RMSEP = 0.108) in detection of different fructose syrup concentrations in adulterated honey	Liu et al. (2016)
Floral origin of honeys	0.5 to 3.5 THz	ATR THz-TDS	PCA PLS-DA CA	Acacia honey, medlar honey, vitex honey	PLS-DA model differentiated different honeys in the frequency range of 0.5 to 1.5 THz Method accuracy = 88.46% for validation set	Liu et al. (2018)
Crystallization of sucrose	0.1 to 3 THz	ATR THz-TDS	PLS	ATR silicon crystal Sugar solution (70 g/l00 mL) Sugar solution placed directly on the ATR silicon crystal Test period: 60 min THz spectra was recorded every 10 min	ATR spectrum was time-dependent, and the absorption of sugar solution dropped over time At the low frequency end of the spectrum, THz waves propagated much deeper into the sugar solution Over time, the solution transformed into a solid glass Crystallization began after 50 h and progressed to a crystalline material after 58.5 h ATR spectra showed a series of phonon bands THz pulsed imaging is an effective method for monitoring the buildup of a sugar coatings in confectionary products	May and Taday 2013)
Cellulose and Sugar detection	0.5 to 2.5 THz	THz TDS	FDTD	Nano-antenna array-based sensing chip Saccharides: mannose, galactose, glucose, arabinose, fructose maltose, sucrose, cellulose glycogen, and amylose Non-saccharide sweeteners: aspartame and acesulfame K	D-Glucose: peaks at 1.4 and 2.05 THz Sucrose: Peaks at 1.4 and 1.8 THz Fructose: absorbance at 1.7 and 2.1 THz Cellulose did not show any specific spectral feature A good agreement was found between experimental results and FDTD calculations Beverages with different sugar content had distinct transmittance features between 1.5 and 2 THz Nano-antenna sensing chip could sensitively and selectively detect carbohydrates at micro-mole concentrations The THz nano-antenna sensing chip can be used in non-invasive blood-sugar monitoring	Lee et al. 2015)
Sugar and alcohol content of alcoholic beverages	0.1 to 1.1 THz	THz-TDS	NA	THz-TDS with a high-index silicon window Reflection mode Sugar (0, 12%) and alcohol (0, 30%)	Addition of ethanol to water significantly decreased refractive index and absorption coefficient of the solution Added sugar did not affect the dielectric properties of the solution No clear change was observed in the refractive index at low concentrations of sugar (less than 20%), but a small decrease was noted in the absorption coefficient Suitable for continuous monitoring of beverage production	Møller et al. (2007)

(*Continued*)

Table 8–Continued.

Application and Product	THz range	Mode/THz Type	Chemometrics	Experiment details	Findings	Reference
Real-time monitoring of fermentation & sugar concentrations in water	0.75 to 1.1 THz	THz-TDS	NA	First report of real-time monitoring of the fermentation process Sugar solutions (0.3 to 45% sugar by weight) Test period: 30 min	Sugar-specific reflection spectra were observed between 0.858 and 0.935 THz Highest THz reflection sensitivity for sugar mixtures was between 0.858 and 0.935 THz and in the frequency range of 0.913 to 1.023 THz for ethanol mixtures LOD for sugar was 1.5 % sugar and 0.3 % for ethanol	Fawole and Tabib-Azar (2016)
Reducing sugar ternary mixture	0 to 3 THz	THz-TDS	PCA ANN PLS	Different concentration s of pure α-lactose monohydrate, D(−)fructose, and citric acid Mode-locked Ti-sapphire laser	Concentration of the reducing sugar in a mixture was predicted using PLS and ANN with a similar RMSE<0.9%	El Haddad et al. (2014)
Sorbitol crystals	0.6 to 2.4 THz	THz-TDS	DFT	α-sorbitol Two cocrystal forms of sorbitol: sorbitol-pyridine and sorbitol-water	Sorbitol-pyridine was less stable than sorbitol-water Combination of simulated and experimental vibrational spectra can be a useful tool for quality assessment of quantum models, interpreting the intermolecular and studying thermodynamic relationships	Dierks and Korter (2017)
Effect of sugar type on yeasts growth	0.75 to 1.1 THz	THz-TDS	NA	Horn antenna Three different samples: (1)yeast and water; (2) Yeast, water, and normal sugar; (3) yeast, water, and zero calorie sweetener (sucralose)	Artificial sweeteners resulted in vigorous bubbling in the solution and maximum growth of yeast Artificial sweeteners and sugar had significant change in reflection coefficient at 1.0152 THz Sugar solutions: Changes in THz reflection spectrum at 14 and 28 min for normal. Splenda and normal sugar solution had changes of 60 dB and 15 dB, respectively Control sample: 8 dB change	Fawole et al. (2015)
Dielectric properties of sugar and alcohol solutions	0 to 1.5 THz	THz-TDS	NA	Reflection mode Sugar solution (0 to 75%) Alcohol solution (0 to 100%) Samples: water, carbonated mineral water, degassed mineral water, carbonated soft drink, and degassed soft drink Temperature: room temperature	Real and imaginary part of the dielectric function were measured for water, carbonated mineral water, degassed mineral water, carbonated soft drink, and degassed soft drink Reflection THz-TDS can detect interfering components, such as color and organic precipitates, in commercial beverages and liquors	Jepsen et al. (2007)
Dielectric properties of solid polycrystalline glucose	0 to 3 THz	THz-TDS	PLS FDTD DFT	Anhydrous polycrystalline glucose pellets	Multiple characteristic absorption peaks between 0.2 and 2.2 THz were related to the complex dielectric function of polycrystalline glucose Lorentz dielectric model was found the best fit for the complex dielectric function of glucose	Sun and Zou (2016)

(*Continued*)

Table 8–Continued.

Application and Product	THz range	Mode/THz Type	Chemometrics	Experiment details	Findings	Reference
Effect of carbohydrates on the solvation dynamics of water	1 to 4 THz	THz-TDS	NA	p-Ge laser Monosaccharide (glucose) Disaccharides (lactose and trehalose)	A linear increase (2 to 4%) in the absorption coefficient was observed between 1 and 3 THz for all three carbohydrates Changes in the THz absorption were correlated to (1) the number of hydrogen bonds between water molecules and carbohydrate and (2) the molar concentration of the solute	Heyden et al. 2008)
Hydration state of saccharides	0.2 to 3 THz	ATR THz-TDS	NA	Monosaccharides: mannose, glucose, and galactose Disaccharides: maltose and sucrose Low concentration solutions (0.292 M) Temperature: 25 °C	Number of hydration water around mono and disaccharides were calculated in low concentration solutions (0.292 M) Number of hydration water for maltose = 21.1 and sucrose = 21.9, mannose = 10.5, and galactose = 11.2 Hydration number of glucose was 15.2 Hydration number decreased with an increase in the concentration of solution THz TD-ATR: a valuable tool for studying the global hydration state and gain information about water dynamics around solutes in a solution	Shiraga et al. 2013)
Quantification of starch content	3 to 13.5 THz	THz-TDS	NA	THz spectroscopy under vacuum condition 2nd derivative of the Savitzky-Golay treatment Starch suspension (2% w/w), amorphous and crystalline glucose Mung beans germinated under white LED light for 18h and then kept at dark for 6h, repeated for 1 to 7days at 26 °C, freeze-dried seedlings were grounded	Crystalline starch: absorption peaks at 5, 7.8, 9, 10.5, 12.1, and 13.1 THz Crystalline glucose: absorption peaks at 8.4, 12, and 12.7 THz One-day germinating mung bean seedling: absorption peaks at 5, 7.9, 9, 10.5, 12.2, and 13.1 THz Four-day and 7-day germinating mung bean seedling: absorption peaks at 9, 10.5, 12.2, and 13.1 THz Hydrolyzed mung bean seedling: absorption peaks at 10.5, 12.2, and 13.1 THz The absorption peak at 9 THz disappeared after hydrolysis with amylase High correlation was observed between the estimated starch content based on the intensity of the peak at 9 THz with the measured starch content by chemical methods (r = 0.98, RMSE = 4.7%)	Nakajima et al. (2019)

NA, not applicable; **PCA**, principal component analysis; **PLS**, partial least squares; **CA**, cluster analysis; **DA**, discriminant analysis; **ANN**, artificial neural networks; **DFT**, density functional theory; **FDTD**, finite difference time domain simulation; **PBE**, Perdew-Burke-Ernzerhof exchange-correlation functionals; **HF**, Hartree-Fock function; **RMSE**, root mean square error; **RMSEC**, root mean square errors of calibration; **RMSECV**, root mean square errors of cross-validation; **RMSEP**, root mean square errors of prediction.

Table 9–Application of THz imaging and spectroscopy techniques in chocolate studies.

Application and Product	THz range	Mode/THz Type	Chemometrics	Experiment details	Findings	Reference
Chocolate bars	0 to 3 THz	THz-TDS	NA	Both transmittance and reflection imaging Chocolate bars with different thickness and fillings	Embossed letters in a chocolate bar were distinguished based on the thickness differences and the scattering effects 3-D representations of layered objects with reflectance THz imaging	Mittleman et al. (1999)
Chocolate bars	0 to 3 THz	THz-TDS	NA	Femtosecond laser source 2-D THz transmission image Scanning speeds of 0.55 m/s Chocolate bars filled with stones, glass and meal pieces Packaged in plastic foil	Contaminants were detected between 0.4 and 0.5 THz with a spatial resolution of less than 1 mm More time delay was reported for the higher refractive index differences	Jördens et al. (2006)
Chocolate bars with contaminants	0 to 3 THz	THz-TDS	NA	Assembled TERA K15 THz-TDS system in transmission geometry Temporal scanning range of 300 ps Scanning speeds of 0.55 m/s Plastic packaged	Suitable for thicker chocolates Can detect contaminants in complex chocolate products (for example waffles or truffles)	Koch and Krok (2006)
Foreign bodies in chocolate	0.4 to 0.75 THz	THz-TDS	NA	Femtosecond laser source Silicon-on-sapphire antenna Scanning speed of 0.5 m/s Nuts, glass, stone, or plastic particles A fringe projection scanner was used for detection of glass contaminants	Analyzed the shape of the temporal waveform Pure chocolate: a single THz signal Nut-contaminated chocolates: two peaks Foreign bodies: different refractive indexes from nuts Desirable ingredients: specific shape and height of THz waveform Glass particles: detected based on (1) number of the peaks and (2) by measuring temporal position of the peaks Glass particles and nuts had similar intensity images The spatial position of the contaminant was clear in the delay image for the pulse maximum False alarms (double pulse) observed when nuts were not completely embedded inside the chocolate bar	Jördens and Koch (2008)
Chocolate contaminants	0 to 2.5 THz	THz-TDS	NA	Small glass and stone pieces in chocolate with different thickness	Small glass and stone pieces were detected based on their refractive indexes and their double-pulse shapes	Ung et al. (2007)
Real-time quality assurance of chocolate products	0 to 3 THz	THz-TDS	NA	Two-point measurement at an isosceles triangle To avoid the problems associated with minor thickness variations, signal intensity was calculated as summation of a temporal spacing with two-line scans	Irregularly shaped curves due to different thickness Maximum intensity was observed for pure chocolate Contaminants: changed the shape of the pulse and resulted in time delay Grooves: resulted in early arrival of THz pulse and smaller intensity Fast and nondestructive method for quality assurance of chocolate by focusing on the whole THz waveform and two-point measurement of the terahertz wave-form	Joerdens et al. (2006)

(*Continued*)

Table 9–Continued.

Application and Product	THz range	Mode/THz Type	Chemometrics	Experiment details	Findings	Reference
Thin layers of chocolate	0.45 to 3 THz	THz-TDS	PCA PLS	THz and FTIR spectroscopy Transmittance mode Special sample holder Mercury-arc lamp source Mylar multilayer beam splitter Frequency resolution: one wavenumber (approx. 30 GHz) Each measurement performed < 100 s	Shape of the absorption spectra was a key feature in separation of different substances PLS model was used for identification and classification of unknown samples Sample-dependent information was used for creation of a PLS model Binary form class membership classified pure and mixtures samples with a good accuracy	Pohl et al. (2014)
Identification of melted parts of a chocolate bar	210 GHz	CW	NA	Modified sub-THz transmission imaging system Reflection mode F-Theta lens (used for an extended scan area with high spatial resolution) Polygonal mirror Conical horn antenna Scanning speed of 80 mm/s	Melting defects in packaged chocolates were identified High-resolution imaging technique (identified a pattern with 2.83 mm line-width at 210 GHz) Wide range of detection (150 mm) Smaller beam size resulted in better image quality	Ok et al. (2015)
Chocolate contaminants	140 GHz	CW	NA	Transmission mode Circular and conical horn antennas Schottky diode detector Contaminants: paper clip (8 to 34 mm; 1-mm thick), maggot (9-mm-long and 1.4-mm-thick), and mealworm (16-mm-long and 2-mm-thick)	The new settings yielded a higher-resolution and a better beam focusing with a less expensive source (140 GHz) Small foreign bodies were detected in a chocolate bar with a high image resolution Image resolution = 0.2 mm/pixel	Ok et al. (2018)
Melamine in chocolate powder	0 to 1.3 THz	THz-TDS	NA	Fast scan mode (30 measurements in 1 s) Melamine (0 to 10 wt %) Chocolate powder particle size: 50, 160, and 255 μm	Regardless of the thickness and type of the packaging material, three distinct melamine peaks (at 2, 2.26, and 2.6 THz) were detected Images at 2 THz were dose-dependent LOD < 13% and $R^2 > 0.913$ showed the efficacy of THz imaging for rapid and nondestructive detection of melamine in chocolate	Baek et al. (2014)

NA, not applicable; **PCA**, principal component analysis; **PLS**, partial least squares.

Table 10–Application of THz imaging and spectroscopy techniques in fatty acid and oil studies.

Application and Product	THz range	Mode/THz Type	Chemometrics	Experiment details	Findings	Reference
Plant oils and animal fats	0.2 to 2 THz	THz-TDS	NA	Mode-locked Ti:sapphire laser Ultra-short (100 fs) pulses Half wave splitting plate LT-GaAs photo-conductor ZnTe crystal detector Plant oil samples (peanut, corn, sesame, vegetable and chili) Animal fat samples (pork and beef fat) Sample thickness: up to 3 mm Transmission mode	Oil samples: increase in the THz frequency increased the absorption coefficient and decreased refraction index Sesame oil: lowest absorption coefficient (7.6126 cm^{-1}) and highest refraction value (1.618) Pepper oil: highest absorption coefficient (11.083 cm^{-1}) at 1 THz Peanut oil: lowest refraction value (1.474) Beef fat: refraction indices of 1.4 (solid state) and 1.52 (liquid state) Pork fat: refraction indices of were reported as 1.51 (solid state) and 1.52 (liquid state) Thick oil sample (3-mm thickness) showed time delay in the transmitted THz wave signal compared to a thin sample (2-mm thickness) Both thin and thick samples had similar absorption peaks Both absorption coefficients and analyzed refraction indices were compared to perceive if any systematic phenomena exist THz fingerprint spectrum and information for some plant oils and animal fats generated	Hu et al. (2005)
Optical properties of peanut oils	0.2 to 2.5 THz	THz-TDS	NA	Modified THz system Mode-locked Ti:sapphire laser producing 100 fs pulses at 800 nm Coplanar strip line antenna fabricated on a semi-insulating (SI) GaAs wafer Two highly resistive silicon lenses ZnTe crystal detector Peanut oil samples (unused peanut oil, 5-min and 10-min boiled peanut oils)	Effect of boiling on peanut oil was studied Unused peanut oil sample: time delay of 8.33 ps Both 5-min and 10-min boiled peanut oil samples: 8.46 ps time delay Supplementary peaks behind the main peanut oil spectra were due to the Fabry-Pérot effect 5-min boiled peanut oil: absorption peak at 1.22 THz 10-min boiled peanut oil: peaks at 1.14, 1.20, and 1.26 THz	Li et al. (2008)
Optical parameter of vegetable oils	0.2 to 1.5 THz	THz-TDS	NA	Oil samples: peanut, rapeseed, soybean, and sunflower seed Iterative algorithm was used to enhance accuracy of the optical parameter extraction	Sunflower seed oil: time delay of 2.13 ps Soybean, peanut, and rapeseed oil: 2.1 ps time delay relative to an empty quartz cuvette Accuracy of the optical parameter extraction for THz-TDS was enhanced	Jiusheng Li (2010)

(*Continued*)

Table 10–Continued.

Application and Product	THz range	Mode/THz Type	Chemometrics	Experiment details	Findings	Reference
Physio-chemical changes of oils during heating	0.05 to 2 THz	THz-TDS	NA	Mode-locked Ti:sapphire laser Designed a fixed sandwich-structure sample holder to eliminate random errors due to alignment Oil sample sealed in a 70-μm-thick LDPE bag and pressed between two stiff HDPE sheets. Aluminum retaining mounts held the whole structure Mechanical micrometers adjusted sample thickness between 0 and 5 mm To minimize the noise fluctuations: each measurement was from the average of 1000 consecutive scans Oil samples: canola, coconut, extra virgin olive, rice bran, refined olive, and sunflower Heating time: 5 min heating beyond the smoke point of each oil	Fiber-coupled THz-TDS system in transmission-mode was used to monitor effect of heat on cooking oils A peak at around 5 ps was observed for the reference THz pulse after the start of the 80 ps measurement window Different oils at a certain thickness: Similar refractive indices and Fabry-Pérot spectra At 0.5 THz optimal thickness was 5 mm 1 mm thickness is optimal for frequencies around 2 THz Very minor changes in the absorption coefficient of cooking oils heated above their smoke point	Dinovitser et al. (2017)
Identification and discrimination of edible cooking oils from swill-cooked dirty oils	0.2 to 1.3 THz	THz-TDS	PCA SVM	Ti:sapphire laser p-type GaAs wafer ZnTe crystal detector Oil sample: common edible oil and swill-cooked oil collected from the frying boilers	Clean edible oils and dirty oils had very similar pulses of waveforms Clean edible oils and dirty oils had different absorbance features PCA and SVM: highest first principal component score with 97.4% contribution rate PC1 score of dirty oils: 0.5 PC1 score of normal edible oils: 2.3 SVM directly identified swill-cooked oils SVM model precision: 100% Combination of THz and chemometrics can be used for rapid identification and discrimination of swill-cooked oils and protection of consumers' health	Zhan et al. (2016)
Identification of edible oils	1 to 14 THz	THz-TDS	fsPLS biPLS iPLS GA-PLS-DA	Special THz system setup Mode-locked Ti:sapphire femtosecond laser Parabolic mirrors DSTMS crystals Customized a 0.5 mm-thick stainless-steel sheet cuvette attached to PE films on each side Conditions: under N_2, low humidity (less than 1%), Temp (298 K) Oil samples: Corn, peanut, pepper oil, sunflower seed, and sesame	All oil samples had absorption between 1.5 and 3.5 THz GA-PLS model: best prediction accuracy GA-PLS-DA model: RESEP = 0.1786, Rp = 0.9920, and highest classification accuracy (100%) Combination of chemometric methods with THz spectroscopy is an effective method for identification and differentiation of edible oils	Yin et al. (2016)
Dielectric properties of corn oil	0.2 to 1.5 THz	THz-TDS	NA	Mode-locked Ti:sapphire laser producing 100-fs pulses Coplanar strip line antenna fabricated on a semi-insulating (SI) GaAs wafer ZnTe crystal detector Conditions: under N_2, room temperature	Studied effect of boiling on spectral characteristics of corn oil 5-min boiled corn oil samples: absorption peaks at 1.437, 1.352, and 1.246 THz 10-min boiling: absorption peaks at 1.458, 1.352, and 1.268 THz Time delays of 8.53 ps and 8.4 ps were noticeable in the THz spectrum of 5-min and 10-min corn oil samples	Li et al. (2009)

(*Continued*)

Table 10–Continued.

Application and Product	THz range	Mode/THz Type	Chemometrics	Experiment details	Findings	Reference
Main components of rice bran oil	0.2 to 1.6 THz	THz-TDS	DFT	Mode-locked Ti:sapphire laser Coplanar strip line antenna fabricated on a semi-insulating (SI) GaAs wafer ZnTe crystal detector Conditions: under N_2, room temperature	Octadecanoic acid and hexadecanoidc acid were detected in rice bran oil Good agreement between theoretical and experimental results THz-TDS technique for detection and identification of main components in edible oil	Li et al. (2009)
Hydrogenation of peanut oil (effect of conventional cooking process)	0.2 to 2.2 THz	THz-TDS	NA	Oil samples: unheated and heated (in a frying pan on conventional oven) Oil samples added to PE powder with a 1:1 weight ratio Liquid cell: 580 μm thick Heating process: used a conventional gas stove, 5 min	No obvious differences in viscosity, smell or color was reported Absorption peaks were observed between 1 and 1.6 THz Significant increase in THz absorption of peanut oil after 5 min direct heating	Ung et al. (2010)
Dielectric function of water in butter, lard, and vegetable oils	0 to 2 THz	THz-TDS	NA	Femtosecond laser Four off-axis paraboloidal mirrors Si lens detector Butter, lard, rapeseed oil and grapeseed oil	Unique THz spectrum for imaginary and real parts of the dielectric function of oils Refractive indices of rapeseed oil and grapeseed oil were 1.51 and 1.52. Butter had a water pool size of 1 to 25 μm	Møller et al. (2010)
Dielectric properties of olive oil	0.2 to 2.5 THz	THz-TDS	NA	Mechanical chopper at 2 kHz was used to modulate the pump beam and increase the SNR Conditions: under N_2 in an acryl box	Absorption coefficient and refractive index of olive oil were measured with and without Fabry-Pérot resonator THz-TDS is a useful tool for characterization of olive in the far-infrared region	Li and Yao (2008)
Geographical origin of olive oils	0.1 to 4 THz	THz-TDS	PCA RF GA BPNN LS-SVM	Extra virgin olive oils from different geographical regions (Australia, Greece, Italy, and Spain)	Olive oil samples had different absorbance spectra and fatty acid compositions GA-LS-SVM: high accuracy (96.25%) in prediction set Combination of THz spectroscopy with chemometric methods: simple, fast, and on-site discrimination method for extra virgin olive oils	Liu et al. (2018)
Unsaturated fatty acids and saturated fatty acids	0.2 to 12 THz	THz-TDS	NA	Unsaturated fatty acids (oleic, linoleic, and linolenic acids) Saturated fatty acids (stearic and palmitic acids)	Several sharp peaks were observed for saturated fatty acids while unsaturated fatty acids showed two distinct peaks (at 247 and 328 cm^{-1}) representing the carboxylic group THz absorbance of fatty acids was concentration-dependent	Jiang et al. (2011)
Elaidic acid	0.5 to 2.5 THz	THz-TDS	DFT	B3LYP algorithm of density functional was used to simulate the structure and vibrational frequencies of the elaidic acid molecule Conditions: under N_2, room temperature	Average refractive index of elaidic acid = 1.43 Absorption peaks: mainly caused by the intermolecular and intramolecular vibrations jointly Good agreement between the experimental and theoretical results was reported Provided THz fingerprint of elaidic acid for detection purposes	Kang et al. (2011)

NA, not applicable; **PCA**, principal component analysis; **PLS**, partial least squares; **fsPLS**, full spectra PLS; **biPLS**, backward interval PLS; **iPLS**, interval PLS; **PLSR**, partial least squares regression; **DA**, discriminant analysis; **GA**, genetic algorithm; **LS**, least-squares; **SVM**, support vector machine; **BPNN**, back propagation neural network; **DFT**, density functional theory; **RF**, random forest pattern recognition method; **RMSEC**, root mean square errors of calibration; **RMSECV**, root mean square errors of cross-validation; **RMSEP**, root mean square errors of prediction.

Table 11–Application of THz imaging and spectroscopy techniques in amino acid and protein studies.

Application and Product	THz range	Mode/THz Type	Chemometrics	Experiment details	Findings	Reference
Bovine serum albumin, collagen, and calf thymus DNA	0.06 to 2 THz	THz-TDS	NA	Two pulsed THz spectroscopy systems based on photoconductive switches Hertzian dipole antennas Parabolic mirrors Transmission mode Used specific data collection and sample preparation techniques to eliminate etalon effects Lyophilized powders (with 200 mg PET and without PET filler) Pellet thickness: 7.5 mm Pellet density was measured at 66% relative humidity	All samples had good agreement with Beer's law behavior Collagen absorbance had a rapid increase with increasing frequency DNA and BSA showed linear increase in the absorbance Dry DNA had a refractive index of 1.3 at 0.7 THz First study on the structural forms of the molecules using crystallographic measurements First report of pulsed THz spectroscopy for measuring refractive index and low-frequency absorption spectrum of biomolecules as a function of relative humidity	Markelz et al. (2000)
Biotin-avidin sensor	0.1 to 1 THz	Differential THz-TDS (DTDS)	NA	Femtosecond laser source generating 150 fs pulses at 86 MHz GaAs wafer ZnTe crystal detector Glass microscope slides (0.96 mm thick) Conditions: room temperature and 40% relative humidity	First report on the use of differential THz-TDS for label-free bioaffinity sensingLOD of the method was 0.1 $\mu g\ cm^{-2}$Factors affecting sensitivity of THz sensor: (1) binding affinity of analyte-ligand (2) avidin immobilization on the glass slide (3) film layer homogeneity (4) THz refractive indices of the bound layers	Mickan et al. (2002)
Enhancing avidin–biotin binding	0.1 to 1 THz	Double-modulated THz-DTDS	NA	Femtosecond laser source GaAs semi-conductor emitter wafer ZnTe crystal detector Octadecanol self-assembled modified quartz crystal surface Used small agarose beads to enhance detection of avidin-biotin binding	LOD of the method was 10.3 ng/cm^2 for avidin This new THz-DTDS biosensor uses a combination of high-refractive index agarose beads with biotin-avidin technology and offers a simple, inexpensive and non-invasive method for detection of biological compounds	Menikh et al. (2004)
Dielectric properties of egg white lysozyme	0 to 2 THz	THz-TDS	NA	High-brightness pulsed THz system Femtosecond laser Hertzian dipole antenna Quartz crystal Tri-N-acetyl-D-glucosamine added to egg white lysozyme Thin film (50 to 100 μm thickness) formed onto half of a quartz slide The clean half of the slide was used as a reference	A tagless, universal biosensor for determination of ligand binding in biomolecules in the THz frequency range Absorbance decreased due to the binding effect, but the refractive index was almost independent from binding THz dielectric response of egg-white lysozyme was a function of hydration and binding at different relative humidity levels Dielectric response can be used as an indicator for binding.	Markelz et al. (2004)
Dynamics of lysozyme in water and absorption spectrum of solvated bovine serum albumin	0 to 4 THz	THz-TDS	NA	In-house developed system Gunn oscillator (at 0.139 THz) Harmonic multipliers (up to 0.21 THz) Free-electron lasers (up to 4.8 THz) A variable path length sample cell A sensitive cryogenic composite silicon detector	Molar extinctions of solvated lysozyme exhibited a fast increase with frequency (0.075 to 0.105 THz) but stayed almost constant between 2 and 3.72 THz A low-frequency cutoff in THz dynamics observed between 0.2 and 0.3 THz Absorption spectrum of solvated bovine serum albumin was between 0.3 and 3.72 THz	Xu et al. (2006a) Xu et al. (2006b)

(*Continued*)

Table 11–Continued.

Application and Product	THz range	Mode/THz Type	Chemometrics	Experiment details	Findings	Reference
Classification of all 20 α-amino acids	0.2 to 3 THz	THz-TDS	NA	Mode-locked Mai-Tai Laser InAs and ZnTe wafer Amino acid disks (diameter = 13 mm, thickness = 1 mm) α-amino acids: glycine, alanine, valine, isoleucine, leucine, serine, threonine, cysteine, methionine, aspartic acid, glutamic acid, asparagine, glutamine, lysine, arginine, histidine, proline, tryptophan, phenylalanine, and tyrosine	First classification of amino acids based on their THz spectra and molecular structures Glycine: sharp peak at 2.53 THz and a very weak peak at 2.30 THz Alanine: peaks at 2.23, 2.56, and 2.73 THz Valine: peaks at 1.11, 1.7, 2.12, 2.22, 2.52, 2.64, and 2.8 THz Isoleucine: peaks at 0.85, 1.08, 1.40, 1.70 2.40, and 2.7 THz Leucine: peaks at 0.68, 0.85, 1.46, 1.64, 2.14, 2.56, 2,74, 2.88, and 2.96 THz Dicarboxylic group of amino acids (Asp and Glu) having a carboxyl group (COOH): Glutamic acid: peaks at 1.23, 2.03, 2.23, 2.46, 2.64, and 2.75 THz Aspartic acid: peaks at 1.35 and 2.58 THz Hydroxylic amino acid group (Thr and Ser) having a hydroxyl group (OH) addition on their side chain: Serine: distinct peaks at 2.01 and 2.71 THz and a very weak peak at 2.4 THz Threonine: sharp peaks at 1.41 and 2.14 THz and wider peaks at 1.11 and 2.58 THz Monocarboxylic diamino acids (His, Lys, and Arg) with amino group (NH_2) on the side ring or the side chain: Lysine: a very distinct peak at 2.25 THz and small peaks at 1.26, 1.79, and 2.64 THz Arginine: sharp peak at 2.6 THz and small stretched peaks at 0.99, 1.47, and 2.02 THz Histidine: sharp peaks at 0.88, 1.65, and 2.24 THz and a wide peak at 2.38 THz Carboxamide group (Asn and Gln), having an amino group (NH_2) and a carbonyl group (C = O): Asparagine: a very sharp peak at 1.64 THz and a wide peak at 2.26 THz Glutamine: peaks at 1.70, 2.14, and 2.42 THz Sulfur-containing amino acids: Methionine: peaks at 1.06, 1.88, 2.7, and 2.94 THz Cysteine: peaks at 1.40, 1.70, 2.33, 2.61, and 2.94 THz Aromatic group (Phe and Tyr) have an aromatic ring on the side chain: Phenylalanine: main peak at 2.52 THz and small peaks at 1.23, 1.99, and 2.72 THz Proline: main peak at 2.64 THz, small peaks at 1.69, 2.08 THz Heterocyclic amino acid: Tryptophan: sharp peaks at 1.43, 1.82, and 2.26 THz and wide peaks at 0.91, 1.20, and 2.57 THz	Wang et al. (2009)

(*Continued*)

Table 11–Continued.

Application and Product	THz range	Mode/THz Type	Chemometrics	Experiment details	Findings	Reference
Torsional vibrational modes of tryptophan	0.2 to 2 THz	THz-TDS	DFT	Mode-locked Ti:sapphire laser ZnTe crystal Two parabolic mirrors Conditions: under N_2, room temperature	Peak at 1.842 THz: assigned to C1-C9 ring torsional motion Peak at 1.435 THz: related to C11-C12 torsional motion Tryptophan film had a refractive index of 1.18 Refractive index of tryptophan powder was 1.27	Yu et al. (2004)
Optical density of Amino acids	0 to 4 THz	THz-TDS	NA	Femtosecond laser LT-GaAs emitter Parabolic mirror Amino acid samples: L-histidine, L-cysteine, L-glutamic acid, L-glutamic acid sodium salt, and L-glutamic acid hydrochloric salt Concentration range (0.2 to 1 mol/L)	L-Glu had sharp peaks at 1.22, 2.03, 2.46, 2.68, 2.80, and 3.24 THz Strong peaks at 1.22 and 2.03 THz were selected as marker bands for plotting the average optical density Two linear models with $r = 0.99$ Concentrations of L-His L-Cys, and L-Glu in mixed samples was calculated with errors of less than 11% (for concentration>0.45 mol/L) and 20% (for concentration> 0.22 mol/L)	Ueno et al. (2006)
Spectral characteristics of L-tyrosine and L-glutamic acid	0.2 to 2 THz	THz-TDS	DFT	Femtosecond laser Ga-As photoconductive emitter Four off-axis ZnTe crystal Parabolic mirror Conditions: under N_2, room temperature (295K)	Average refractive index of L-tyrosine: 1.47 Average refractive index of L-glutamic acid: 1.56 Good agreement between the theoretical calculations with the experimental data	Yan et al. (2008)
Non-destructive quantification of amino acids in dietary supplements	0.5 to 3 THz	THz-TDS	NA	Femtosecond laser LT-GaAs photoconductive antenna for both generation and detection of THz pulses Amino acid tablets (10-mm diameter and 0.8-mm thickness) wrapped in paper	Wrapped and unwrapped samples had very similar spectral pattern Good agreement between calculated and experimental spectrums Recovery ratio of 12% for L-Ile, L-Gln, and L-Arg L-Val: recovery ratio: 29% L-leu: recovery ratio: 59%	Ueno et al. (2011)
Binary mixture of amino acids	0 to 2.5 THz	THz-TDS	AsLS iPLS PLS	Femtosecond laser ZnTe-based semiconductor antenna AsLS was used to reduce the possible background contributions and calculate the baseline Latin partition was used to divide samples into prediction and calibration sets	Glutamic acid and glutamine: different absorption spectrum iPLS: more effective model for both glutamine and glutamic acid (RMSEP = 0.39 ± 0.02) $R^2 = 0.9904$ for glutamine $R^2 = 0.9906$ for glutamic acid	Lu et al. (2016)
Ternary amino acid mixture	0 to 3 THz	THz-TDS	PLS SVM	MSC, Savitzky-Golay smoothing, wavelet transform, and first derivative were used Amino acids: L-tyrosine, L-glutamine, and L-glutamic acid	L-tyrosine, L-glutamine, and L-glutamic acid had different characteristic absorption SVM model with MSC pre-processing: highest yield and most accurate prediction	Zhang et al. (2017)
Ternary amino acid mixture	0 to 1.8 THz	THz-TDS	TM PLS	Fiber laser ZnTe-based semiconductor antenna detector Tchebichef image moment (TM) Amino acids: L-tyrosine, L-glutamine, and L-glutamic acid)	Extinction coefficients, absorption coefficients, and refractive indices of tyrosine, glutamic acid, and glutamine calculated TM method resulted in R2 = 0.9595 and RMSEp < 1.2601 More reliable and accurate model compared to PLS	Lu et al. (2018)

(*Continued*)

Table 11–Continued.

Application and Product	THz range	Mode/THz Type	Chemometrics	Experiment details	Findings	Reference
Absorption spectrum of L-histidine and L-histidine hydrochloride monohydrate	0.5 to 4 THz	THz-TDS	DFT	Quantum chemical calculations were performed to simulate the vibrational properties of amino acids Powder X-ray diffraction (PXRD) performed to check the structures of L-histidine and L-histidine hydrochloride monohydrate	L-histidine: sharp peaks at 1.41, 2.09, 2.47, 2.80, 3.37, and 3.97 THz and weak peaks at 0.77, 1.73, and 2.99 THz L-histidine hydrochloride monohydrate: noticeable peaks at 2.22, 2.37, 2.90, and 3.20 THz and less distinct peaks at 0.89 and 1.62 THz Observed a shift towards higher frequencies and sharper absorption bands when the temperature was reduced At low temperature, the peak at 1.62 THz of L-histidine hydrochloride monohydrate spectrum split into two distinct peaks Measured PXRD pattern matched with CCDC open database	Zong et al. (2018)
Vibrational spectra of phenylalanine	0.2 to 2.2 THz	THz-TDS	HF	Phenylalanine and PE disks (diameter = 13 mm and thickness = 1 mm)	Torsional vibrational modes of phenylalanine molecule investigated Phenylalanine absorption peaks at 1.23 and 1.99 THz	Li et al. (2006)
Vibrational characteristics of L-phenylalanine and it's monohydrate	0.5 to 4.5 THz	THz-TDS	DFT	PXRD and DSC-TG examinations used for studying molecular packing patterns and thermodynamic properties Conditions: low temperature (−180 °C) and room temperature (25°C)	L-phenylalanine absorption peaks were sharper and stronger at −180 °C At room temperature, L-phenylalanine had sharp peaks at 2.81 and 4.19 THz and less noticeable bands at 1.17 and 1.99 THz L-phenylalanine monohydrate had bands at 0.93, 1.48, 3.09, 4.03 THz and small peaks at 1.71 and 1.92 THz At low temperature, anhydrous L-Phe: a new peak at 2.30 THz and the broad peak at 2.81 THz split into three peaks (2.85, 3.22, and 3.41 THz)	Pan et al. (2017)
Protein hydration and aspects of collective water network dynamics	0.2 to 1 THz	THz-TDS	NA	Semiconductor p-Ge laser in a closed-cycle helium cryostat Picosecond time scale Kinetic THz absorption studies of hydration dynamics during protein folding Condition for model peptides: at low hydration levels, at frequency range of 1.2 to 3 THz	A non-linear THz absorbance response was observed Theories and models for better understanding of the concentration-dependent features observed with THz absorbance Developed a tool for time-resolved studies Solvent dynamics were coupled to secondary structure formation of proteins Reported that the water network had been rearranged prior to protein folded to its native conformation	Born and Havenith (2009)
Peptides at low hydration level	0.2 to 1 THz	THz-TDS	NA	Model peptides: *N*-acetyl-tryptophan-amide, *N*-acetyl-leucine-amide, *N*-acetyl-leucine-methylamide, *N*-acetyl-glycine-amide, and *N*-acetyl-glycine-methylamide	THz absorption coefficients of model peptides in aqueous solution were concentration-dependent Dramatic decrease in THz absorption when the number of water molecules per solute was less than 18 to 20 (signature for the breakdown of peptide-water network motions) Hypothesis: a minimum number of hydration waters is necessary to activate the peptide-water network motions	Born et al. (2009)

NA, not applicable; **PLS**, partial least squares; **iPLS**, interval PLS; **AsLS**, asymmetric least squares; **SVM**, support vector machine; **DFT**, density functional theory; **RF**, random forest pattern recognition method; **TM**, Tchebichef image moment method; **HF**, Hartree-Fock function; **RMSEP**, root mean square errors of prediction; **RMSEC**, root mean square errors of calibration; **RMSECV**, root mean square errors of cross-validation.

Table 12–Detection of vitamins using THz imaging and spectroscopy techniques.

Application and Product	THz range	Mode/THz Type	Chemometrics	Experiment details	Findings	Reference
Riboflavin and related compounds	0 to 4.5 THz	CW	NA	Riboflavin, lumiflavin, lumichrome, alloxazine, and D-mannitol	Both the intensity and position of their THz spectrum were temperature-dependent	Takahashi et al. (2005)
Riboflavin and astaxanthin	0 to 2.5 THz	THz-TDS	NA	Tablet diameter = 12 mm and thickness = 1 mm	Riboflavin was more absorptive to THz waves and had strong peaks at 1.03, 1.17, 1.54, 1.92, 2.23, 2.36, and 2.47 THz Pure astaxanthin had peaks at 0.99, 1.49, and 2.13 THz	Wang et al. (2010)
L-ascorbic acid	0.2 to 2.4 THz	THz-TDS	DFT	Ti:sapphire laser with 68fs pulse duration A large-aperture GaAs photoconductive antenna A pair of parabolic mirrors ZnTe electro-optic crystal Pellet diameter = 13 mm and thickness = 1.2 mm Conditions: room temperature	L-ascorbic acid: Strong peaks at 1.80, 2.05, 2.21, and 2.34 THz Peaks at 2.05 and 2.34 THz were assigned to phonon or intermolecular modes Peaks at 1.8 and 2.21 THz were related to intra-molecular vibrations Refractive index of L-ascorbic acid: between 1.77 and 1.83	Binghua et al. (2008)
L-ascorbic acid	0.2 to 2.4 THz	THz-TDS	DFT	Ti:sapphire laser GaAs photoconductive antenna A pair of parabolic mirrors ZnTe electro-optic crystal B3LYP algorithm of DFT was used for simulation	Reported both the experimental and theoretical vibrational frequencies of L-ascorbic acid A good agreement between the theoretical and experimental results was found	Cao et al. (2009)
Vitamin C in aqueous solution	0.6 to 13.5 THz	FTIR-ATR	iPLS Full spectrum PLS	Mercury lamp as a THz-generating device L-alanine triglycine sulfate as detector	iPLS model with five PLS factors showed better performance and vitamin C quantification at lower frequencies Prediction performance of vitamin C using the iPLS model had RPD an of 4.57 Their method had a low standard error of prediction of 1.49 and an RER of 11.996	Suhandy et al. (2011)
Vitamin C in aqueous solution	0.6 to 13.5 THz	FTIR-ATR	PLSR	PLSR model was validated through full cross-validation	An acceptable ratio prediction to deviation value (RPD = 3.53)	Ogawa et al. (2011)
L-ascorbic acid and thiamine (vitamin B1)	0.1 to 3.5 THz and 8 to 10 THz	THz-TDS and FTIR	NA	FTIR with a highly sensitive silicon bolometer detector	A new FTIR fingerprint peak found between 0.3 and 0.5 THz Thiamine peaks appeared in and extended frequency range (8 to 10 THz) in FTIR spectroscopy Thiamine: peaks at 8.75, 8.85, 9.00, 9.30, and 10.30 THz L-ascorbic acid had low absorption	Li et al. (2015)
Identification and characterization of vitamin C, B1, B2, and B6	0.2 to 2.6 THz	THz-TDS	DFT	Diode-pumped mode-locked Ti:sapphire laser Sample thickness: 1 mm; diameter: 13 mm vitamin C, B1, B2, and B6	Vitamin C had peaks at 1.08, 1.49, 1.82, 2.02, and 2.34 THz Peaks at 1.08 and 1.82 THz were related to phonon or intermolecular mode Peaks observed at 2.02 and 2.34 THz were due to the scissoring of the ring and ring torsion, respectively Vitamin B1 had peaks at 1.11 and 1.5 THz Vitamin B6 showed a single peak at 1.71 THz Vitamin B2 had distinct peaks at 0.38, 0.62, 0.82, 1.02, 1.17, 1.52, 1.93, 2.19, and 2.42 THz	Yu et al. (2009)

NA, not applicable; **fsPLS**, full spectra PLS; **iPLS**, interval PLS; **PLSR**, partial least squares regression; **DFT**, density functional theory; **RPD**, residual predictive deviation.

Table 13–Detection of alcohol using THz imaging and spectroscopy techniques.

Application and Product	THz range	Mode/THz Type	Chemometrics	Experiment details	Findings	Reference
Alcohol content of alcoholic beverages	0.1 to 1.1 THz	THz-TDS	NA	A self-referenced reflection THz-TDS Compared the double and triple Debye model parameters for some water-alcohol mixtures with the reported data in the literature	Imaginary and real part of the dielectric function measured Simultaneous detection of sugar and alcohol Higher accuracy achieved at low alcohol concentrations	Jepsen et al. (2007)
Dielectric properties of alcoholic beverages and liquors	0.1 to 1.1 THz	THz-TDS	NA	Pure water, ethanol in water, and sugar in water	The method is independent of carbonation and yeast content Both the refractive index and the absorption coefficient decreased significantly when ethanol was added to water Addition of sugar (<20%) did not affect the dielectric properties of the liquid and refractive index, but a small reduction in the absorption coefficient was observed	Jepsen et al. (2007)
Alcohol production real-time monitoring	0.75 to 1.1 THz	THz-TDS	NA	Frequency-domain THz dielectric spectroscopy A diagonal horn antenna (aperture diameter = 1.6 mm) Water-ethanol and water-sugar mixtures	Highest ethanol sensitivity: between 0.913 and 1.023 THz Highest sugar sensitivity: between 0.858 and 0.935 THz LOD of 1.5% for sugar; LOD of 0.3% for ethanol	Fawole and Tabib-Azar (2016)
Dielectric properties of mono-hydroxy alcohols	0.5 to 10 THz	THz-TDS	NA	Pulsed THz waves generated from ambient air plasma Combination of experimental observations, ab initio quantum calculations and all-atom molecular dynamics simulations Mono-hydroxy alcohols: methanol, ethanol, 1-butanol, 1-propanol, and 2-propanol	Dielectric response had contribution from three damped harmonic oscillators and a Debye relaxation processAlcohols had frequency-dependent spectrum from 2 to 6 THzThree types of motions were identified: (1) the overall motion of alcohol molecules results in a rise to peak at 2 THz (2) alkyl group oscillations affect the peaks between 4 and 6 THz (3) the movement of H-bonded OH groups increase the peak amplitude at higher frequency range	Sarkar et al. (2017)
Wettability of aliphatic monohydric liquid alcohols	0.1 to 1 THz	THz-TDS	NA	Photoconductive dipole antenna Silicon lens Quartz liquid cells Polynomial fitting Aliphatic monohydric liquid alcohols: methanol, ethanol, 1-propanol, and 1-butanol 4-μL drop of each alcohol into a container cell	Strength of the transmitted THz pulse was proportional to the path depths of the liquid and has a non-uniform distribution for the liquids Increasing the alcohol alkyl chain increased the surface wettability Methanol showed the maximum depth followed by ethanol and1-propanol The minimum depth was reported for 1-butanol	Huang et al. (2018)

NA, not applicable.

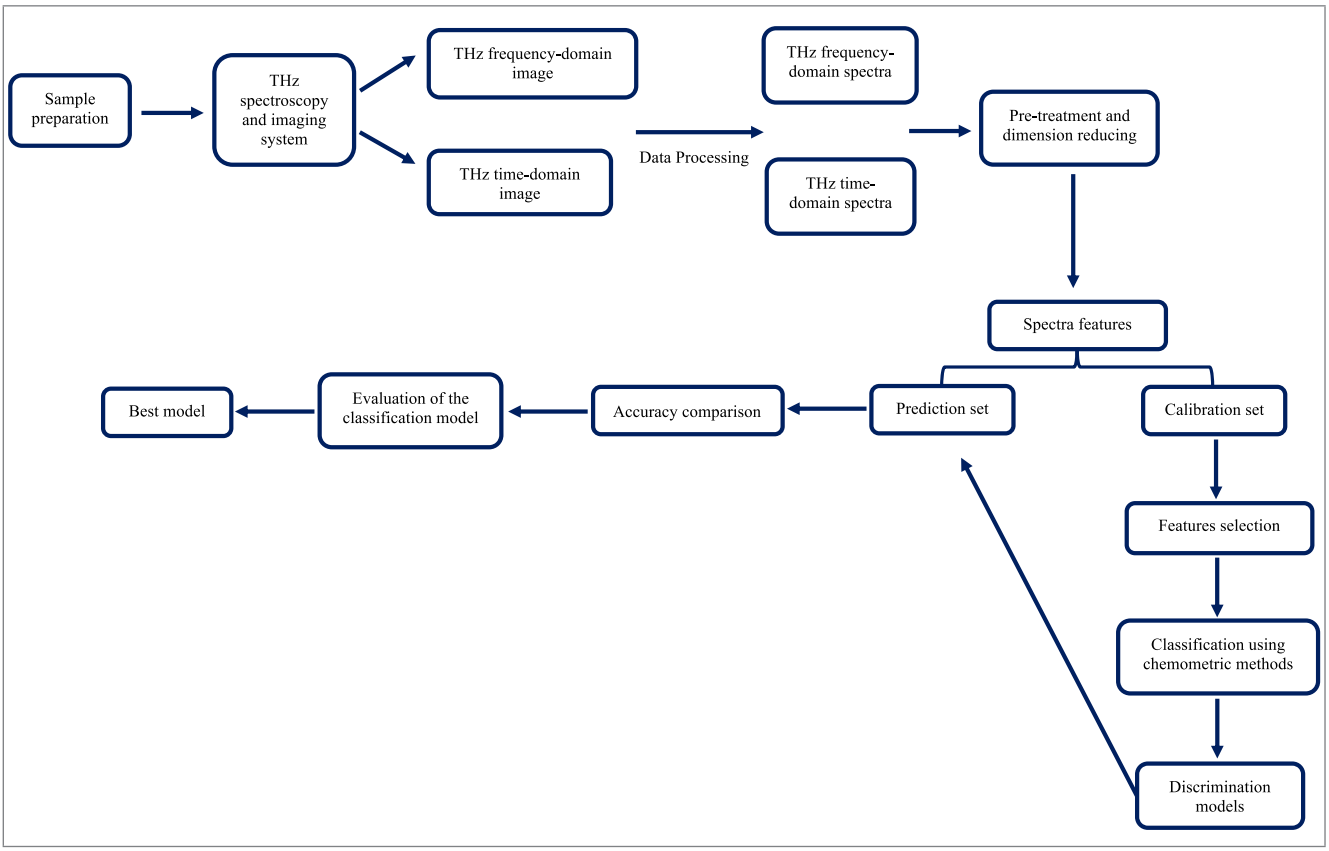

Figure 2–The steps involved in data acquisition and data analysis based on the THz images for identification and discrimination purposes (based on the process reported by Wang et al., 2017 and Liu et al., 2019).

insects based on their water content (Table 1). Han, Park, and Chun (2011) used a sub-THz gyrotron as a radiation source to produce a CW at 408 GHz for real-time inspection of foreign bodies (Han et al., 2011). Using the first version of their gyrotron system, that is, KG1, they detected metallic and soft objects in a cracker (Han, Park, Ahn, Lee, & Chun, 2012). They also showed that their system can perform real-time inspection for in-shell peanuts and distinguish between full and empty peanut shells. Modifying their system, the group developed a second version of a miniature gyrotron, that is, KG2, for 0.4-THz real-time food inspection (Han, 2013).

CW-THz imaging was used to detect both high- and low-density objects in instant noodles (Lee, Choi, Han, Woo, & Chun, 2012). Due to the wave diffraction from the edges, fine details were not observed in THz images from high-density foreign bodies, for example, granite and aluminum pieces. However, they showed that CW-THz was able to detect cricket and maggot pieces and that the maggot pieces were not visible under X-ray. To increase the SNR ratio and overcome the spatial resolution limitation in THz imaging, Kim et al. (2012) used a CW-THz imaging system with a horn antenna. The horn antenna increased transmitted power over sixfold, and metallic cubes, stones, paper, grasshoppers, and mealworms were detected in flour and instant noodles (Table 1). The method had a relatively high sensitivity, and images with a spatial resolution up to 500 μm were captured.

Bessel beams are non-diffracting in nature and can be used in THz imaging for food applications. Gaussian beam and quasi-Bessel beam (QBB) THz imaging were compared for detecting foreign objects in noodles. Using QBB sub-THz imaging, Ok, Choi, Park, and Chun (2013) detected crickets in noodles at 210 GHz with a high spatial resolution and very sharp peaks. They used a point scanning method for characterization of QBB and realized that the wavefront shape was affected by the performance of QBB. They suggested that high-speed THz-QBB together with broadband detection can be an effective noninvasive inspection method if performed over large sample areas (Ok et al., 2013). Insects, metals, and polymers in milk powder were detected using a sub-THz wave Gaussian beam that was focused by a lens with a low f-number. High-resolution images could even be observed from objects with low water content under transmission mode (Ok, Kim, Chun, & Choi, 2014). In another study, the group used a reflection-mode CW-THz imaging system for detection of low-density objects, such as insects and plastics (Ok et al., 2014). Using a beam-steering tool, they achieved a high-speed operation with a good agreement between the scan length of the aspheric F-Theta scanning lenses and the spatial resolution (Table 1). Combining a polygonal mirror scanner with an F-Theta lens, used for an extended scan area with high spatial resolution, Ok et al. (2015) identified foreign objects with a scanning speed of 80 mm/s. Crickets in noodles and defects in chocolate were identified with a high resolution (up to 2.83 mm), wide range of detection (150 mm), and fast scanning speed (80 mm/s). They suggested that by minimizing the beam size and adjusting the concave mirror and optical design of the F-Theta lens, the image quality could be improved. Later, Ok et al. (2018) investigated the sub-wavelength imaging resolution under transmission mode and achieved higher-resolution and a more cost-effective scanning. Better beam focusing was obtained with a less expensive source (140 GHz). Although the interfacial geometry between a food matrix and foreign bodies strongly affect THz images, their

method detected a 1-mm-thick paper clip in a chocolate bar with a high image resolution (0.52 λ) and a long depth of focus (5 λ).

Detection of toxic and harmful compounds

Aflatoxins (AFs) are a group of toxic fungal metabolites that can cause severe health problems in human and animals (Afsah-Hejri, Jinap, Hajeb, Radu, & Shakibazadeh, 2013). High-performance liquid chromatography (HPLC), ELISA, and liquid chromatography/tandem mass spectrometry (LC-MS/MS) are the most widely used detection methods for aflatoxins in food and feed (Afsah-Hejri, Jinap, & Radu, 2013). Despite the high sensitivity and accuracy, these analytical methods are destructive and time consuming. Chen and Xie (2014) investigated the possibility of using a combination of THz-TDS with chemometric methods as a nondestructive tool for detection of aflatoxins in peanut oil. They used stepwise multiple linear regression (SMLR) and partial least squares regression (PLSR) to build quantitative models and evaluated the performance of their methods by comparing the results with the results of two spectral pretreatment methods. They showed that the SMLR model was more stable but had a slightly lower prediction precision. Based on the degree of correlation, they recognized that only some frequencies were related to aflatoxin B_1 (AFB_1) concentration (Table 2). Results at 1.11 THz and 0.72 THz represented 92.9% of the practical information related to the AFB_1 concentration. Using the data at 1.11 and 0.72 THz, a good SMLR model was developed, and its root mean square errors of calibration (RMSEC), root mean square errors of cross-validation, (RMSECV), and corresponding correlation coefficient (R) values are presented in Table 2 (Chen & Xie, 2014). Although the accuracy of their method was slightly lower than the routine analytical methods for AFB_1, Chen and Xie (2014) showed that the combination of THz-TDS with chemometric methods can be used as a fast and nondestructive tool for quantification of AFB_1 in peanut oil. They also detected AFB_1 in corn samples, which was extracted using immunoaffinity columns and then exposed to THz radiation. No noticeable absorption peaks were observed in the THz region, meaning that an information-fusion method is needed for identification of AFB_1 in corn samples (Zhao, Lian, & Zhang, 2015). For their quantitative analysis, they improved the Dempster-Shafer (D-S) method, a common data fusion method that combines joint confidence levels with probability. They first performed their test with different AFB_1 concentrations and then eliminated the interference factors to find the optimal D-S model. They successfully detected AFB_1 in all samples and determined the correct concentration of AFB_1 in 94% of the samples.

Ge, Jiang, Lian, Zhang, and Xia (2016) performed a similar study on different aflatoxin extracts. They analyzed the absorption data using chemometric methods, such as partial least squares (PLS), principal component regression (PCR), support vector machine (SVM), and principal component analysis (PCA)-SVM. To evaluate the performance of the proposed model, the R and root mean square error (RMSE) were calculated. In quantitative measurement studies, improved prediction accuracy will be achieved with higher values of R and lower values of RMSE. They observed that linear regression models, such as PCR and PLS, were more precise for the AFB_1 range of 1 to 50 μg/mL while nonlinear-regression-based models (PCA-SVM and SVM) showed more accuracy in the range of 1 to 50 μg/L. Values for prediction accuracy and R are presented in Table 2. To validate the practicability of their models, Ge et al. (2016) applied their THz-chemometric method on mildewed maize acetonitrile extracts and successfully quantified AFB_1 in the samples in less than 5 s (Table 2). Although the quantification time of the THz-chemometric method is less than that of chromatographic methods, the results are not satisfying enough to replace chromatographic methods with THz-based quantification. For example, the limit of detection (LOD) of a quadrupole time-of-flight mass spectrometry coupled with liquid chromatography and electrospray ionization was 0.19 μg/kg for both aflatoxins B_1 and G_1 and 0.02 μg/kg for both aflatoxins B_2 and G_2 and the overall recoveries for all four aflatoxins ranged between 57.1% and 108.7% (Sirhan, Tan, & Wong, 2013).

In a recent study, the combination of THz spectroscopy with chemometric methods quantified AFB_1 in soybean oil with high accuracy (Liu, Zhao, Wu, Liu, Yang, & Zheng, 2019). Liu et al. (2019) used some pretreatment methods such as PCA and *t*-distributed stochastic neighbor embedding (*t*-SNE) to convert the data set into matrix and visualize the similarities. Using a back propagation neural network (BPNN), an excellent classification model was acquired with *t*-SNE pretreatment. The coefficient of prediction for the BPNN combined with *t*-SNE was 0.9948. Their method successfully determined 1 μg/kg of AFB_1 in soybean oil with a prediction accuracy of 90%. Due to the implementation of pretreatment methods, their method had a higher coefficient of prediction compared to the methods reported by Chen and Xie (2014) and Ge et al. (2016). Liu et al. (2019) showed that pre-treatment methods can be used on high-dimensional data sets to omit unnecessary information from THz signals and achieve a higher accuracy in the prediction set. The combination of THz spectroscopy with chemometrics and pretreatment methods has the potential practical application for determination of aflatoxins in the edible oil industry but some improvements on the signal processing methods, specifically for large data processing are needed. Rapid and inline detection is an important factor for detection of toxins in food, and new THz spectroscopy systems should meet this requirement. In addition, detection of various toxins requires implementation of different chemometric methods that need to be improved accordingly. One of the weaknesses of THz-based quantification methods is that the LOD of THz-based methods is still very low compared to the chromatographic methods. Most of the chromatographic methods have a very good LOD and limit of quantification (LOQ). In a recent study, the LOD and LOQ of an LC-MS/MS method were reported as 0.11 and 0.36 μg/kg, respectively, for total aflatoxins in maize (Ouakhssase, Chahid, Choubbane, Aitmazirt, & Ait Addi, 2019). They reported a recovery range of 70% to 110% for all aflatoxins (except AFB_2) at concentrations between 1 and 10 μg/kg.

Melamine is a synthetic-rich nitrogen compound that has been illegally added to food products to increase protein content. According to the World Health Organization (WHO), the tolerable daily intake of melamine for human consumption is 0.2 mg/kg of body mass (Åkesson, Point, & di Caracalla, 2010). If melamine is absorbed into the bloodstream, crystals will form in renal tubules, causing kidney malfunction and failure. Numerous incidents of high levels of melamine contamination of food products has raised a food safety concern and created a demand for a rapid and accurate detection method. Ung, Fischer, Ng, and Abbott (2009) used THz-TDS for detection of melamine in infant milk powder. To determine the baseline detection limit, THz results were compared with Fourier-transform infrared spectroscopy (FTIR) results. Cui, Mu, Wang, Zhang, and Zhang (2009) observed absorption peaks at 1.99 and 2.29 THz for pure melamine and mixtures of more than 10% melamine + milk powder and polyethylene. A linear relationship was found between the ratio of melamine in the mixture and the absorption coefficient. They observed sharp and distinct absorption peaks in samples with high levels of melamine. They

also calculated the vibration of melamine crystals using density functional theory (DFT).

Baek, Lim, and Chun (2014) investigated the expediency of detecting melamine in foodstuff using THz-TDS. Milk powder, chocolate powder, and flour were tested with or without packaging materials of different thicknesses. Regardless of the thickness and type of the packaging material, distinct melamine peaks at 2, 2.26, and 2.6 THz were detected in all food mixtures. Images at 2 THz were observed to be dose-dependent. Fluorescent-based methods are very selective and accurate for detection of melamine. Su et al. (2019) used a FAM–aptamer–G-quadruplex construct for detection of melamine in plastic water cups. Their method had a LOD of 6.32 nM and recovery ranging from 97.15% to 101.92%.

THz-TDS was used for detection of some harmful food additives. *O*-phenylphenol and thiabendazole, preservatives applied to the surfaces of lemons, bananas, and grapes showed to induce chromosomal aberrations in rats. EDTA, often added to canned food and mayonnaise to preserve their color and flavor, has been related to low blood pressure. Saccharin, used as sugar substitute in ice cream and soft drinks, has been recognized as a causative agent for uterine cancer in rats. Yoneyama, Yamashita, Kasai, Ito, and Ouchi (2007) detected EDTA-2Na, saccharin, *o*-phenylphenol, and thiabendazole using THz. They designed a specific membrane device for holding food additive samples in solution. Their specific membrane device helped them to overcome a distribution deviation problem that was observed in previous studies in which sapphire or silicon plates had been used. For saccharin in both solution and pellet form, three signature peaks were observed as well as for thiabendazole. For *o*-phenylphenol, only one signature peak was detected for the pellet form while two peaks were observed in solution. For EDTA-2Na, no peaks were observed for solution form, but two signature peaks were observed for the pellet form (Table 2).

Auramine O (AO), a yellow color diphenylmethane dye, is still legally added to some food products in certain developing countries; however, it is a carcinogen that has been reported to cause bladder, prostate, lung, and stomach tumors (IARC, 2010). Zhang, Li, Chen, and Qin (2017) used a combination of THz spectroscopy with an improved PLSR model for detection and quantification of AO in medicinal herbs. The new 2DCOS-PLSR resulted in a fast, reagent-free, and accurate quantitative analysis of AO (Table 2). In another study, Zhang and Li (2018) implemented multiple regression analysis on THz spectral data and showed that the combination of variable contribution sorting with stacked partial least squares had the best performance in quantification of AO in pollen typhae. The performance of their later model was higher than that of their previous model (Table 2) and did not require special pretreatment or chemical consumption, but it was lower than the performance of chromatographic methods. In a study performed to simultaneously quantify three food colorants, the LOD of the HPLC method for AO was reported as 0.0125 μg/g (Tatebe et al., 2014). Although THz-based methods are fast and convenient but need improvements to be used for on-site detection of harmful compounds.

Isomers of trichloroanisole (TCA) are reported as contaminants in several foods and beverages. TCA derivatives are responsible for the muddy flavor in drinking water and have also been identified in sake, raisins, and rice. A well-known derivative, 2,4,6-TCA is responsible for cork taint in wine. Several product recalls have been reported due to odors caused by TCA on packaging materials. Hor, Lim, Federici, Moore, and Bozzelli (2008) observed three strong peaks for 2,4,6-TCA in the solid phase (Table 2). High volume fractions of TCA showed only a weak absorption peak. Chlorine placement had a significant impact on the THz spectrum of other TCA isomers.

Talc powder is used as an inert carrier for food coloring and as a separating agent in bakery, seasonings, table salts, and dried food. THz spectral characteristics, such as the absorption coefficient and refractive index, were used for detection of talc powder in flour (Xiao-li & Jiu-sheng, 2011).

Antibiotic detection

The presence of antibiotics in food of animal origin represents a serious risk to human health. Redo-Sanchez et al. (2011) used real-time THz to study 11 commonly used antibiotics in food and feed samples. They detected specific fingerprints for eight antibiotics (Table 3). The LOD and image resolution were not specified in their study. Massaouti, Daskalaki, Gorodetsky, Koulouklidis, and Tzortzakis (2013) used THz fingerprints to detect antibiotics at very low concentration (as low as 0.01 w/w) in honey as well as mixtures of antibiotics and insecticides in honey. In the frequency range of 0.5 to 2.6 THz, specific absorption peaks were observed for the sulfonamide family of antibiotics (sulfapyridine, sulfathiazole) (Table 3). Amitraz and tetracycline had featureless spectra in that frequency range. Performing the study in a wider frequency range (0.5 to 6 THz) using a 100 μm GaP crystal, tetracycline exhibited four peaks, and amitraz showed a strong resonance peak.

Qin, Xie, and Ying (2014) detected tetracyclines hydrochloride (TCsH) in infant milk powder. All TCsHs showed clear absorbance spectra (Table 3). They observed an increase in the absorbance when the concentration of the antibiotic increased. Samples that contained a mixture of antibiotic and milk were not detectable at very low antibiotic concentration due to the interaction of the molecules with their surrounding solid medium. Applying PLSR and partial least squares discriminant analysis (PLS-DA) to their spectral data, they quantitatively classified TCsH groups with an accuracy between 83.33% and 100%. An accuracy of 100% was obtained for the model of the doxycycline hydrochloride and tetracycline hydrochloride (TCH) groups; they also built PLSR models for predicting the concentration of TCsH in infant milk powder.

Qin, Xie, and Ying (2015) used PLSR to build a calibration model for tetracycline hydrochloride (TC-HCl) and showed that THz spectroscopy combined with the PLSR model can be used for nondestructive and rapid prediction of TC-HCl residue in food powders. In powder samples, the absorption coefficient increased significantly with increase in concentration. For powder samples, the PLSR model was a good quality control tool (Table 3), but it was not suitable for liquid samples. In order to improve the sensitivity of their method and also expand the application to liquid samples, the group used metamaterials (Qin, Xie, & Ying, 2016). The sensitivity of the method for TCH was improved by a factor of 10^5 for a trace amount of TCH (as low as 0.1 mg/L) in a solution. In a subsequent study, they determined the complex refractive indices for TCH solutions by incorporating the attenuated total reflection technique (ATR) into THz-TDS, creating the ATR THz-TDS (Qin, Xie, & Ying, 2017). The complex refractive index curve of pure milk and pure water has a similar shape. Adding TCH to milk and water lowered each of their complex refractive indices, but no sharp change was detected. The combination of the PLSR model with THz spectral data was also successful in quantification of chlortetracycline hydrochloride (CCH) and TCH in chicken and rice samples (Table 3) (Wang et al., 2018).

A metasurface is two-dimensional version of a metamaterial that is used in high-sensitivity sensors. An extraordinary sensitive THz detection method using metasurfaces was developed to detect trace amounts of kanamycin sulfate in liquid form (Table 3); metasurfaces resulted in a higher sensitivity than silicon (Xie, Gao, Shu, Ying, & Kono, 2015).

The presence of antibiotic residue in feed directly affects the quality of food of animal origin. Three fluoroquinolones were detected in feed matrices using THz (Table 3). Using BPNN, an excellent classification model was acquired with no pretreatment (Long, Li, & Liu, 2018).

Detection of microorganisms

Rapid and accurate detection of microorganisms is vital for food safety control. Currently time-consuming culturing methods, molecular methods, and mass spectroscopy techniques are being used for bacterial detection. Conventional methods are based on biochemical and phenotypic tests and usually take days or weeks, in the case of slow-growing microorganisms. The procedure of the conventional methods is complex, and the LOD is between 10 and 100 CFU/mL. Molecular methods are also complex, but are fast and have LOD of several genome equivalents. Mass spectroscopy techniques are reagent-free, very fast, and simple, with an LOD of between 10^5 and 10^6 CFU/mL (Yang, Yang, Luo, & Fu, 2016). None of these methods can detect microorganisms inside a package or differentiate between dead and living bacteria. THz spectroscopy is a reagent-free, simple, and fast technique that can see-through the packaging material and is able to differentiate between living and dead organisms. Bioparticles (for example, yeasts and bacterial cells) have a relatively low absorption coefficient, allowing THz radiation to propagate through them. Cell components (for example, proteins and genetic material) have distinct absorption coefficients and contribute to the THz signature of bacterial spores or cells. In 2002, THz imaging was used for detection of harmful bacteria in packages and envelopes (Wang, Ferguson, Mannella, Abbott, & Zhang, 2002). The biosignature of *Bacillus subtillis* spores was studied by Brown, Bjarnason, Chan, Lee, and Celis (2004). Three distinct transmission signatures were observed for *B. subtillis*, both in dilute and concentrated samples below 1.2 THz (Table 4). The resolution of their spectrum was not good due to the poor SNRs. To improve the SNR, Yu, Alimova, Katz, and Alfano (2005) used THz-TDS in the far-IR region. Dipicolinic acid, a major constituent of bacterial spores, showed absorption at 1.54 THz. They concluded that *B. subtilis* spores can be detected by the absorption band at 1.54 THz, and can serve as a marker for spore detection, and the refractive index was 2 for *B. subtilis* spores. In another study, Johnson, Valentine, and Sharpe (2005) compared the mid-IR with the far-IR (that is, THz) relative intensities of *Bacillus* spores. Even at a high spore concentration, very weak THz absorption spectra was observed compared to the mid-IR amide I band, which is used for spore detection.

Transmission spectra of *Escherichia coli* and *B. subtilis* suspensions were studied in the sub-THz region (Bykhovski et al., 2005). They first analyzed the contribution of DNA to the THz spectra of the entire bacterial cell and observed that the DNA of *E. coli* and *B. subtilis* had a measurable difference in their THz transmission spectrum. They also observed a good correlation between the chromosomal DNA signature and the corresponding signature of the cells and spores. In another study, Globus et al. (2012) showed that FTIR spectroscopy in the sub-THz region was sensitive enough for characterization of *E. coli* and *B. subtilis* based on their spectral features. Their method had a good sensitivity and reliability (Table 4). Mazhorova et al. (2012) developed a bacteria sensor using the evanescent mode of a suspended core fiber in THz-TDS mode. They used a specific arrangement for their sample holder (Table 4) and detected *E. coli* at the concentration range of 10^4 to 10^9 CFU/mL at 0.7 THz.

Berrier, Schaafsma, Nonglaton, Bergquist, and Rivas (2012) used THz plasmonic antennas to increase the sensitivity limit of films coated with bacterial cells. They detected a monolayer of bacteria and selectively identified their Gram type. The structural differences in the cell wall as well as differences in the cell components resulted in a signal change and subsequently, differentiation between *E. coli* and *B. subtilis*.

THz metamaterials are used to increase the sensitivity of the method. Metamaterials have the potential to be used for fabrication of selective microbial sensors. The sensing ability of metamaterial sensors depends on the substrate composition and deposition of the analyte together with the resonance effects (O'Hara et al., 2008). Park et al. (2014) used metamaterials operating at the THz frequency range for rapid and real-time detection of bacteria, yeast, and fungi. The micro-sized gap property of THz metamaterials and compatibility of the gap size with the size of microorganisms makes them ideal platforms for sensitive detection of bacteria, yeast, and fungi (Table 4). THz metamaterials are also very sensitive to the elements near the surface, promising good sensing in aqueous environments without notable loss in the THz wave transmission (Park et al., 2014). This method was sensitive to the surface number density of the microorganisms located at the surface of metamaterials and can be used in fabrication of bacteria-specific biosensors.

Kurita et al. (2014) used nickel mesh sensors for detection of *E. coli*. Metallic mesh sensors are thin metallic films with square apertures arranged periodically on them, showing transmission peaks at particular resonant frequencies known as "extraordinary transmission" (Kurita et al., 2014). Dielectric materials, such as microorganisms, affect the transmission spectra of the mesh, resulting in a frequency shift, which makes the metallic mesh act as a label-free sensor. Their method was not sensitive enough for food inspection purposes (Table 4).

Bacterial detection using THz spectroscopy is challenging (Yang et al., 2016). THz spectroscopy has limited sensitivity due to the size mismatch between bacterial cells and THz wavelength. The typical size of a bacterial cell is 1 to 3 μm, and THz radiation has a wavelength of 300 μm at 1 THz. This size mismatch leads to a low scattering cross section during quantification of bacterial cells. THz metamaterials and antennas can be used to enhance coupling between THz radiation and bacterial cells, increasing the sensitivity. Nanoantennas with a 5-μm-wide slot can significantly increase sensitivity.

Gram-negative bacteria have a different dielectric response to THz waves than Gram-positive bacteria due to their different cell structure. Also, living and dead bacterial cells show distinct THz spectrum due to their different molecular motion. Yang et al. (2016) performed a study to distinguish between living and dead microorganisms and found that their absorption patterns are different (Table 4). Recently, they used CW-THz for rapid and label-free identification of microorganisms at different living states (Yang et al., 2017). The group developed an accurate electrical bacterial growth sensor for *E. coli* with $R = 0.977$.

Wessel, Schmalz, Cahill, Gastrock, and Meliani (2013) Wessel et al. (2013) designed contactless, label-free, efficient, and reliable THz-based biosensors for automated yeast cell cultivation

monitoring. Their biosensors were based on the fact that an increase in the number of yeast cells within a single compartment induces a detectable change in the average permittivity. Song and Wang (2009) designed a phase sensitive biosensor working at 7 GHz. Their radio frequency device had a high sensitivity, that is, more than 20 dB compared to a conventional transmission line, and could detect very small dielectric property changes. Modifying the microfluidic system based on polytetraflurorethylene (PTFE) tubes previously designed by Song and Wang (2009) and Wessel et al. (2013) successfully detected a trace number of samples (Table 4).

In another study, Park, Son, Choi, Kim, and Ahn (2014) used THz slot antennas to visualize yeast cells, molds, and bacteria in the THz frequency range. Due to their high THz dielectric constant, yeast cells proved to be ideal for optimizing THz-based microbial sensors (Table 4). Fawole, Sinha, and Tabib-Azar (2015) monitored the fermentation process and studied the effect of normal sugar and artificial sweeteners on the growth of *Saccharomyces cerevisiae* using THz (Table 4). Surprisingly, artificial sweeteners resulted in vigorous bubbling in the solution, and maximum growth of yeast colonies was observed within 24 min. Solutions containing aspartame or sucralose showed maximum growth of yeast and generation of CO_2 bubbles.

Moisture content measurement

Water intensely absorbs THz radiation while other food components exhibit different absorption coefficients. Lipids, starch, and protein have absorption coefficients that are 20, 50, and 100-times smaller than water in the THz region (Qin et al., 2013). Therefore, one of the most apparent applications of THz spectroscopy is its employment in moisture content quantification (Federici, 2012). The moisture content of food affects the texture, mechanical strength, taste, microbial growth, shelf life, and overall quality of a food product. The methods used for moisture analysis of food, such as oven drying, distillation, MW, and near-IR spectroscopy, are time consuming, destructive, and require sample preparation. In 2005, Chua et al. first attempted to measure the moisture content in food samples (Chua et al., 2005). They performed their tests on crushed wheat grains with different moisture levels. To avoid scattering due to unevenly shaped grains and achieve homogeny, they used an ultrasonic sieve and collected particles less than 45 mm in diameter. They made a special sample holder for their experiment (Table 5). Apparent absorption spectrums were observed for all moisture levels. Initially, they could not differentiate between them as each absorption spectra represented data from both free water molecules in the crushed grains and the extended water network of the sample. They deducted the spectra of the wetted samples from the spectrum of the dry samples and observed a linear correlation showing that samples at 18% moisture level had the highest absorption.

THz spectroscopy was used as a robust, noninvasive, and rapid method for measuring the moisture content of intact wafers (Parasoglou et al., 2009). They performed their initial test on dehydrated wafers and observed a linear relationship between moisture content and peak-to-peak amplitude (Table 5) (Parasoglou et al., 2010). They observed that below 0.6 THz, the relative absorbance of water was significantly higher than the other ingredients of the wafer and the scattering effect of pores in the wafer was small. However, above 0.6 THz, the scattering effect of pores was dominant and weakened the THz signal absorbed by water.

The water content of instant coffee powder was measured in the sub-THz region (Yasui & Araki, 2005). Adding a micro-structured photoconductive antenna to the system enabled the group to measure the moisture content of coffee powder in the glass bottles. Significant changes were observed in the transmission spectra of instant coffee after 3.5 hr of exposure to forced humidity (Table 5) (Yasui & Araki, 2011).

The simplest amino acid, glycine, is a water-soluble compound. Glycine solutions are used as food additives in protein drinks and food supplements. Ogawa, Cheng, Hayashi, and Fukunaga (2009) performed ATR THz-TDS to measure the water content of glycine powder and aqueous glycine solution. After eliminating the spectrum of water, they achieved three distinct absorption peaks for dissolved glycine (Table 5). Glycine powder had a different absorption spectrum.

In addition to water content, the condition of the water molecules in food samples can be studied with THz spectroscopy (Jepsen et al., 2007). The plane-wave density functional method was used to predict and allocate the vibrational modes in crystal molecules. Vibrational frequencies were assigned to certain modes of the sucrose crystal. A different frequency range was used for the noncrystalline system (Table 5) and the index of refraction and absorption coefficient were measured. Outcomes showed good agreement between the results from alcoholic beverages samples with properties of the reference mixtures. The accuracy of the measurement depended on the stability of the sample at the test temperature.

Interactions of water molecules with the atoms of packaging films were studied with THz-TDS (Inamo, Sakai, Kiwa, & Tsukada, 2016). Gas barrier films have water molecules in them that interact with other atoms of the film and subsequently affect the diffusion speeds of the gases. Inamo et al. (2016) used a time-delay system in their high-speed THz-TDS, reducing the signal acquisition time to 0.5 s. Polycarbonate films were stored in humidity-controlled containers, and a linear relationship between the amount of water molecules in the film and the spectral intensity was observed. THz-TDS can be used in evaluation of gas barrier films and observation of water molecules inside a sample.

Relative humidity (RH) is a critical factor in food processing and food safety. Shin et al. (2017) built a low-cost polymer-based humidity sensor that works in the THz region. Polymer-based materials have unique properties, such as variation in their hydrophobic or hydrophilic properties, after exposure to humidity. Thus, humidity variation will result in a dielectric behavior change. This is the basic for sensing and monitoring RH using polymer-based materials. Increase in the thickness of the film due to the coating moved the resonance frequency to a lower frequency and also increased the effective refractive index (Table 5). They also performed a finite-difference time-domain (FDTD) simulation of the guided-mode resonance (GMR) sensor and observed a good estimate for water absorbed by polyvinyl alcohol (PVA)-coated GMR sensor. It was demonstrated that the water content in the PVA film was increased up to 6% as relative humidity was increased up to 70% at 20 °C. While the PVA-coated GMR sensor appears to be a good candidate for inexpensive and highly sensitive RH sensing, future studies are needed to improve temperature-dependent RH sensing techniques.

Ions influence both the dynamics and structure of their surrounding water molecules, and ion hydration is particularly important in stabilization and destabilization of other molecules in food. THz vibrational signatures of the hydrated ions in aqueous salt solutions were studied (Funkner et al., 2012) and specific cation and anion bands related to the vibrational modes of the ions and their hydration shells were found (Table 5). THz absorption

of salt solutions was found to be concentration-dependent and strictly linear.

Sodium bis(2ethylhexyl)sulfosuccionate (AOT) is an ionic surfactant used to make water-in-oil microemulsions. THz-TDS was used to study the dielectric properties of systems containing water in butter as well as water-AOT,-heptane (W-AOT-H) (Møller, Folkenberg, & Jepsen, 2010). An increase in the dielectric function of the real and imaginary part of the confined water pool was observed for the W-AOT-H system. No surface vibrational modes in the W-AOT-H system water pools were noticed. Water in butter was considered as bound water. A unique THz spectrum of rapeseed oil, grapeseed oil, and lard were also reported (Table 5).

Inspection, identification, and quality control

Yan, Zhang, and Ying (2007) discussed the unique properties of THz waves and their applications in quality control of food and agricultural products. Food packages are usually inspected for packaging flaws, but channel leaks (ranging from 10 to 100 μm in diameter) are difficult to detect with the naked eye. Air-filled and water-filled channel defects in plastic packages were detected using a real-time THz-TDS (Morita, Dobroiu, Otani, & Kawase, 2005). Absorption coefficient differences were used for detection of water-filled channels whereas the refraction index differences were the basis of detection for air-filled channel defects. Channel defects in polyethylene films were successfully detected (Table 6). Very tiny objects, such as hair, can also be detected with THz spectroscopy (Hiromoto et al., 2013).

Reflection mode THz-CW was used by Ok et al. (2014) as a rapid and low-cost quality inspection method, and they were the first to report CW sub-THz transmission imaging results. They developed a wide-range detection, high-speed scanning, and high-resolution imaging technique (Table 6). Both defects in chocolate bars as well as crickets in noodle flour were detected using this method. Image quality was improved when the beam size was minimized (Ok et al., 2015).

At a specific THz frequency, the absorption coefficient and refractive index can be mapped with two-dimensional coordinates, and food material can be quantified using the refractive index. Based on the absorption coefficients, complex refractive indices and a 2-D data map, Shin et al. (2018) detected embedded insects and defects in sugar and milk powder (Table 6). Each food sample exhibited a unique optical characteristic, but the refractive indices and absorption coefficients of different insects were similar.

The use of X-ray inspection of food with active substances has raised the concern of residual radiation and radiation damage to the food. Kim et al. (2012) performed a study to enhance CW-THz imaging for food inspection by using a horn antenna to enhance the spatial resolution, resulting in a high spatial resolution of up to 500 μm (Table 6). They compared their results with X-ray images and concluded that a horn antenna CW-THz imaging system proved to be a sensitive tool for nondestructive inspection of the soft organic objects inside flour and powders.

Lack of a powerful THz source is one of the obstacles in sub-THz real-time imaging. To overcome this obstacle, Han et al. (2011) used a gyrotron as a radiation source for active real-time imaging and employed a focused beam that scans point-by-point over the sample. At the sub-THz region, gyrotrons are capable of generating excellent output power with a good output beam pattern for detection of non-dense fragments in food products, thus gyrotrons are very suitable for illuminating the entire imaging area and maintaining the power density above the LOD of array detectors. Later, they developed the first version of a compact sub-THz gyrotron, that is, KG1, for real-time food inspection. Their small and inexpensive imaging system worked in the 0.1 to 1 THz region. The KG1 operated at 0.2 THz, and a diode-type magnetron injection gun was used to accelerate the electron beams. Defects in crackers and peanut hulls were detected using a miniature sub-THz gyrotron (Table 6) (Han, 2013).

Hadjiloucas, Walker, and Bowen (2010) analyzed THz images and linked the imaginary and real parts of the refractive index of some confectionary samples to creaminess and characterized some food hydrocolloids. They used PCA and advanced classification techniques with linear or nonlinear classifiers to distinguish between different states in the sample.

An active THz imaging system based on a quasioptical system and a network analyzer was used for quality control of food and agricultural products (Etayo et al., 2011). Defects, stacked objects, holes, and unwanted objects were differentiated based on the differences in their level of absorption, transmission, and reflection (Table 6). Their system had a good resolution and could be used for detection of small fragments, layers, thickness control, and measuring the number of slices.

The quality of Chinese green tea was measured using THz-TDS by acquiring the refractive index and absorption spectrum of 80 samples over the range of 0.2 to 1.5 THz (Xi-Ai et al., 2011). Back propagation artificial neural network (BPANN), naive Bayes, and least squares support vector machines (LS-SVM) were used to perform a multi-class classification on the results, and LS-SVM showed the best classification results.

Particle size affects both the blending process and the uniform distribution of compounds in a powder mixture. Typically, powders have particle size between 75 and 300 mm, which can be detected with THz imaging in the range of 0.1 to 4 THz. THz-TDS was used as a rapid and highly sensitive technique for monitoring powder flows and controlling particle size in an optically opaque tube (May et al., 2009). A clear relationship was observed between the measured scattering losses and the size of particles flowing through a tube at THz frequencies. Also, THz pulsed-imaging and ATR THz-TDS configuration was used to study the crystallization progress and monitor the buildup of sugar coatings on some products (May & Taday, 2013). The ATR spectra of the sugar solution were found to be time dependent (Table 6). At the beginning of the test (0 hr), the spectrum appeared to be overshadowed by water absorption. The absorption of the sugar solution decreased over a period of 50 hr. Crystallization began after 50 hr and at approximately 58.5 hr, crystalline material was formed.

Meat freshness is usually determined through time-consuming and destructive methods, such as chemical and microbial tests, sensory evaluation, biosensors, and chromatography methods. THz-TDS was used to monitor the process of deterioration and differentiate between preserved and bad meat (Huang et al., 2015). They observed differences in the time domain as well as in the absorption coefficient of the samples during the deterioration process. Variations were caused by decomposition of tissue material and reduction of water content (Table 6).

Insect infestation is one of the major problems affecting the quality of pecans. At present, infected nuts are cleaned through a mechanical cleaning method consisting of floating them in chemical solution and hand picking under UV lamps. The technique is costly, tedious, and inefficient. Li et al. (2010) developed a specific THz-TDS and performed a study on the feasibility of applying THz as a non-destructive method for quality evaluation of pecans. Due to the THz power source penetration limitation, they used slices of nutmeat, the inner separator, and the shell. They observed that the absorption coefficient was increased at higher THz wavelength. The inner separator, shell, and nutmeat were differentiated

based on absorption coefficient curves at frequencies higher than 1.2 THz. They successfully detected dead and living insects in pecans based on their differences in water content and absorption coefficient in the THz region.

Foxtail millet is a rich-amino acid cereal widely consumed in East Asia. Lu, Zhang, Zhang, Yang, and Xiang (2016) combined THz-TDS with chemometrics for quantitative and qualitative analysis of binary mixture of amino acids in foxtail millet. L-Glutamine and L-glutamic acid have similar properties and chemical structures. Binary mixtures of L-glutamine and L-glutamic acid were prepared and mixed with foxtail millet matrix. Different absorption spectra were observed for glutamic acid and glutamine between 0.3 and 1.9 THz. To reduce the possible background contributions, asymmetric least squares (AsLS) was used for calculation of the baseline. For quantitative analysis purposes, PLS and interval partial least squares (iPLS) regressions were applied to the absorption spectra data. The performance of the models was assessed, and iPLS was more effective than PLS for both glutamine and glutamic acid (Table 6). The interval with the lowest RMSECV was considered a feasible model interval. The interval dataset ranging from 1.20 to 1.37 THz provided the best results for the PLS model. Multivariate curve resolution alternating least squares (MCR-ALS) was applied to distinguish pure components in the samples.

A single reducing sugar or a mixture of reducing sugars are used as food additives for adjusting the flavor of some food products. Specific titration methods, spectrophotometry, atomic absorption spectrometry, gravimetry, and pulsed electrochemical method are used for qualitative and quantitative analyses of binary and ternary mixtures (Li & He, 2007). El Haddad et al. (2014) used a combination of THz spectroscopy and chemometric methods for quantitative and qualitative analyses of a ternary mixture of reducing sugars. PCA was applied to correctly locate the samples into a ternary diagram and manage data compression. They used artificial neural networks and PLS regression for quantitative analysis. RMSE was used to evaluate the performance of the model for quantitative purposes. The method predicted the concentration of the constituents with an RMSE less than 0.9%.

Somatic cell count is a leading indicator of milk quality. There is no nondestructive and practical method for detection of somatic cells in milk. Naito et al. (2011) used a combination of THz spectroscopy with chemometric methods for detection of somatic cells. They modified the ATR THz-TDS system by adding a temperature controller below a high resistance silicon ATR prism in the Fourier transform THz spectrometer. The results (Table 6) indicated that the addition of a temperature controller to the ATR prism reduced the error due to temperature changes, thus improving the system.

Ge et al. (2016) studied the vibrational frequencies and geometric structures of six preservatives. Using DFT, the vibrational and structural frequencies of the samples were calculated and compared with the experimental data (Table 6). They concluded that THz absorption peaks at low frequencies could be assigned to intermolecular, intramolecular collective motion, or phonon modes.

There are carcinogenicity concerns associated with consumption of *tert*-butylhydroquinone (TBHQ), a preservative commonly added to unsaturated oils. Zhang, Cai, and Shen (2011) detected different concentrations of TBHQ based on their absorption spectra and refractive index in the frequency range of 0.2 to 2.2 THz.

Yan et al. (2018) used a combination of THz spectroscopy and chemometrics for rapid identification and quantification of three flavonols that have a similar structure. The fast Fourier transform method was applied to transform the THz-TDS spectrum into the frequency-domain and obtain the spectral distribution. They employed extreme learning machine, *k*-nearest-neighbors, and random forest (RF) pattern recognition methods to develop their qualitative discrimination models. Using the RF model, they achieved an exceptional discrimination (Table 6). Two regression algorithms, PLSR and LS-SVM, were used form quantitative models relating concentrations of the samples with THz spectra information. The LS-SVM model produced better results with higher residual predictive deviation, higher prediction coefficient, and low root mean square error of prediction for all three flavonols.

Adulteration detection

Food adulteration is a top food safety concern. Consumption of melamine-adulterated food, such as milk, will result in renal failure and kidney stones. Table 7 lists melamine detection studies using THz spectroscopy (Baek et al., 2014; Cui et al., 2009; Ung et al., 2009). Other forms of adulteration in dairy products include the addition of glucose or fat powder. Chemometric methods can analyze data based on pattern recognition. Liu (2017) applied PCA and SVM-discriminate analysis (SVM-DA) on the THz spectrum of the samples to identify adulterated dairy products. Intense absorption characteristics were observed over 0.38 to 1.5 THz, which was related to the presence of fat in the samples. The THz characteristics of skim milk and low-fat milk samples are explained in Table 7. Satisfactory results were obtained by using SVM-DA in classification of adulterated milk samples; a specificity of 100% and sensitivity of 88.62% were achieved.

The addition of high-fructose corn syrup to honey is a common adulteration, and current methods for differentiation of pure honey from adulterated honey are expensive, time consuming, and labor intensive. Liu, Zhang, and Han (2016) combined THz-TDS with chemometric methods for rapid and nondestructive quantification of high-fructose syrup content in Acacia honey. They initially pretreated the spectra by Savitzky-Golay smoothing prior to building a PLS model (Table 7). Their results confirmed the effectiveness and reliability of the technique in detection of adulterated honey. Further, the floral sources of honeys were identified using ATR THz-TDS (Liu, Zhang, Yang, & Han, 2018). They evaluated the absorption coefficient of three honeys by some chemometrics methods. PCA, PLS-DA, and cluster analysis were used to obtain information about the botanical origins of the honeys and demonstrate the differences of three honey categorizes (Table 7). The PLS-DA model proved to be suitable for identification of honey origin. In their recent study, the group used a combination of THz spectroscopy with chemometric methods to differentiate the geographical origin of olive oils (Liu et al., 2018). Olive oil samples showed differences in their THz absorbance spectra and fatty acid compositions. The combination of a genetic algorithm (GA) with the least square-SVM method resulted in an excellent classification with an accuracy of 96.25% for the prediction set. They showed that combination of THz spectroscopy with chemometric methods can be used as a simple and fast method for on-site discrimination of extra virgin olive oils.

There are some concerns associated with consumption of transgenic products. The methods for identification of transgenics are DNA-based, time consuming, and expensive. Recently, THz spectroscopy and imaging has been used for identification and discrimination of transgenics. Figure 2 shows the main steps involved in data acquisition and data analysis based on the THz images for discrimination of transgenics. Liu et al. (2019) used PCA combined with RF, BPNN, LS-SVM, and a GA to screen and classify four olive oils with different geographical origins. All samples showed differences in their absorbance spectra and fatty acid

compositions. The combination of a GA and LS-SVM resulted in an excellent classification with an accuracy of 96.25% in the prediction set. Then, the combination of THz spectroscopy with PLS, weighted linear discriminant analysis (WLDA), and successive projection arithmetic (SPA) was used for discrimination of transgenic camellia oil (Liu et al., 2019). A high classification accuracy was achieved with the SPA-WLDA model (correct discrimination rate, 96.53%) showing that the combination of THz spectroscopy with chemometric methods can be used for discrimination of oils from transgenic seeds.

The most common adulterant in turmeric is yellow chalk powder, Calcium carbonate with yellow dye, which makes it is very unsafe to consume. The acid method, which uses HCl, is not accurate enough and cannot quantify the extent of adulteration in turmeric. Nallappan, Dash, Ray, and Pesala (2013) used THz spectroscopy to detect different concentrations of yellow chalk powder in packaged turmeric. Pure and adulterated samples showed completely different spectra. Peaks at 6.3 THz were considered as yellow chalk powder adulteration.

Detection of carbohydrates and sweeteners

ATR-THz spectroscopy combined with a chemometric method was used for quantification of glucose in aqueous solutions. Suhandy et al. (2012) acquired the absorbance spectra of glucose solutions using a THz-based Fourier transform spectrometer and developed calibration models with PLS regression for preprocessing of the original spectra. The best results achieved by the calibration model used Savitzky-Golay second derivative spectra.

D- and L-Glucose are enantiomers. D-Glucose is the main source of energy for living organisms while L-glucose is a low-calorie sweetener. It is challenging to differentiate between them, but THz-TDS has reportedly been used in identification of both glucose and uric acid (Upadhya, Shen, Davies, & Linfield, 2003). Two sharp absorption peaks and a minor peak were observed for D-glucose whereas L-glucose displayed a sharp peak and noise (Table 8). THz absorption of L-glucose was completely temperature-dependent, and the most distinct absorption peaks were detected at low temperatures. Different spectral features were observed for sucrose. Although sucrose embodies glucose in its molecular structure, the spectral features were found to be different, which could originate from intermolecular vibrations.

Structural isomers, such as glucose and fructose, have different physio-chemical properties. Zheng, Fan, Liang, and Yan (2012) used THz-TDS and molecular modeling to identify glucose and fructose. Glucose and fructose represented different THz spectra at room temperature. They used gaseous-state theory within the linearity combination of the atomic orbital method to investigate the conformation and simulate the molecules. The harmonic vibrational frequencies and ground-state structures of the isomers were determined by the Hartree-Fock (HF) function and DFT. Based on the numerical results, the density function B3PW91 was applicable for the reproduction of bond length whereas the density function B3LYP was more suitable for the replication of bond angle. Performing some calculations on isolated-molecules, Zheng et al. (2012) explained that the differences between the THz spectrum of glucose and fructose was due to the combination of intermolecular (for example, hydrogen bonds) and intramolecular motions (for example, covalent bonds).

Anhydrous and monohydrate forms of saccharides have different food applications. As an example, anhydrous glucose is used in candy production while monohydrated glucose is consumed for the quick enhancement of energy. Zheng, Fan, Li, and Tang (2014) investigated the dehydration kinetics of monohydrated glucose using THz-TDS and solid-state theory. Anhydrous and monohydrated glucose displayed different THz spectra at room temperature. In the earlier study, Zheng et al. (2012) observed three bands for monohydrated glucose whereas in the 2014 study, two more spectral features in the same frequency region were attained, which was the first time the two new spectral features of monohydrated glucose had been reported. The spectral differences between the two studies was explained based on the crystalline unit cell. For simulation studies, Perdew–Burke–Ernzerhof exchange-correlation functionals was used. Solid-state calculations provided satisfactory spectral reproduction. It was determined that the THz features of anhydrous glucose came from the interactions of glucose molecules whereas for monohydrated glucose, these features originated from the intermolecular modes of glucose–glucose and water–glucose molecules. Calculations showed that a specific peak of monohydrated glucose (at 1.8 THz) was related to the intermolecular interactions of glucose–water molecules. It is critical to measure the stability of molecules in a solution. There are two key factors in defining complex dielectric properties: amplitude stabilization and phase stabilization. Tajima, Nakamura, Shiraga, Ogawa, and Ajito (2016) improved the phase stability by developing a double-beam CW-THz with a photonic phase modulator in the sub-THz region. They built a specific THz-based system for glucose hydration sensing using an integrated photonic phase modulator (Table 8). Different concentrations of glucose solutions were tested to understand water–glucose interactions. They observed that the Fabry-Pérot (FP) effect resulted in large waves in the transmission characteristics of glucose solutions. This phenomenon reduced the accuracy of the dielectric constant measurement. They finally mitigated the FP effect in the liquid cell window by incorporating a simple calibration procedure. The overall signal stability was significantly enhanced, and a sub-THz liquid sensor with high measurement stability was successfully developed for both modeling and characterization purposes.

THz absorption spectrums of some pentoses were studied (Ge et al., 2006). A unique THz fingerprint of pentoses revealed their molecular structure (Table 8). This study demonstrated that THz-TDS is a flexible tool for differentiating between optical isomers and quantitating biomolecules in a low frequency range.

It is critical to quantify the amorphous and crystalline content of a milled material. The presence of crystalline seeds will extend the surface area of the amorphous phase in the milled material and make it very sensitive to moisture and temperature. Smith, Hussain, Bukhari, and Ermolina (2015) used THz pulsed spectroscopy to quantify the crystallinity of ball-milled anhydrous β-lactose in order to control the milling process. The amount of residual crystallinity was evaluated using THz and differential scanning calorimetry (DSC). PLS was used for analyzing the specific bands between 1.16 and 1.8 THz (representing anhydrous β-lactose). They compared the residual crystallinity of β-lactose with α-lactose monohydrate (the hydrated counterpart of β-lactose). They observed that α-lactose monohydrate produced 20% to 30% more amorphous material than β-lactose during the test period (Table 8). During the milling process, a monotonic decrease in crystallinity was observed for the milled samples of β-lactose. During the early time period of the test, THz results delivered a lower estimate for the amount of residual crystallinity than that calculated from the DSC data. It was stated that the lower estimate from THz might be related to the recrystallization of the amorphous form during sample preparation. They concluded that while DSC was a more reliable method than THz for measuring the crystallinity of anhydrous β-lactose after

milling, THz was the method of choice for measuring α-lactose monohydrate.

Fructose syrup was detected in acacia honey using a combination of chemometric methods and ATR THz-TDS (Liu et al., 2016; Liu et al., 2018). The PLS model was reliable and effective in detection of different concentrations of fructose syrup in authentic honey while the PLS-DA model helped to differentiate between honeys of different floral origin (Table 8). May and Taday (2013) used ATR THz-TDS and THz pulsed spectroscopy to monitor crystallization of sucrose and buildup of sugar coatings on confectionary products. THz-TDS spectroscopy on an ATR window was employed to follow phase transition (from aqueous phase into a glassy state), and THz pulsed imaging was used to investigate the final product (Table 8). They observed that the ATR spectra were time dependent and the absorption of sugar solution decreased over time. ATR spectra showed a series of phonon bands, which are collective excitation of atoms in a typical crystalline structure.

Lee et al. (2015) developed a label-free, nondestructive, noncontact THz-TDS sensing system for molecular detection of carbohydrates in food samples. They used nano-antennas to increase the detection sensitivity and selectivity of the method. Sucrose, D-glucose, fructose, and cellulose showed unique spectral features (Table 8). They also presented color contour plots of THz fingerprinting for two non-saccharide sweeteners and some saccharides. FDTD calculations were used to describe the performance of the sugar antenna with molecular concentration. Experimental results were in good agreement with FDTD calculations. They proposed a model that could explain the molecular-selective detection. The performance of the method was tested using a fructose antenna for detection of sugars and artificial sweeteners in some popular beverages. They observed distinct differences in THz transmittance of some beverages with different sugar contents. They concluded that their THz nano-antenna sensing chip could sensitively and selectively detect carbohydrates at micro-mole concentrations.

Møller, Merbold, Folkenberg, and Jepsen (2007) used self-referencing reflection THz-TDS to measure small volumes of aqueous solutions. They used a high-index silicon window in their reflection THz-TDS system to split the input THz pulse into two parts. The measurement was then performed by recording the two pulses that emerged from the reflection unit. The addition of ethanol to water significantly decreased the refractive index and absorption coefficient of the solution. The addition of sugar to water did not affect the dielectric properties of the sample. No clear change was observed in the refractive index at low concentrations of sugar (less than 20%), but a small decrease was noted in the absorption coefficient. The reflection THz-TDS system enabled the researchers to simultaneously quantify ethanol and sugar in a solution without sample preparation.

Controlling and maximizing ethanol yield is a key parameter in the fermentation process. Ethanol production requires an online monitoring system that does not contaminate the fermentation broth. Fawole and Tabib-Azar (2016) used THz for real-time monitoring of the fermentation process. They observed that both sugar and ethanol mixtures were selective to THz frequencies (Table 8). This frequency selectivity was due to the FP effects at the wall of the sample holder. They reported the LOD and the highest THz reflection sensitivity for sugar mixtures and ethanol mixtures.

As previously explained, the combination of THz spectroscopy and chemometric methods were used for analyses of a ternary mixture of reducing sugars (Table 8) (El Haddad et al., 2014). Thermally stable D-sorbitol is usually used as bulking agent and additive in sugar-free formulations. Sorbitol has several hydrogen bonding contacts and conformational flexibility. These features result in co-crystallization of sorbitol with solvent molecules and complex crystalline polymorphism. Dierks and Korter (2017) used THz spectroscopy to study the structure and stability of two cocrystal forms of sorbitol (sorbitol-pyridine and sorbitol-water). First, sorbitol crystals were grown and identified with powder X-ray diffraction and single-crystal X-ray diffraction. Later, THz-TDS and solid-state DFT were used to analyze the structure and intermolecular motions of the crystals. The crystal forms were then compared with the anhydrous-sorbitol polymorph. Simulated THz spectra of α-sorbitol, sorbitol–pyridine, and sorbitol–water were compared with the experimental data. Results showed that sorbitol–pyridine was far less stable than sorbitol–water. The lower stability of sorbitol–pyridine could be due to the disruption of its intermolecular hydrogen bond network.

Fawole et al. (2015) evaluated the effect of sugar type on the growth of yeasts. The frequency-averaged reflection was measured for three different samples (Table 8). Surprisingly, artificial sweeteners resulted in maximum growth of yeast and bubble production. A significant change was observed in THz reflection coefficient for both normal sugar and artificial sweeteners at 1.0152 THz.

Jepsen, Møller, and Merbold (2007) investigated the dielectric properties of aqueous sugar and alcohol solutions with reflection THz-TDS. The accuracy of the method was determined by the SNR, and the method showed high accuracy at low concentrations of alcohol. The real and imaginary part of the dielectric function was measured for some drinks. Through simultaneous measurement of the real and imaginary part of the dielectric function, two or more ingredients can be determined in an aqueous solution.

Sun and Zou (2016) used THz-TDS to investigate the dielectric properties of solid polycrystalline glucose. They analyzed the transmission data of anhydrous polycrystalline glucose pellets and calculated the complex dielectric function. Calculations were made using the Fresnel equation, and the complex dielectric function was then considered as the initial value for the reverse fitting process. FDTD was used for fitting purposes. The complex dielectric function of glucose was acquired by implementation of the least square's method. DFT simulated the vibrations of polyglucose and single glucose molecules. They also studied the dielectric properties of glucose in connection with its absorption mechanism. Multiple characteristic absorption peaks were found between 0.2 and 2.2 THz, which were related to the complex dielectric function of polycrystalline glucose. They found a specific absorption peak in the real part of the complex dielectric function, which could be related to the anomalous dispersion within the full width half maximum of the absorption peak. Both experimental and FDTD simulation results revealed that the Lorentz dielectric model was the best fit for the complex dielectric function of glucose. They concluded that the characteristic absorption peaks of polycrystalline glucose mainly originated from collective intermolecular vibrations, such as crystal phonon modes and hydrogen bonds.

Bulk water absorbs THz radiation more than highly concentrated proteins (solutions, biomolecule solids, or films). However, it was found that a mixture of protein and water can absorb THz more than a bulk water sample alone. It is possible only with the contribution of the hydration water as a third material. The presence of proteins, if affected by the surrounding water molecules, can affect the tested features of water, especially the relaxation degree and the rate of reorientation in the network. The water molecules, by tumbling and diffusing by the hydrogen bonding network, cause the hydrogen bond to be made and broken, which

results in this reorientation. As the absorption coefficient is sensitively dependent on the dynamical reorientation of dipole moments on a picosecond timescale, measuring THz absorption is an effective tool with which to probe this. In a comprehensive study, Born and Havenith (2009) introduced three basic concepts for THz spectroscopic hydration studies: THz excess, THz defect, and spectral density. They showed successful application of two of their model concepts, THz excess and THz defect, to carbohydrates, such as glucose, trehalose, and lactose. They used the models to correlate the characteristics of both monosaccharides and disaccharides with the THz absorbance spectra.

In order to find answers for the effect of carbohydrates on the solvation dynamics of water in solutions, Heyden et al. (2008) studied the absorption spectrum of some solvated sugars (one monosaccharaide and two disaccharides). All three carbohydrates showed a linear increase in their absorption coefficient. The effect of different layers of the hydration shell was discussed (Table 8), and they concluded that monosaccharides, such as glucose, have slighter influence on the surrounding water molecules than lactose and trehalose.

Shiraga, Ogawa, Kondo, Irisawa, and Imamura (2013) conducted a study on the hydration state of saccharides to evaluate the global hydration state. ATR THz-TDS was used to characterize the global hydration state and define the refractive index of saccharide solutions. The complex refractive index for both water and carbohydrate solutions was measured. They showed that the global hydration state was related to the steric configuration of hydroxyl groups and the number of hydrophilic groups in saccharide molecules. The number of hydration water molecules around both monosaccharides and disaccharides were calculated in low concentration solutions (Table 8). The number of hydration water molecules were almost twice as much for maltose and sucrose than that of mannose and galactose, possibly because of the number of hydrophilic groups in disaccharides. The hydration number of glucose was 15.2. It was observed that with an increase in the concentration of each solution, the hydration number decreased.

Enzyme or acid hydrolysis is usually used for quantification of starch in food products. Recently, THz spectroscopy was used for quantification of starch in germinating seedlings (Nakajima, Shiraga, Suzuki, Kondo, & Ogawa, 2019). They showed that 1-day seedlings had a similar THz spectra to that of standard starch, but the absorption peaks gradually changed during the germination period (Table 8). They used α-amylase to hydrolyze the 1-day seedlings as well as the standard starch and obtained their THz absorption peaks. The peak at 9 THz was sensitive to the changes in starch and disappeared after hydrolysis. They showed that the constituent saccharides did not affect the peak at 9 THz. The peak at 9 THz was selected as an indicator for monitoring starch during germination, and the intensity of this peak was used for quantification of starch content in mung beans. They compared the starch content of the 1-day-old mung bean seedling with the native potato starch and observed higher intensities for the 1-day-old seedlings, which they related to the starch structure being different. Although their method was accurate ($r = 0.98$), the sampling procedure was destructive and purification pretreatments were required. More studies are needed to confirm the feasibility and practicability of the method.

Chocolate studies

The foremost applications of THz for chocolate goes back to the studies performed by Mittleman et al. (1999). Focusing on the intensity and the phase of the signal, they presented a series of THz images from chocolate bars with different thicknesses and those with almond fillings. As chocolate itself does not absorb much THz radiation, other components inside the chocolate bar absorb more THz radiation and become visible. The embossed letters can be distinguished in a chocolate bar THz image due to the thickness differences and the scattering effects. They compared transmission and reflection imaging for chocolate bars and concluded that the reflectance imaging system was able to provide unique capabilities, such as 3D representations of layered objects.

Chocolate is low in moisture and high in fat, making it a relatively THz-transparent product. Jördens et al. (2006) used 2D THz transmission imaging to detect foreign objects in chocolate (Table 9); glass particles and stones absorbed THz waves and affected the scattering profile of transmitted THz. It was observed that the shape of the wave was changed, and the transmitted intensity decreased due to the high absorption and scattering loss. Metal contaminants were found to reflect THz radiation. Since in a production line, every chocolate bar needs to be inspected within 0.1 s, they conducted a series of tests by moving the chocolate bars in steps of 0.5 mm/s to test the applicability of THz for real-time inspection. Chocolate bars were moved using a glass splinter, and a waterfall plot of THz waveforms was measured. Time delay was observed due to the difference in the refractive indices. More time delay was reported for the higher refractive index differences. They also observed that thickness variations resulted in signal change, for example, a pulse delay of 1.7 ps was observed for a maximum thickness variation of 0.64 mm. The presence of millimeter-scale contaminations inside the chocolate bar changed the shape of the THz pulses. Two smaller pulses appeared close to each other, which were generated by two portions of the main THz pulse. One traveled alongside the contaminant, and the other traveled through it, experiencing a time delay due to the higher refractive index of the contaminant. As the first THz pulse was smaller than the main THz pulse, a dip was observed in the sum of two line scans, indicating the contamination. They concluded that THz-TDS can be used as a contactless, nondestructive technique for detection of very fine nonmetallic objects in chocolate. Koch and Krok (2006) assembled a THz-TDS system to study pure and contaminated thick chocolate products. They claimed that complex chocolate products (for example, waffles or truffles) can be inspected with their THz-TDS system.

Foreign bodies can be distinguished from nuts based on their refractive indexes, as well as the shape and height of transmitted THz waves (Jördens & Koch, 2008). Pure chocolate had a single THz signal while chocolates with nuts showed a double-pulse structure due to the differences in the refractive indexes of nuts and chocolate (Table 9). The shape and the height of the THz waveform was used to differentiate between desirable and unwanted ingredients. Any peak that appeared earlier or later in time than the pure chocolate spectrum was considered as a contaminant. Both the intensity image (0.5 to 0.75 THz) and the temporal position delay image for the pulse maximum were considered for detection of glass particles. No difference was observed between the glass particles and nuts in the intensity image. False alarms (double pulse) were observed when the nuts were not completely embedded inside the chocolate bar. The reason is that any localized differences in thickness (different refractive indices) will cause a change in the length of the optical path, resulting in a double pulse structure waveform. Finally, they included the height profile in the image processing measurements to reduce the false alarm rate. The application of this technique in other industries was discussed by Wietzke et al. (2009).

In a similar work, Ung, Fischer, Ng, and Abbott (2007) reported THz-TDS imaging for detection of contaminants in chocolate of

different thicknesses. Joerdens, Rutz, Hasek, and Koch (2006) discussed the prospect of using THz for real-time quality assurance of chocolate products. The difference in the thickness of chocolate bars resulted in irregularly shaped curves during line scan measurement. They observed that the signal was at a maximum when THz pulses scattered through pure chocolate. The presence of a groove resulted in early arrival of the THz pulse and subsequently, smaller intensity. Pure and consistent chocolate pieces were identified based on time delays and peak shapes. Pohl, Debmann, Dutzi, and Hübers (2014) used multivariate analysis to differentiate between different substances based on their THz transmittance spectra (Table 9). PCA and PLS were used to distinguish different substances and obtain a prediction model, respectively. The shape of the absorption spectra was a key feature in separation of different substances. A PLS model based on the THz spectra of known substances was built and used for identification and classification of unknown samples. They used a class membership in binary form (0, 1), with 1 for pure substance, to identify and classify pure samples and mixtures.

Ok et al. (2014) detected melting defects in chocolate bars using a CW sub-THz transmission imaging system with a polygonal mirror and were the first to report CW sub-THz transmission imaging using a beam steering tool to increase the speed of detection. They achieved wide-range detection, high-speed scanning, and a high-resolution imaging technique (Table 9). The quality of the image was improved when the beam size was minimized (Ok et al., 2015). In another study, a paper clip, maggot, and buried mealworm were detected in chocolate bars. The method had a high resolution, wide range of detection, and fast scanning speed (Table 9). In 2018, Ok et al. suggested that by minimizing the beam size, adjusting the concave mirror and optical design of the F-Theta lens the image quality can be improved (Ok et al., 2018). They compared some subwavelength focusing parameters, such as beam diameters, Bessel beam focusing, and Gaussian beam focusing, with the parameters used in a previous study. The new settings in their later study yielded a higher-resolution and a more cost-effective scanning. They obtained better beam focusing with a less expensive source (140 GHz). Even though the interfacial geometry between a food matrix and foreign bodies affect THz images, both metallic objects and nonmetallic objects in a chocolate bar were detected with high image resolution.

Regardless of the thickness and type of packaging material, melamine was detected in chocolate powder using THz-TDS (Baek et al., 2014) and appeared as three distinct peaks (Table 9). Some differences in the sensitivity among wrapping materials was observed. Chocolate powder covered with two layers of wrapping material showed a reduction in the sensitivity due to the combined effects of chemical composition and the particle size of the wrapping material.

Fatty acids and oil studies

Hu, Guo, Wang, and Zhang (2005) published the first report on the optical properties of plant oils and animal fats in the THz region. They studied the absorption coefficient and refraction indices of five plant oil samples and two animal fat samples (Table 10). Samples showed different refraction indices, and the absorption coefficient was found to be temperature dependent. For all oil samples, an increase in the THz frequency resulted in an increase in the absorption coefficient and a slow decrease in the refraction index. The lowest absorption coefficient was observed for sesame oil. Pepper oil showed the highest absorption coefficient at 1 THz. The refraction indices ranged from 1.466 to 1.66. At 1 THz, the lowest and the highest refraction indices belonged to peanut oil and sesame oil, respectively. For animal fat samples, the absorption coefficient increased with increasing THz frequency, but no change was observed in the refraction index of the samples. Due to the greater phase transformation temperature, beef fat showed a more pronounced variation in its refraction index compared to that of pork fat (Table 10). The thickness of the samples resulted in a time delay but did not change the shape of the peaks.

Li, Yao, and Li (2008) were the first to use THz-TDS to investigate the effect of boiling on peanut oil. A mechanical chopper at 2 kHz was used to modulate the pump beam and increase the SNR. They also enclosed their THz system in a N_2-supplied acryl box to prevent the absorption of THz waves by atmospheric water vapor. A time delay was observed for the pulse of the samples (Table 10). They also observed several supplementary peaks behind the main peanut oil spectra, revealing the FP effect. A frequency increase resulted in escalation of the power absorption coefficient and reduction in the refractive index of the samples. Toxins were also identified in peanut oil by using a combination of THz-TDS and chemometric methods (Chen & Xie, 2014).

In another study, optical parameters of some vegetable oils were investigated (Jiusheng, 2010). An iterative algorithm was used to enhance the accuracy of the parameter extraction for THz-TDS. The pulse of the samples relative to the reference pulse showed a time delay. Oil samples showed a time delay relative to the pulse of an empty quartz cuvette (Table 10). As in a prior study, they mentioned the FP effect as several supplementary peaks behind the main oil spectra were observed. The refractive indices of oil samples showed a gradual decrease as THz wave frequency increased. The intermolecular vibrations were clearly spotted in the frequency range of 1.1 to 1.5 THz, revealing hydrogen-bond bending. Furthermore, the spectra of oil samples could be attributed to both intermolecular and intramolecular vibration modes in the THz region. Like the previous study, the power absorption coefficients increased with an increase in the frequency of the THz wave. It was reported that about 20% variation for the absorption coefficients and the refractive indices of all vegetable oils could be observed if the conventional data extraction algorithms were used. In the current study, the accuracy of the optical parameter extraction for THz-TDS was enhanced by using an iterative algorithm, and the dielectric properties of vegetable oils were accurately analyzed.

THz-TDS was used to monitor the physio-chemical changes of some cooking oils after heat treatment at the smoke point (Dinovitser, Valchev, & Abbott, 2017). They designed a specific sandwich-structure sample holder for their study (Table 10). A peak at approximately 5 ps was observed for the reference THz pulse after the start of the 80 ps measurement window. They observed similar refractive indices and FP spectra for all different oils at a given thickness. The effect of oil sample thickness on the dynamic range was measured. They observed that the best measurement at low THz frequencies was achieved when a thick sample was used, while thin samples resulted in optimum measurements at high THz frequencies (Table 10). The spectra of all different oil samples were very similar spectra, and the optical parameters of the samples were greater than 1 THz. They observed very minor changes in the absorption coefficient of the cooking oils heated above their smoke point. Their result was in contrast with the findings of Zhan, Xi, Zhao, Bao, and Xiao (2016) who reported significant spectral differences between edible oils and swill-cooked oils.

Swill-cooked oils or gutter oils is a term used in Southeast Asia for frying oils repeatedly used or cooking oils recycled from waste oils collected from restaurants and other sources. Zhan et al.

(2016) employed a spectral-mathematical (T-Math) strategy to identify and discriminate edible cooking oils from swill-cooked dirty oils using THz-TDS. They observed very similar pulses of waveforms but different absorbance features at several frequencies for clean edible oils and dirty oils. PCA and SVM were employed for identification and classification of oils. PCA and SVM amplified the differences, and normal edible oils showed the highest first principal component score with 97.4% contribution rate (Table 10). SVM directly identified swill-cooked oils with a precision of 100%. Yin, Tang, and Tong (2016) used a combination of THz spectroscopy and chemometric methods, such as discriminant analysis (DA), GA, and PLS-DA, for identification of edible oils. They customized a sample holder (Table 10) and performed their study under nitrogen and low humidity. The THz absorption spectrum of all oil samples was observed between 1.5 and 3.5 THz. Full spectra PLS, backward interval, and iPLS algorithms were employed to verify the performance of the classification method. The best prediction accuracy was achieved by the GA-PLS model. The GA-PLS-DA model had the smallest RMSE of prediction, the largest R of prediction, and highest classification accuracy (Table 10).

Li, Zhao, and Xu (2009) reported the effect of boiling on the spectral characteristics of corn oil. They used an iterative algorithm to improve the accuracy of the parameter extraction for THz-TDS spectroscopy. They observed a slow decrease in the refractive indices of the corn oil samples as the THz wave frequency increased. An increase in the power absorption coefficients was reported when THz wave frequency increased. Depending on the heating time, oil samples had different absorption spectra and different time delays (Table 10). In another study, the group identified the main components of rice bran oil using THz-TDS (Li, Zhao, & Li, 2009). Based on the THz absorption spectrum, they identified octadecanoic acid and hexadecanoic acid in rice bran oil. DFT provided theoretical spectra, which was in good agreement with the experimental results. Ung, Ng, and Abbott (2010) expanded upon those prior studies and evaluated the ability of THz to detect saturated fats in heated samples (Ung et al., 2010). No clear differences in viscosity, smell, or color were reported for heated oil samples, and they observed absorption patterns similar to those reported in previous studies. Li et al. (2008) observed changes after 10 min of boiling, but Ung et al. (2010) reported a significant increase in THz absorption of peanut oil after 5 min of direct heating.

Møller et al. (2010) investigated the dielectric properties of butter, lard, and vegetable oils. Each oil presented a unique THz spectrum for the imaginary and real parts of the dielectric function. The refractive indices of vegetable oils were measured (Table 10). The imaginary and real parts of the dielectric function of water in butter was also studied. Other researchers used THz-TDS to study the dielectric properties of nonedible/industrial water-oil complexes (Cunnell et al., 2009; Gorenflo et al., 2006).

Li and Yao (2008) modified their previous system and investigated the optical properties of olive oil. A mechanical chopper was used to increase the SNR. They used a novel iterative algorithm to improve the data extraction algorithms and enhanced the accuracy of the parameter extraction for THz-TDS. Both the absorption coefficient and the refractive index of the olive oil samples were measured with and without an FP resonator.

The combination of THz-TDS and chemometrics helped researchers to differentiate between extra virgin olive oils from different geographical regions (Liu et al., 2018). PCA combined with RF, GA, BPNN, and LS-SVM was used to screen and classify olive oils. All samples showed differences in their absorbance spectra and fatty acid compositions. The combination of GA and the LS-SVM method resulted in an excellent classification with a high accuracy in the prediction set (Table 10).

The structural dynamics of fatty acids and their analogues were studied to build a THz spectral database. Jiang, Ikeda, Ogawa, and Endo (2011) obtained the absorption spectra of some unsaturated fatty acids and saturated fatty acids and discussed the relationship between the chemical structure and the THz spectrum of fatty acids and their analogues. Several sharp peaks were observed for saturated fatty acids whereas unsaturated fatty acids showed two distinct peaks, representing the carboxylic group (Table 10). They noticed that THz absorbance of fatty acids was concentration dependent.

Elaidic acid, the trans isomer of oleic acid, is the main *trans*-fat found in hydrogenated vegetable oils. Elaidic acid lowers HDL cholesterol and increases the risk of heart diseases. Kang et al. (2011) studied the optical properties of elaidic acid using THz-TDS. The B3LYP algorithm was used to simulate the structure and vibrational frequencies of the elaidic acid molecule. The observed absorption peaks were mainly caused by the intermolecular and intramolecular vibrations, jointly. Good agreement between the experimental and theoretical results was reported.

Amino acids and protein studies

Within the past two decades, THz spectroscopy has been widely used for quantification of proteins as well as studying the intermolecular interactions and conformational changes in proteins. Markelz, Roitberg, and Heilweil (2000) published the first report on application of pulsed THz spectroscopy to inspect collective vibrational modes of biomolecules. They also developed specific data collection and sample preparation techniques. Protein denaturing and hydration resulted in an FIR absorption increase. No FP effect was observed in measurement of absolute absorbance when RH was less than 5%. All samples displayed good agreement with Beer's law behavior (Table 11). They also studied the structural forms of the molecules using crystallographic measurements. This was the first report of the use of pulsed THz spectroscopy to successfully measure the refractive index and low-frequency absorption spectrum of biomolecules as a function of RH. Cherkasova, Fedorov, Nemova, and Pogodin (2009) observed some dose-dependent changes in both the intensity and the spectral characteristics of albumin at 3.6 THz.

Biotin is a vitamin and an essential cofactor, which needs to be consumed through food or supplements (Staggs, Sealey, McCabe, Teague, & Mock, 2004). Biotin is also used in biotin–avidin and biotin–streptavidin sensors used for detection of proteins. The first report on the use of differential THz-TDS spectroscopy for label-free bioaffinity sensing was published in 2002 (Mickan et al.). Binding was determined by evaluating the transmission of biotin bound to the sensor protein avidin. They used a pure avidin glass microscope slide (reference slide) and a half-biotin half-avidin slide (test slide). Based on the degree of binding and the refractive indices of biotin to avidin, far-IR transmission changes were measured (Table 11). They emphasized that the sensitivity of their THz sensor depended on following factors: the binding affinity of the analyte-ligand, avidin immobilization on the glass slide, film layer homogeneity, and THz refractive indices of the bound layers. In a similar study, Menikh, Mickan, Liu, MacColl, and Zhang (2004) used small agarose beads to enhance detection of avidin–biotin binding using a double-modulated THz-DTDS system.

Markelz, Knab, Chen, Cerne, and Cox (2004) developed a tagless, universal biosensor for determination of ligand binding in biomolecules in the THz frequency range. They demonstrated the THz dielectric properties of egg white lysozyme. They observed that the absorbance decreased due to the binding effect, but the refractive index was almost independent from binding. It was also reported that the THz dielectric response of egg white lysozyme was a function of hydration and binding at different RH levels.

Xu, Plaxco, and Allen (2006a) directly measured the low-frequency vibrational modes of proteins and studied the collective dynamics of lysozyme in water. They developed a THz absorption spectrometer specifically for strongly absorbent compounds. In order to detect the weakened radiation, they added a variable path length sample cell and a sensitive cryogenic composite silicon detector to their system. They used their specific spectrometer for measuring the molar extinction of solvated lysozyme. The molar extinctions of solvated lysozyme showed a fast increase with frequency (Table 11) but afterward, stayed almost constant. Their observation was in agreement with the previously published theoretical models. In another study, Xu, Plaxco, and Allen (2006b) measured the absorption spectrum of solvated bovine serum albumin and reported an increase in the vibrational modes with frequency increase.

Amino acids, the building blocks of proteins, carry out important functions in the body. There have been several reports on the application of THz in amino acid studies (Ma, Zhao, Dai, & Ge, 2008). One of the foremost amino acid studies using THz was performed by Wang, Li, Zhang, and Zhang (2009) who studied the absorption spectrum of all twenty α-amino acids, presented in Table 11. They correlated THz spectral features with the molecular structures of α-amino acids and for the first time, classified amino acids based on their THz spectra and molecular structures. Amino acids showed different THz spectral features in the frequency range of 0.2 to 3 THz. They concluded that an absorption peak between 2.52 and 2.64 THz is associated with the carboxyl group, peaks between 2.23 and 2.3 THz are linked to the amino group, and the peak at 2.73 THz is related to the methyl group. The presence of a terminal hydroxyl group on the side chain affected methyl groups and reduced the number of absorption peaks. The group also built a database on amino acids and reviewed some THz applications in amino acids studies (Tang, Lin, Chen, & Zhang, 2009).

The absorption coefficient, refractive index, and low-frequency torsional modes of tryptophan (powder and film) were measured using THz-TDS (Yu et al., 2004). Two dominant torsional vibrational modes were observed. They used a density-functional calculation to assign the origins of the torsional vibrations to the ring and chain of the tryptophan molecule. The peaks observed at 1.842 and 1.435 were assigned to the C1-C9 ring torsional motion and C11-C12 torsional motion, respectively (Table 11). Wang et al. (2009) reported similar results.

In 2006, Ueno, Rungsawang, Tomita, and Ajito (2006) investigated the optical densities of some amino acids. The molar absorption coefficients were calculated by averaging the THz spectra at several different concentrations of amino acids. L-Glutamic acid (L-Glu) showed sharp peaks at 1.22, 2.03, 2.46, 2.68, 2.80, and 3.24 THz. Their findings were slightly different from those of Wang et al. (2009) who observed a very small peak at 2.23 THz. A peak at 3.24 THz was reported by Ueno et al. (2006), and they selected the strong peaks at 1.22 and 2.03 THz as marker bands for plotting the average optical density. Two linear models were used to analyze the plots, and good R values were found. The standard $\alpha m(\nu)$ values of amino acids were obtained between 0.5 and 3 THz, and it was observed that the optical density of each amino acid was increased linearly, proportional to its concentration. They successfully calculated the concentrations of L-histidine (L-His), L-cysteine (L-Cys), and L-Glu in mixed samples (Table 11).

Yan et al. (2008) used THz-TDS to obtain the refractive index and absorption coefficient of L-tyrosine (L-Tyr) and L-Glu. They specified that the absorption peaks originated from intramolecular and intermolecular vibrational modes. The average refractive index of L-Glu and L-Tyr is presented in Table 11. DFT was used to attain both vibrational and structural frequencies of the isolated amino acid molecules in the gas phase. Good agreement was reported between the experimental data with the theoretical calculations.

The concentration of L-valine (L-Val), L-leucine (L-Leu), L-isoleucine (L-Ile), L-glutamine (L-Gln), and L-arginine (L-Arg) in dietary amino acid supplements was quantified using THz-TDS (Ueno, Katsuhiro, Kukutsu, & Tamechika, 2011). Two different commercially available amino acid tablets were used to investigate the effectiveness of THz imaging for nondestructive quantitative analysis. A very similar spectral pattern was observed for the wrapped and unwrapped samples. Also, the experimental spectrums were well imitated by the calculated spectrums. The recovery of the method was calculated (Table 11), but the LOD of their method was not reported.

Lu et al. (2016) combined chemometric methods with THz-TDS for quantitative and qualitative analysis of a binary mixture of similar amino acids. L-Glu and L-Gln were mixed with foxtail millet matrix, and the absorption spectrum was measured. L-Glu and L-Gln each showed a different absorption spectrum between 0.3 and 1.9 THz. They combined their spectral observations with AsLS, PLS, and iPLS regressions and reported that iPLS was more effective than the PLS model for both glutamine and glutamic acid (Table 11). THz-TDS was also used for quantification of amino acids with similar properties and chemical structures in a ternary mixture (Zhang, Lu, Liao, & Zhang, 2017). L-Tyr, L-Glu, and L-Gln had different characteristic absorption spectrums between 0.3 and 1.8 THz. PLS and SVM were compared for quantitative analysis purposes. They also used multiplicative scatter correction (MSC), Savitzky-Golay smoothing, wavelet transforms, and the first derivative. The highest yield and the most stable and accurate prediction were achieved by the SVM model with MSC preprocessing. MCR-ALS was applied to increase the resolution of THz spectra. THz spectral profiles of amino acids in a cereal media were consistent with the experimental spectrum of pure amino acids. In their latest study, the group used a novel approach for the quantitative analysis of mixture of ternary amino acids in foxtail millet (Lu, Li, Zhai, Zhang, & Zhang, 2018). The Tchebichef image moment method was applied to extract the information of target amino acids and detect them based on their fingerprint spectra. Their approach was more reliable and accurate comparing to the traditional methods such a PLS (Table 11).

In a very recent study, Zong et al. (2018) investigated the THz absorption spectrum of L-histidine hydrochloride monohydrate. Their spectral observation was different from Wang's (2009) report on histidine. They also compared the absorption spectrum of L-His with L-His hydrochloride monohydrate (LHHM) and observed two unique THz spectrums (Table 11). Six sharp peaks (at 1.41, 2.09, 2.47, 2.80, 3.37, and 3.97 THz and three weak peaks at 0.77, 1.73, and 2.99 THz were observed for L-His. They reported a different pattern with four noticeable peaks and two less distinct peaks for LHHM. They monitored the temperature-dependence of vibrational modes in LHHM. They also noticed a peak split for LHHM at low temperatures. In order to simulate the vibrational

properties of amino acids, quantum chemical calculations were performed. They calculated the individual vibrational modes of LHHM by adopting solid-state DFT. They showed that the THz absorption spectrum mostly reveals the collective vibrational motions of the whole amino acid molecule. In order to check the structures of L-histidine and LHHM, they carried out powder X-ray diffraction (PXRD) and recorded the pattern of both compounds. The measured PXRD pattern of both powder forms satisfactorily matched with the data in the open database of the Cambridge Crystallographic Data Centre. They concluded that THz spectroscopy is sensitive to temperature, composition, and structure and the THz fingerprints of amino acids can be used for identification and detection purposes.

Li, Zheng, and Wang (2006) reported both the theoretical and experimental vibrational spectra of phenylalanine (Phe). They reported only two absorption peaks at 1.23 and 1.99 THz, whereas Wang et al. (2009) later observed four absorption peaks. In this study Li et al. (2006) used HF method at the 6–31G level for calculation and visualization of the vibrational modes of the Phe molecule and found a good agreement between experimental and theoretical results. Recently, Pan et al. (2017) investigated the low-frequency vibrational characteristics of L-phenylalanine (L-Phe) and its monohydrate form. They observed a distinct THz absorption spectrum for anhydrous and hydrous L-Phe. In order to simulate the vibrational modes of amino acids, they used the information obtained from the crystal structures of amino acids and performed DFT calculations. The results of their theoretical method showed a good agreement with the experimental observations. They also investigated the molecular packing patterns and thermodynamic properties of the anhydrous and hydrous form of L-Phe by using PXRD, differential scanning calorimetry, and thermogravimetry examinations. They stated that the characterized features of L-Phe mainly originated from the collective vibration of the molecules whereas it was more related to the hydrogen bond interactions between water molecules and L-Phe in its monohydrate form. L-Phe has temperature-dependent absorption peaks and sharp and strong peaks observed at low temperatures (Table 11). At room temperature, only the band at 1.99 THz was consistent with that reported by Wang et al. (2009). The monohydrate form of L-Phe had four strong peaks, and two less noticeable bands. At low temperatures, the anhydrous form of L-Phe had a new peak at 2.30 THz and a broad peak at 2.81 THz that was split into three peaks (Table 11). A shift in absorption peaks were observed when temperature increased. They concluded that the THz spectrum of amino acids are temperature sensitive and THz fingerprints can be used for identification and detection purposes.

Niehues, Heyden, Schmidt, and Havenith (2011) used molecular dynamics (MD) simulations and THz spectroscopy to study hydrophilic and hydrophobic solutes. Peptides and amino acids in aqueous solutions were measured in frequencies less than 2.7 THz, and a good correlation was observed between the polarity and hydrophobicity of the solute and the THz absorption of the solvating water. They also used MD simulations to study the effect of hydrophilic and hydrophobic model particles on water dynamics. They linked the changes in the THz absorption spectrum of solvated amino acids to the vibrational density of states in the hydration water around the model particles. They compared the hydrophilic and hydrophobic solutes and reported a stronger increase in the oxygen vibrational density of solvating water molecules and THz absorption for hydrophilic solutes.

In 2009, Born and Havenith published a manuscript on the aspects of collective water network dynamics. Previous studies showed that at high protein concentrations, THz absorbance was linearly dependent on protein concentration. Born and Havenith (2009) established a new method to define THz absorption coefficients of solvated biomolecules. They observed a nonlinear THz absorbance response that unraveled a concentration of protein at which the dynamical hydration shells start to overlap. They introduced some theories and models for better understanding of the concentration-dependent features observed with THz absorbance. They also performed kinetic THz absorption studies of hydration dynamics during protein folding and developed a tool for time-resolved studies. They also studied the solvation of some model peptides at low hydration levels (Table 11). Ebbinghaus et al. (2008) showed the pH-dependence of the protein hydration shell and the major changes in the THz absorption pattern of aqueous proteins.

Antifreeze glycopeptides (AFGPs) are among the newest subjects in peptide studies. AFGPs can regulate ice nucleation, control ice crystal growth, and create viable conditions at very low temperatures. Due to their unique properties, AFGPs are molecules of great interest for food scientists. AFGPs can be used in frozen food products, such as ice cream, ice slurries, and fruits and berries. AFGPs can also inhibit ice recrystallization and the Ostwald ripening process, which is very important in water-in-oil emulsions. Urbańczyk, Góra, Latajka, and Sewald (2017) reviewed the latest research on understanding the relationship between the structure of AFGPs and their activity as well as the behavior of the hydration shell around AFGPs. The combination of THz spectroscopy and computational methods was tested. THz spectroscopy helps to better understand the role of hydration water in contact with the protein surfaces and its impact on protein stability.

Detection of vitamins

THz spectroscopy has been used to measure the low-frequency vibrations of vitamin B2 (riboflavin) and some of its related compounds (Takahashi, Ishikawa, Nishizawa, & Ito, 2005). It was found that both the intensity and position of the THz spectrum of vitamin B2 were temperature-dependent. Takahashi et al. (2005) used high precision quantum chemical calculations for measuring the vibrational mode of the compounds. Later, Wang et al. (2010) used THz-TDS for detection of intracellular metabolites, such as vitamins. Riboflavin appeared to be more absorptive to THz waves and showed sharp and strong peaks (Table 12). Riboflavin and astaxanthin were then detected inside the bacterial cells with shifts in position of the absorption peaks.

Vitamin C (ascorbic acid) has a specific role in the metabolism of some proteins and chelation with some metals. Binghua, Guangxin, and Zekui (2008) studied the THz absorption spectrum, index of refraction, and vibrational modes of L-ascorbic acid (Table 12) and stated that the absorption spectrum of L-ascorbic acid originates from both intermolecular and intramolecular vibrational modes. Peaks that appeared at 2.05 and 2.34 THz were assigned to phonon or inter-molecular modes while peaks at 1.8 and 2.21 THz were related to intramolecular vibrations. They also used DFT to simulate the vibrational frequency and structure of L-ascorbic acid. In another study, the group reported both the experimental and theoretical vibrational frequencies of L-ascorbic acid using a B3LYP algorithm of DFT (Cao, Zhang, Hou, Huang, & Zhou, 2009). They compared the THz absorption spectrum of supplementary vitamin C tablets with those of L-ascorbic acid and found some distinct fingerprint spectra in THz region, showing a good agreement between the theoretical and experimental results. In a study performed by Suhandy, Yulia, Ogawa, & Kondo, 2011) a combination of FTIR-ATR THz spectroscopy with iPLS

regression was used for quantification of vitamin C in aqueous solution. They used iPLS regression for selection of both the variables and spectral regions to develop a calibration model. The performance of their iPLS model was then evaluated by comparing it to that of the full-spectrum PLS model. The iPLS model with five PLS factors showed better performance and lower standard error of prediction for quantification at lower frequencies. Their method also improved ratio prediction to deviation and ratio error range values (Table 12). The L-ascorbic acid content of 33 samples of vitamin C solutions (3% to 21%) was quantified using ATR-THz spectroscopy (Table 12) (Ogawa, Kondo, & House, 2011). In another study, THz-TDS and FTIR were used to detect L-ascorbic acid and thiamine (vitamin B1). Results of both THz-TDS and FTIR fingerprints were consistent except that a new FTIR fingerprint peak appeared in the low frequency region (Table 12). That specific peak was only detected by the highly sensitive silicon bolometer detector used in FTIR spectroscopy (Li, Li, & Jiang, 2015).

Yu, Huang, Wang, Zhao, and Zhang (2009) used combination of THz-TDS and DFT calculation for identification and characterization of some vitamins, and good agreement was observed between their theoretical and experimental data. Their theoretical results assigned most of the absorption peaks to the intramolecular modes. For vitamin C, they reported five peaks (Table 12). The peaks observed at 1.8 and 2.34 THz were also reported by Binghua et al. (2008). Peaks below 2 THz were assigned to phonon or intermolecular mode and peaks appeared at frequencies higher than 2 THz were related to the scissoring of the ring and ring torsion. Specific absorption peaks were reported for vitamin B1, B6, and B2 (Table 12). The observed peaks for riboflavin (vitamin B2) were similar to those reported by Wang et al. (2009) except for the peaks at 0.38, 0.62, and 0.82 THz.

Alcohol studies

Møller et al. (2007) employed a self-referenced reflection THz-TDS in the frequency range of 0.1 to 1.1 THz to quantify both the alcohol and sugar content of beverages. They measured the refractive index and the absorption coefficient of pure water, ethanol in water (30% w/w), and sugar in water (12% w/w). They showed that their method was independent of carbonation and yeast content. Both the refractive index and the absorption coefficient decreased significantly when ethanol was added to water. The addition of sugar did not affect the dielectric properties of the liquid. As a result, the addition of small amount of sugar (<20%) did not change the refractive index, but a small reduction in the absorption coefficient was observed. In another study, the group investigated the dielectric properties some of commercial alcoholic beverages and liquors using reflection THz-TDS spectroscopy (Jepsen, Møller, & Merbold, 2007). They measured both the imaginary and the real part of the dielectric function and determined two ingredients (sugar and alcohol) simultaneously. Higher accuracy was achieved at low alcohol concentrations.

Fawole and Tabib-Azar (2016) demonstrated a noninvasive real-time monitoring of a 30-hr fermentation process using frequency-domain THz dielectric spectroscopy. The sensitivity range and LOD of the method for sugar and alcohol is presented in Table 13.

Sarkar, Saha, Banerjee, Mukherjee, and Mandal (2017) reported the complex dielectric properties of five mono-hydroxy alcohols. They realized that the major contribution to the complex dielectric spectra of alcohols was from the fast hydrogen-bond rupture, the motions of the H-bonded OH groups, and the motion of alkyl chains. The spectrum of all alcohols was frequency-dependent between 2 and 6 THz (Table 13). Huang et al. (2018) studied the wettability of some aliphatic monohydric liquid alcohols and reported a non-uniform distribution for the liquids (Huang et al., 2018) and showed that the surface wettability increased by increasing the alcohol alkyl chain (Table 13).

Current Pitfalls and Future Prospects of THz Technology

THz spectroscopy is a safe, nondestructive, noninvasive, convenient method with great flexibility and broad applications. Despite its potential applications, THz technology has some limitations and drawbacks listed below.

Cost

The high cost of a THz source and detector is a critical factor affecting its commercial use (Hochrein, 2014; Wang et al., 2018). Although the cost has been decreasing during the past few years, it is still too high for use in some applications. Besides, the process of optimizing a THz system for food inspection and monitoring purposes is labor-intensive and expensive (Gowen et al., 2012).

Water and high moisture compounds

Besides the low speed of data acquisition, the major limitation in THz spectroscopy is the absorption of THz waves by water (Mathanker et al., 2013). Application of THz in the food industry is limited due to strong absorption of THz radiation by water (Qin et al., 2013). Modern THz systems have lessened this challenge by using higher radiant powers. Despite all the improvements, identification of some solid compounds is still challenging depending on their extent of hydration (Smith & Arnold, 2011). Implementation of some spectral processing methods or specific sample preparation techniques may be helpful.

Scattering effect

The scattering effects, the major problem in both transmission and reflection modes of THz spectroscopy, is due to the inhomogeneity of food (Qin et al., 2013; Redo-Sanchez et al., 2013). The physical variation of a sample, such as irregular shape and different particle size, influence the refractive index and adversely affect the quality monitoring process (Gowen et al., 2012). Grinding the sample and compressing it into a fine and smooth pellet can reduce the scattering effects. Using algorithms, such as the Karhunen Loeve transform, can also be useful for extracting the spectral data and minimizing the scattering effects (Qin et al., 2013).

Limited penetration

THz radiation penetration depth is dependent on several factors such as the properties of the food material, thickness of the sample, power of the THz source, wavelength of THz radiation, and its angle at the food sample (Smith & Arnold, 2011). The composition, shape, and water content of a food sample also affect the penetration depth of THz radiation at a specific frequency. Water significantly limits the penetration depth. Limited penetration of THz radiation is more problematic in liquids than solids. Using THz in reflection mode can reduce the extent of this issue. However, it is not necessary to operate in reflection mode if the power of transmitted beam is increased (Redo-Sanchez et al., 2013). In the case of microorganism detection in liquid samples, performing THz spectroscopy using ATR THz-TDS with quartz cuvettes can resolve this problem to some extent (Qin et al., 2013).

Thickness of the sample and effect of food matrices and wrapping materials

Although THz is a powerful tool for in-line detection of moisture content in dry food, one of the limitations in measuring the moisture level of food by THz is the thickness of the sample. THz spectroscopy is suitable for samples with a thickness of <1 mm (Chua et al., 2005). Samples with thickness >1 mm appear opaque at frequencies >0.7 THz. There are two ways to avoid this problem: (1) the measurements should be performed at the low-frequency THz region or (2) the samples must be dried or frozen (Qin et al., 2013). The reason is that THz absorption by liquid water is decreased at the low-frequency THz region, and dehydrating or freezing will omit the absorption of THz radiation by liquid water without altering or damaging the sample (Smith & Arnold, 2011).

The presence of impurities or the differences in the thickness of a food sample, such as a chocolate bar, can affect the THz spectrum (Qin et al., 2013). Performing reflectance spectroscopy through ATR module is the best way for thick, highly scattering and strongly absorbing samples (Smith & Arnold, 2011).

Studies showed that THz imaging can successfully detect harmful compounds in packaged food, but the sensitivity of the method is affected by the combined effects of chemical composition and the particle size of the wrapping material (Baek et al., 2014). They showed that the THz absorption peak of melamine was affected by the food matrix, such as flour, chocolate, and milk powder. They also showed the effect of wrapping materials and reported a significant sensitivity decrease for large particle size food matrix with two layers of wrapping material.

Limited LOD for chemicals

Studies showed that THz in combination with chemometric methods can rapidly detect and quantify harmful chemicals and toxins in food samples (within 5 s). Despite the latest improvements in the quantification of toxins using THz spectroscopy, the LOD of the method needs improvement (Chen & Xie, 2014; Ge et al., 2016). Although sample preparation time is longer for chromatographic and immune assay methods, but these methods have very good LOD for chemicals. Using the combination of THz spectroscopy with chemometric methods, the best reported LOD for detection of AFB_1 was 1 μg/kg (Liu et al., 2019), while the LOD of a fluorescent probe-based method was 3.1 pg/mL for AFB_1 (Wang et al., 2019). The LOD of a real-time immune-PCR method was 0.03 ng/mL for total aflatoxins (Ren et al., 2019).

Limited sensitivity and low LOD for detection of microorganisms

THz is a reagent-free, fast, and simple operational procedure, with great ability to differentiate between dead and living bacteria; however, the LOD of THz spectroscopy is still low compared to conventional culturing and molecular techniques (Liu et al., 2018). The best LOD reported was for *E. coli* (LOD = 10^4 CFU/mL) by Mazhorova et al. (2012) while the LOD of an impedimetric biosensor for *E. coli* was reported as 48 CFU/mL (Lin, Pillai, Lee, & Jemere, 2019). A real-time PCR method showed the best LOD for detection of bacterial contaminates in food samples. LOD = 10^1 genome copies was reported for *E. coli* in oysters (Miotto et al., 2019).

Application specificity

Most of the high-speed THz systems are application-specific and are based on sampling from a sub-region THz frequency to match the desired response (Gowen et al., 2012). In order to use a THz system in a manufacturing and processing line, the system must be specifically optimized for that particular product and purpose. This process is usually long and labor-intensive.

Possible Future Advances in THz Technology

Although much progress has been made in THz hardware, THz imaging techniques, and sample preparation methods, THz imaging still has a long way to go from an experimental research tool to a practical control device. THz imaging has some attractive features and is worthy of further research. Possible areas for future studies include the following:

Decreasing the cost of THz technology

Due to the high cost of the technology, the majority of the THz systems are used in research and academic areas. One of the reasons for the high price of the THz system is its low sales volume. In fact, if more applications are revealed, demand for THz systems will increase, and consequently the cost will decrease. On the other hand, it is said that the high price of the technology is a limiting factor for its application. Further research and development are needed to design a THz imaging system with sources and detectors that are low-cost and efficient and improve the probability of the THz instrumentation and technology.

Studying the interaction of THz with food materials

Water is a strong THz wave absorber, and studies showed that the reaction of food to THz radiation depends on the type of water and the level of water in the food. Water can be in the form of free or bound water in the food. A THz image of a water-in-oil emulsion depends on the type of water and the size of the water pool. Møller et al. (2010) showed the effect of the real and imaginary part of water pool on the THz spectra. The level of hydration also affects the low-frequency vibrational modes of proteins. Born, Weingärtner, Bründermann, and Havenith (2009) stated that a minimum number of hydrations is required to activate the peptide-water network and achieve a good THz spectrum. Ogawa et al. (2009) showed that the hydrogen bonding of water molecules and amino acids affects the vibrational mode in the amino acid molecule. Despite many publications in agriculture and the food industry, the interaction of THz radiation with food products has not yet been described in detail. Further research is needed to investigate the interaction of THz with food materials and implementation of some simulation algorithms might be helpful in this respect (Ung et al., 2007).

Improving temperature-dependent sensing techniques

Moisture content monitoring is very important for dried foods. The conventional electrical RH sensors are temperature-dependent, expensive, and need periodic maintenance. Guided-mode resonance (GMR) sensors can work in THz range, and Shin et al. (2017) showed that the PVA-coated GMR sensor is a good candidate for inexpensive and highly sensitive RH sensing. Although the PVA-coated GMR sensor was very sensitive to humidity changes at 20 °C, future studies are needed to improve temperature-dependent RH sensing techniques.

Improving frequency-dependent sensing techniques

In the past few decades, many studies have focused on building sensors that can detect chemical and biomolecules without the labeling process. Waveguide sensors and THz micro-resonators have proven to be useful for liquid samples (O'Hara et al., 2008). Frequency selective surfaces and metamaterials are very small in size, highly sensitive, and have a tunable resonant frequency response

in the THz range. Further research is required to efficiently utilize metamaterials as sensing devices and build frequency selective surface-based sensors.

Improving the LOD and accuracy

The presence of toxic compounds in food is a serious food safety concern. A good detection technique must be able to detect and quantify trace amount of toxins in food. Rapid and online detection of harmful compounds is also a need of the food industry. Although THz spectroscopy proved to be a fast and reliable method for detection of harmful chemicals in food, it has a low LOD compared to the routine chemical and immunoassay methods. Further research is needed to improve the LOD and accuracy of prediction models for food contaminants (Ge et al., 2016; Redo-Sanchez et al., 2013).

Improving THz systems and instruments using multiple technologies

In order to make a fast, accurate, and highly efficient THz system for in-line used at food industries, multiple technologies must be implemented in the next generation of THz systems. Improvement in the scan rate for real-time analysis, implementation of femtosecond laser sources, and use of antireflective coatings to achieve a higher level of throughput would be helpful. The use of nanomaterials can improve spatial resolution and imaging contrast (Smith & Arnold, 2011; Ung et al., 2007). Improvements in the signal processing methods (specifically for large data processing), is also needed.

Improving the performance of THz systems

THz system performance is characterized by its imaging speed, spectral resolution, spatial resolution, and the amount of information the system can provide (Ung et al., 2007). For example, a clear absorption peak will help to develop algorithms for food quality control purposes (Redo-Sanchez et al., 2013). Although current THz systems provide clear absorption peaks, more research is needed to develop algorithms for self-automated and real-time systems. Some compact and turnkey THz systems (such as Zomega Mini-Z and Micro-Z systems) capable to operate at waveform rates of 500 Hz have been developed, however such systems are very expensive (Gowen et al., 2012). A cost-effective THz imaging system with high performance would be very helpful in food applications.

Increasing data rate

THz applications in a manufacturing sector require inspection of a large volume of products per unit time. In a normal manufacturing environment, usually 100 to 10,000 units of products must be inspected per minute. THz system must have a high data rate (number of items to be inspected per unit time) to meet the requirements of the manufacturing company (Redo-Sanchez et al., 2013). Increasing the data rate or scanning speed is a critical factor leading to the success of THz technology and its industrial applications.

Building a THz database

Many of the THz applications in the food industry are based on the detection of a specific spectra. Unfortunately, there is no specific THz database library for food products. Building a THz database library for all food products is impractical and impossible, but a THz database library for the main food components can simplify the prediction and detection processes (Ung et al., 2007).

Optimizing software implementation

Researchers showed that several statistical and chemometric methods can be used for analyzing and processing the THz spectral data. In order to find a good model, different statistical and chemometric methods should be tested. This process is long and time-consuming. Chemometrics as well as statistical methods should be integrated into future THz instruments to automatically analyze the results (Yang, Smith & Arnold, 2011; Yang et al., 2016).

Developing label-free biosensors and improving the SNR

Rapid and accurate detection of microorganisms is vital for food safety control. Currently the time-consuming culturing methods, DNA-based methods and some electrochemical biosensors are being used for bacterial detection. Studies showed that THz-based technique can detect pathogens in food products based on their specific THz spectral characteristics (Globus et al., 2012; Park et al., 2014; Wessel et al., 2013; Yang et al., 2017). Future generations of THz systems must focus on developing fast, convenient, and label-free biosensor for detection of bacteria in food. Further research is required to develop a noninvasive real-time monitoring THz technique for microorganisms (Yang et al., 2016). Lab-on-a-chip devices used for bacterial detection need further improvement in terms of substituting the current materials with less absorptive materials, such as silicon or quartz and also adoption of sensitive room-temperature detectors (Yang et al., 2016).

Conclusions

Not only can THz waves pass through a wide variety of foods and packaging materials, but they can also be used for identification and characterization purposes. THz imaging is a great alternative to X-rays in food inspection and quality control processes and has been successfully used in non-invasive detection of harmful compounds, toxins, and microorganisms in food. The geographical origin of a food as well as adulteration can be determined with this technique. THz spectroscopy is also a good tool for characterization of food components. Although applications of THz imaging and spectroscopy in the food industry are attractive, the technique has some pitfalls that need to be considered. The cost of the THz equipment is still very high for most applications, the technique has limited sensitivity and low LOD, high SNR, is thickness-dependent, and sample preparation is required for some applications. There is no database library available for food applications. Future research is needed to increase the scanning speed and sensitivity of the method. Fast and cost-efficient THz systems can be developed through implementation of compact and more efficient sources and detectors. In recent years, a few useful THz systems have been developed. Although much more work is required to improve the technique, THz technology is establishing itself as a powerful tool with great detection and quantification ability in the food industry. A wide range of food applications is expected for THz spectroscopy in the near future.

Acknowledgment

The authors would like to sincerely thank Mrs. Elizabeth Northeimer for reviewing the commercial food engineering aspects and English editing the completed manuscript.

Author Contributions

Dr. Afsah-Hejri researched and developed the content of the introduction, food applications, and THz pitfalls and future research sections in addition to compiling and revising the completed document. Dr. Hajeb assisted Dr. Afsah-Hejri with some of the food

application tables. Ara designed and illustrated the figures. Dr. Ehsani critically reviewed the overall manuscript.

Conflict of Interest

The authors declare that there are no conflicts of interest.

List of abbreviations

Abbreviation	Full form
ANN	Artificial neural networks
AsLS	Asymmetric least squares
biPLS	Backward interval PLS
BPANN	Back propagation artificial neural network
BPNN	Back propagation neural network
CA	Cluster analysis
D-S	Dempster–Shafer method
DA	Discriminant analysis
DFT	Density functional theory
FDTD	Finite difference time domain simulation
fsPLS	Full spectra PLS
GA	Genetic algorithm
HF	Hartree-Fock function
iPLS	Interval PLS
LS	Least-squares
LS-SVM	Least squares-support vector machine
MCR-ALS	Multivariate curve resolution alternating least squares
NB	Naive Bayes
PBE	Perdew-Burke-Ernzerhof exchange-correlation functionals
PCA	Principal component analysis
PCR	Principal component regression
PLS	Partial least squares
PLSR	Partial least squares regression
PWDF	Plane-wave density functional method
RF	Random forest pattern recognition method
RMSE	Root mean square error
RMSEC	Root mean square errors of calibration
RMSECV	Root mean square errors of cross-validation
RMSEP	Root mean square errors of prediction
RPD	Residual predictive deviation
SLR	Stepwise linear regression
SMLR	Stepwise multiple linear regression
SPA	Successive projection arithmetic
SVM	Support vector machine
TM	Tchebichef image moment method
WLDA	Weighted linear discriminant analysis

References

Afsah-Hejri, L., Jinap, S., Hajeb, P., Radu, S., & Shakibazadeh, S. (2013). A review on mycotoxins in food and feed: Malaysia case study. *Comprehensive Reviews in Food Science and Food Safety*, *12*(6), 629–651. https://doi.org/10.1111/1541-4337.12029

Afsah-Hejri, L., Jinap, S., & Radu, S. (2013). Occurrence of aflatoxins and aflatoxigenic *Aspergillus* in peanuts. *Journal of Food, Agriculture and Environment*, *11*(3–4), 228–234.

Åkesson, M. T., Point, C. C., & di Caracalla, V. D. T. (2010). Proposed draft maximum levels for melamine in food and feed (N13-2009). http://www.fao.org/tempref/codex/Meetings/CCCF/cccf4/cf04_05e.pdf

Akyildiz, I. F., Miquel, J., & Han, C. (2014). Terahertz band: Next frontier for wireless communications. *Physical Communication*, *12*, 16–32. https://doi.org/10.1016/j.phycom.2014.01.006

Baek, S. H., Lim, H. Bin, & Chun, H. S. (2014). Detection of Melamine in foods using terahertz time-domain spectroscopy. *Journal of Agricultural and Food Chemistry*, *62*, 5403–5407. https://doi.org/10.1021/jf501170z

Berrier, A., Schaafsma, M. C., Nonglaton, G., Bergquist, J., & Rivas, J. G. (2012). Selective detection of bacterial layers with terahertz plasmonic antennas. *Biomedical Optics Express*, *3*(11), 2937. https://doi.org/10.1364/BOE.3.002937

Bigourd, D., Cuisset, A., Hindle, F., Matton, S., Fertein, E., Bocquet, R., & Mouret, G. (2006). Detection and quantification of multiple molecular species in mainstream cigarette smoke by continuous-wave terahertz spectroscopy. *Optics Express*, *31*(15), 2356–2358.

Binghua, C., Guangxin, Z., & Zekui, Z. (2008). Far-infrared vibrational spectra of L-ascorbic acid investigated by terahertz time domain spectroscopy. Paper presented at *2nd International Conference on Bioinformatics and Biomedical Engineering, iCBBE 2008* (pp. 47–49), Shanghai, China. https://doi.org/10.1109/ICBBE.2008.18

Blanchard, F., Razzari, L., Bandulet, H., Sharma, G., Morandotti, R., Kieffer, J., . . . Hegmann, F. A. (2007). Generation of 1.5 μJ single-cycle terahertz pulses by optical rectification from a large aperture ZnTe crystal. *Optics Express*, *15*(20), 13212–13220.

Born, B., & Havenith, M. (2009). Terahertz dance of proteins and sugars with water. *Journal of Infrared, Millimeter, and Terahertz Waves*, *30*(12), 1245–1254. https://doi.org/10.1007/s10762-009-9514-6

Born, B., Weingärtner, H., Bründermann, E., & Havenith, M. (2009). Solvation dynamics of model peptides probed by terahertz spectroscopy. Observation of the onset of collective network motions. *Journal of the American Chemical Society*, *131*(10), 3752–3755. https://doi.org/10.1021/ja808997y

Bowman, T., Chavez, T., Khan, K., Wu, J., Chakraborty, A., Rajaram, N., . . . El-Shenawee, M. O. (2018). Pulsed terahertz imaging of breast cancer in freshly excised murine tumors. *Journal of Biomedical Optics*, *23*, 026004–1. https://doi.org/10.1117/1.JBO.23.2.026004

Brown, E. R., Bjarnason, J. E., Chan, T. L. J., Lee, A. W. M., & Celis, M. A. (2004). Optical attenuation signatures of *Bacillus subtillis* in the THz region. *Applied Physics Letters*, *84*(18), 3438–3440. https://doi.org/10.1063/1.1711167

Bykhovski, A., Li, X., Globus, T., Khromova, T., Gelmont, B., Woolard, D., . . . Jensen, J. O. (2005). THz absorption signature detection of genetic material of *E. coli* and *B. subtilis*. Paper presented at Proceedings of the SPIE, Chemical and Biological Standoff Detection III, *5995*, Boston, MA. https://doi.org/10.1117/12.629959

Cao, B., Zhang, G., Hou, D., Huang, P., & Zhou, Z. (2009). Terahertz timedomain spectroscopy of L-ascorbic acid. *Guang Pu Xue Yu Guang Pu Fen Xi*, *29*(7), 1729–1731.

Chavez, T., Bowman, T., Wu, J., Bailey, K., & El-Shenawee, M. (2018). Assessment of terahertz imaging for excised breast cancer tumors with image morphing. *Journal of Infrared, Millimeter, Terahertz Waves*, *39*(12), 1283–1302.

Chen, M., & Xie, L. (2014). A preliminary study of aflatoxin B1 detection in peanut oil by terahertz time-domain spectroscopy. *Transactions of the ASABE*, *57*(6), 1793–1799. https://doi.org/10.13031/trans.57.10725

Cherkasova, O. P., Fedorov, V. I., Nemova, E. F., & Pogodin, A. S. (2009). Influence of terahertz laser radiation on the spectral characteristics and functional properties of albumin. *Optics and Spectroscopy*, *107*(4), 534–537. https://doi.org/10.1134/S0030400X09100063

Chua, H. S., Obradovic, J., Haigh, A. D., Upadhya, P. C., Hirsch, O., Crawley, D., . . . Linfield, E. H. (2005). Terahertz time-domain spectroscopy of crushed wheat grain. Paper presented at *Microwave Symposium Digest, 2005 IEEE MTT-S International* (pp. 2103–2106), Long Beach, CA. https://doi.org/10.1109/mwsym.2005.1517162

Cui, Y., Mu, K., Wang, X., Zhang, Y., & Zhang, C. (2009, August). Measurement of mixtures of melamine using THz ray. In *International Symposium on Photoelectronic Detection and Imaging 2009: Terahertz and High Energy Radiation Detection Technologies and Applications* (Vol. 7385, p. 73851E). International Society for Optics and Photonics. https://doi.org/10.1117/12.835293

Cunnell, R., Luce, T., Collins, J. H. P., Rungsawang, R., Freeman, J. R., Beere, H. E., . . . Zeitler, J. A. (2009, September). Quantification of emulsified water content in oil using a terahertz quantum cascade laser. In *2009 34th International Conference on Infrared, Millimeter, and Terahertz Waves* (pp. 1-2). IEEE. https://doi.org/10.1109/ICIMW.2009.5325604

Dierks, T. M., & Korter, T. M. (2017). Vibrational and energetic analysis of sorbitol crystal forms. Paper presented at *International Conference on Infrared, Millimeter, and Terahertz Waves, IRMMW-THz*. https://doi.org/10.1109/IRMMW-THz.2017.8067032

Dinovitser, A., Valchev, D. G., & Abbott, D. (2017). Terahertz time-domain spectroscopy of edible oils. *Royal Society Open Science*, *4*, 170725. https://doi.org/10.1098/rsos.170275

Dougherty, J. P., Jubic, G. D., Kiser, W. L., Dougherty, J. P., Jubic, G. D., & Kiser, W. L. (2007). Terahertz imaging of burned tissue. Paper presented at *Proceedings of the SPIE. Terahertz and Gigahertz Electronics and Photonics*, *6472*. https://doi.org/10.1117/12.705137

Ebbinghaus, S., Seung, J. K., Heyden, M., Yu, X., Gruebele, M., Leitner, D. M., & Havenith, M. (2008). Protein sequence- and pH-dependent hydration probed by terahertz spectroscopy. *Journal of the American Chemical Society*, *130*(8), 2374–2375. https://doi.org/10.1021/ja0746520

El Haddad, J., De Miollis, F., Bou Sleiman, J., Canioni, L., Mounaix, P., & Bousquet, B. (2014). Chemometrics applied to quantitative analysis of

ternary mixtures by terahertz spectroscopy. *Analytical Chemistry*, *86*(10), 4927–4933. https://doi.org/10.1021/ac500253b

Ergün, S., & Sönmez, S. (2015). Terahertz technology for military applications. *Journal of Management and Information Science*, *3*, 13–16

Etayo, D., Iriarte, J. C., Palacios, I., Maestrojuán, I., Teniente, J., Ederra, I., & Gonzalo, R. (2011). THz imaging system for industrial quality control. Paper presented at *2011 IEEE MTT-S International Microwave Workshop Series on Millimeter Wave Integration Technologies, IMWS 2011*, 172–175. https://doi.org/10.1109/IMWS3.2011.6061867

Fawole, O., Sinha, K., & Tabib-Azar, M. (2015). Monitoring yeast activation with sugar and zero-calorie sweetener using terahertz waves. Paper presented at *2015 IEEE SENSORS - Proceedings* (pp. 19–22). https://doi.org/10.1109/ICSENS.2015.7370322

Fawole, O., & Tabib-Azar, M. (2016). Terahertz quantification of ethanol and sugar concentrations in water and its application for noninvasive real-time monitoring of fermentation. Paper presented at *IEEE MTT-S International Microwave Symposium Digest*, *2016-Augus*, (pp. 0–3). https://doi.org/10.1109/MWSYM.2016.7540132

Federici, J. F. (2012). Review of moisture and liquid detection and mapping using terahertz imaging. *Journal of Infrared, Millimeter, and Terahertz Waves*, *33*(2), 97–126. https://doi.org/10.1007/s10762-011-9865-7

Fitzgerald, A., Wallace, V. P., Jimenez-Linan, M., Bobrow, L., Pye, R., Purushotham, A., & Arnone, D. (2006). Terahertz pulsed imaging of human breast tumors. *Radiology*, *239*, 533–540. https://doi.org/10.1148/radiol.2392041315

Funkner, S., Niehues, G., Schmidt, D. A., Heyden, M., Schwaab, G., Callahan, K. M., . . . Havenith, M. (2012). Watching the low-frequency motions in aqueous salt solutions: The terahertz vibrational signatures of hydrated ions. *Journal of the American Chemical Society*, *134*(2), 1030–1035. https://doi.org/10.1021/ja207929u

García-rial, F., Member, G. S., Montesano, D., Gómez, I., Callejero, C., Bazus, F., & Grajal, J. (2018). Combining commercially available active and passive sensors into a millimeter-wave imager for concealed weapon detection. *IEEE Transactions on Microwave Theory and Techniques*, *67*(3), 1167–1183

Ge, H., Jiang, Y., Lian, F., & Zhang, Y. (2016). Terahertz spectroscopy investigation of preservative molecules. *Optik*, *127*(12), 4954–4958. https://doi.org/10.1016/j.ijleo.2016.02.048

Ge, H., Jiang, Y., Lian, F., Zhang, Y., & Xia, S. (2016). Quantitative determination of aflatoxin B1 concentration in acetonitrile by chemometric methods using terahertz spectroscopy. *Food Chemistry*, *209*, 286–292. https://doi.org/10.1016/j.foodchem.2016.04.070

Ge, M., Zhao, H., Ji, T., Yu, X., Wang, W., & Li, W. (2006). Terahertz time-domain spectroscopy of some pentoses. *Science in China Series B Chemistry*, *49*(3), 204–208. https://doi.org/10.1007/s11426-006-0204-0

Globus, T., Dorofeeva, T., Sizov, I., Gelmont, B., Lvovska, M., Khromova, T., . . . Koryakina, Y. (2012). Sub-THz vibrational spectroscopy of bacterial cells and molecular components. *American Journal of Biomedical Engineering*, *2*(4), 143–154. https://doi.org/10.5923/j.ajbe.20120204.01

Gorenflo, S., Tauer, U., Hinkov, I., Lambrecht, A., Buchner, R., & Helm, H. (2006). Dielectric properties of oil-water complexes using terahertz transmission spectroscopy. *Chemical Physics Letters*, *421*(4–6), 494–498. https://doi.org/10.1016/j.cplett.2006.01.108

Gowen, A. A., O'Sullivan, C., & O'Donnell, C. P. (2012). Terahertz time domain spectroscopy and imaging: Emerging techniques for food process monitoring and quality control. *Trends in Food Science and Technology*, *25*(1), 40–46. https://doi.org/10.1016/j.tifs.2011.12.006

Hadjiloucas, S., Walker, G. C., & Bowen, J. W. (2010). Quantifying consumer perception of foodstuffs using THz spectrometry. Paper presented at *IRMMW-THz 2010 - 35th International Conference on Infrared, Millimeter, and Terahertz Waves, Conference Guide* (pp. 0–1). https://doi.org/10.1109/ICIMW.2010.5612357

Haff, R. P., & Toyofuku, N. (2008). X-ray detection of defects and contaminants in the food industry. *Sensing and Instrumentation for Food Quality and Safety*, *2*(4), 262–273. https://doi.org/10.1007/s11694-008-9059-8

Han, S. (2013). Compact sub-THz gyrotrons for real-time T-ray imaging. Paper presented at *IEEE 2013* (pp. 3–4).

Han, S., Park, W. K., & Chun, H. S. (2011). Development of sub-THz gyrotron for real-time food inspection. Paper presented at *RMMW-THz 2011 - 36th International Conference on Infrared, Millimeter, and Terahertz Waves*, 0–1.

Han, S. T., Park, W. K., Ahn, Y. H., Lee, W. J., & Chun, H. S. (2012). Development of a compact sub-terahertz gyrotron and its application to T-ray real-time imaging for food inspection. Paper presented at *International Conference on Infrared, Millimeter, and Terahertz Waves, IRMMW-THz*, (pp. 6–7). https://doi.org/10.1109/IRMMW-THz.2012.6380390

Han, S. T., Park, W. K., & Chun, H. S. (2011). Development of sub-THz gyrotron for real-time food inspection. Paper presented at *IRMMW-THz 2011 - 36th International Conference on Infrared, Millimeter, and Terahertz Waves* (pp. 0–1). https://doi.org/10.1109/irmmw-THz.2011.6105104

Herrmann, M., Tani, M., Watanabe, M., & Sakai, K. (2002). Terahertz imaging of objects in powders. *IEE Proceedings Optoelectronics*, *149*(3), 116–120. https://doi.org/10.1049/ip-opt:20020185

Heyden, M., Brundermann, E., Heugen, U., Niehues, G., Leitner, D. M., & Havenith, M. (2008). Long-range influence of carbohydrates on the solvation dynamics of water-answers from terahertz absorption measurements and molecular modeling simulations. *Journal of the American Chemical Society*, *130*(17), 5773–5779. https://doi.org/10.1021/ja00781083

Hiromoto, N., Shiba, N., & Yamamoto, K. (2013). Detection of a human hair with polarization-dependent THz-time domain spectroscopy. Paper presented at *2013 38th International Conference on Infrared, Millimeter, and Terahertz Waves (IRMMW-THz)* (pp. 1–2). IEEE.

Hochrein, T. (2014). Markets, availability, notice, and technical performance of terahertz systems: Historic development, present, and trends. *Journal of Infrared, Millimeter, and Terahertz Waves*, *36*(3), 235–254. https://doi.org/10.1007/s10762-014-0124-6

Hor, Y. L., Lim, H. C., Federici, J. F., Moore, E., & Bozzelli, J. W. (2008). Terahertz study of trichloroanisole by time-domain spectroscopy. *Chemical Physics*, *353*(1–3), 185–188. https://doi.org/10.1016/j.chemphys.2008.08.011

Hu, B. B., & Nuss, M. C. (1995). Imaging with terahertz waves. *Optic Lettters*, *20*(16), 1716–1718.

Hu, Y., Guo, L., Wang, X., & Zhang, X. C. (2005). THz time-domain spectroscopy on plant oils and animal fats. Paper presented at *SPIE, Infrared Components and Their Applications* (p. 334). https://doi.org/10.1117/12.580922

Huang, H., Zhao, H., Zhang, B., Su, Y., Jiang, W., Cai, B., . . . Ma, Y. (2018). A terahertz transmission imaging based approach for liquid alcohol wettability investigation. *Infrared Physics and Technology*, *89*, 110–114. https://doi.org/10.1016/j.infrared.2017.12.021

Huang, X. B., Hou, D. B., Huang, P. J., Ma, Y. H., Li, X., & Zhang, G. X. (2015). The meat freshness detection based on terahertz wave. Paper presented at *Photoelectronic Technology Committee Conferences* (Vol. 9795, p. 97953D). https://doi.org/10.1117/12.2211973

Inamo, M., Sakai, K., Kiwa, T., & Tsukada, K. (2016). Application to non-destructive evaluation of gas barrier films using a high-speed terahertz time-domain spectroscopy. Paper presented at *Progress In Electromagnetic Research Symposium (PIERS)* (p. 3921).

International Agency for Research on Cancer. (2010). *Some aromatic amines, organic dyes, and related exposures* (Vol. 99). Lyon, France: IARC Press

Jepsen, P., Cooke, D., & Koch, M. (2011). Terahertz spectroscopy and imaging—Modern techniques and applications. *Laser and Photonics Reviews*, *5*(1), 124–166. https://doi.org/10.1002/lpor.201000011

Jepsen, P., Moller, U., Eichhorn, F., Merbold, H., Folkenberg, J. R., & Clark, S. J. (2007). Terahertz time-domain spectroscopy of crystalline and aqueous systems. Paper presented at *2007 Conference on Lasers & Electro-Optics/Quantum Electronics and Laser Science Conference*, 1740–1741. https://doi.org/10.1007/978-1-4020-6503-3_11

Jepsen, P., Møller, U., & Merbold, H. (2007). Investigation of aqueous alcohol and sugar solutions with reflection terahertz time-domain spectroscopy. *Optics Express*, *15*(22), 14717. https://doi.org/10.1364/OE.15.014717

Jiang, F. L., Ikeda, I., Ogawa, Y., & Endo, Y. (2011). Terahertz absorption spectra of fatty acids and their analogues. *Journal of Oleo Science*, *60*(7), 339–343. https://doi.org/10.5650/jos.60.339

Jin, Q., Williams, K., Dai, J., & Zhang, X.-C. (2017). Observation of broadband terahertz wave generation from liquid water. *Nonlinear Optics*, 50–51.

Jiusheng, L. (2010). Optical parameters of vegetable oil studied by terahertz time-domain spectroscopy. *Applied Spectroscopy*, *64*(2), 231–234. https://doi.org/10.1366/000370210790619663

Joerdens, C., Rutz, F., Hasek, T., & Koch, M. (2006). Towards real-time terahertz quality. Towards real-time terahertz quality IEEE THz Technology, Ultrafast Measurements and Imaging (p. 322).

Johnson, T. J., Valentine, N. B., & Sharpe, S. W. (2005). Mid-infrared versus far-infrared (THz) relative intensities of room-temperature Bacillus spores.

Chemical Physics Letters, *403*(1–3), 152–157. https://doi.org/10.1016/j.cplett.2004.12.095

Jördens, C., & Koch, M. (2008). Detection of foreign bodies in chocolate with pulsed terahertz spectroscopy. *Optical Engineering*, *47*(3), 037003. https://doi.org/10.1117/1.2896597

Jördens, C., Rutz, F., & Koch, M. (2006). Quality assurance of chocolate products with terahertz imaging. *Measurement*, 1–8.

Kaltenecker, K., Zhou, B., Tybussek, K. H., Engelbrecht, S., Lehmann, R., Walker, S., . . . Fischer, B. M. (2018). September). Ultra-broadband THz spectroscopy for sensing and identification for security applications. Paper presented at *2018 43rd International Conference on Infrared, Millimeter, and Terahertz Waves (IRMMW-THz)* (pp. 1–2). IEEE.

Kang, X. S., Zhang, G. X., Chen, X. A., Huang, P. J., Hou, D. B., & Zhou, Z. K. (2011). Terahertz spectroscopic investigation of elaidic acid. *Guang Pu Xue Yu Guang Pu Fen Xi*, *31*(10), 2629–2633. https://doi.org/10.3964/j.issn.1000-0593(2011)10-2629-05

Karagoz, B., Altan, H., & Kamburoglu, K. (2015). Terahertz pulsed imaging study of dental caries. Paper presented at *European Conference on Biomedical Optics* (p. 95420N). Optical Society of America, 1–8. https://doi.org/10.1117/12.2183673

Kawano, Y., & Ishibashi, K. (2008). An on-chip near-field terahertz probe and detector. *Nature Photonics*, *2*(10), 618–621. https://doi.org/10.1038/nphoton.2008.157

Kim, G. J., Kim, J. Il, Jeon, S. G., Kim, J., Park, K. K., & Oh, C. H. (2012). Enhanced continuous-wave terahertz imaging with a horn antenna for food inspection. *Journal of Infrared, Millimeter, and Terahertz Waves*, *33*(6), 657–664. https://doi.org/10.1007/s10762-012-9902-1

Koch, M., & Krok, P. (2006). Quality control of chocolate products with THz imaging. *Menlo Systems*, 1–6. Retrieved from http://www.menlosystems.com/en/stories/application-notes/view/2259

Kurita, I., Suzuki, T., Kondo, N., Kondo, T., Kamba, S., Miura, Y., & Ogawa, Y. (2014). Specific detection of *Escherichia coli* by using metallic mesh sensor in THz region. Paper presented at 2014 URSI GASS (pp. 3–6). https://doi.org/10.1109/URSIGASS.2014.6930066

Lee, D. K., Kang, J. H., Lee, J. S., Kim, H. S., Kim, C., Hun Kim, J., . . . Seo, M. (2015). Highly sensitive and selective sugar detection by terahertz nano-antennas. *Scientific Reports*, *5*, 1–7. https://doi.org/10.1038/srep15459

Lee, Y., Choi, S., Han, S., Woo, D. H., & Chun, H. S. (2012). Detection of foreign bodies in foods using continuous wave terahertz imaging. *Journal of food protection*, *75*(1), 179–183. https://doi.org/10.4315/0362-028X.JFP-11-181

Leisawitz, D. T., Danchi, W. C., Dipirro, M. J., Feinberg, L. D., Gezari, D. Y., Hagopian, M., . . . Zhang, X. (2000). Scientific motivation and technology requirements for the SPIRIT and SPECS far-infrared/submillimeter space interferometers. Paper presented at *SPIE, Astronomical Telescopes and Instrumentation* (pp. 36–46). https://doi.org/10.1117/12.393957

Li, B., Cao, W., Mathanker, S., Zhang, W., & Wang, N. (2010). Preliminary study on quality evaluation of pecans with terahertz time-domain spectroscopy. Paper presented at *SPIE Infrared, Millimeter Wave, and Terahertz Technologies* (p. 78543V1-78543V6). https://doi.org/10.1117/12.882201

Li, B., & He, Y. (2007). Simultaneous determination of glucose, fructose and lactose in food samples using a continuous-flow chemiluminescence method with the aid of artificial neural networks. *Luminescence*, *22*, 317–325. https://doi.org/10.1002/bio.965

Li, C., Li, M., & Jiang, L. (2015). Research on Lascorbic acid and thiamine based on wideband terahertz spectroscopy technique. *Guang Pu Xue Yu Guang Pu Fen Xi*, *35*(3), 595–598.

Li, J., & Yao, J. (2008). Highly precise determination of optical constants in olive oil using terahertz time-domain spectroscopy. Paper presented at *Proceedings of SPIE* (Vol. 7277, pp. 727707-727707–6). https://doi.org/10.1117/12.819784

Li, J., Yao, J., & Li, J. (2008). Terahertz time-domain spectroscopy and application on peanut oils. Paper presented at *SPIE, Photonics and Optoelectronics Meetings: Terahertz Science and Technology* (Vol. 7277, pp. 727705-727705–727706). https://doi.org/10.1117/12.819782

Li, J., Zhao, X., & Li, J. (2009). Experimental study on identifying main component in rice bran oil with terahertz time-domain spectroscopy. Paper presented at *Proceedings of SPIE* (Vol. 7385, p. 73850M–73850M–6). https://doi.org/10.1117/12.835033

Li, J., Zhao, X., & Xu, D. (2009). Optical parameter determination of seed oil with terahertz time-domain spectroscopy. Paper presented at *Proceedings of SPIE* (Vol. 7385, p. 73850N–73850N–6). https://doi.org/10.1117/12.835025

Li, Y., Zheng, Y., & Wang, W. (2006). THz spectrum and vibrational mode of phenylalanine. Paper presented at *IRMMW-THz 2006 - 31st International Conference on Infrared and Millimeter Waves and 14th International Conference on Terahertz Electronics*, 422. https://doi.org/10.1109/ICIMW.2006.368630

Lin, D., Pillai, R. G., Lee, W. E., & Jemere, A. B. (2019). An impedimetric biosensor for E. coli O157: H7 based on the use of self-assembled gold nanoparticles and protein G. *Microchimica Acta*, *186*(3), 169.

Liu, B. H., Zhong, H., Karpowicz, N., Chen, Y., & Zhang, X. (2007). Terahertz spectroscopy and imaging for defense and security applications. *Proceedings of the IEEE*, *95*(8), 1514–1527).

Liu, J. (2017). Terahertz spectroscopy and chemometric tools for rapid identification of adulterated dairy product. *Optical and Quantum Electronics*, *49*(1), 1–8. https://doi.org/10.1007/s11082-016-0848-8

Liu, J., Fan, L., Liu, Y., Mao, L., & Kan, J. (2019). Application of terahertz spectroscopy and chemometrics for discrimination of transgenic camellia oil. *Spectrochimica Acta Part A: Molecular and Biomolecular Spectroscopy*, *206*, 165–169. https://doi.org/10.1016/j.saa.2018.08.005

Liu, W., Liu, C., Hu, X., Yang, J., & Zheng, L. (2016). Application of terahertz spectroscopy imaging for discrimination of transgenic rice seeds with chemometrics. *Food Chemistry*, *210*, 415–421.

Liu, W., Liu, C., Yu, J., Zhang, Y., Li, J., Chen, Y., & Zheng, L. (2018). Discrimination of geographical origin of extra virgin olive oils using terahertz spectroscopy combined with chemometrics. *Food Chemistry*, *251*, 86–92. https://doi.org/10.1016/j.foodchem.2018.01.081

Liu, W., Zhang, Y., & Han, D. (2016). Feasibility study of determination of high-fructose syrup content of Acacia honey by terahertz technique. In *SPIE, Infrared, Millimeter-Wave, and Terahertz Technologie* (p. 100300J1-6). https://doi.org/10.1117/12.2245966

Liu, W., Zhang, Y., Yang, S., & Han, D. (2018). Terahertz time-domain attenuated total reflection spectroscopy applied to the rapid discrimination of the botanical origin of honeys. *Spectrochimica Acta Part A: Molecular and Biomolecular Spectroscopy*, *196*, 123–130. https://doi.org/10.1016/j.saa.2018.02.009

Liu, W., Zhao, P., Wu, C., Liu, C., Yang, J., & Zheng, L. (2019). Rapid determination of aflatoxin B1 concentration in soybean oil using terahertz spectroscopy with chemometric methods, *Food Chemistry*, *293*, 213–219. https://doi.org/10.1016/j.foodchem.2019.04.081.

Long, Y., Li, B., & Liu, H. (2018). Analysis of fluoroquinolones antibiotic residue in feed matrices using terahertz spectroscopy, *Applied Optics*, *57*(3), 544–550. https://doi.org/10.1364/AO.57.000544

Lu, S. H., Li, B. Q., Zhai, H. L., Zhang, X., & Zhang, Z. Y. (2018). An effective approach to quantitative analysis of ternary amino acids in foxtail millet substrate based on terahertz spectroscopy. *Food Chemistry*, *246*, 220–227. https://doi.org/10.1016/j.foodchem.2017.11.016

Lu, S., Zhang, X., Zhang, Z., Yang, Y., & Xiang, Y. (2016). Quantitative measurements of binary amino acids mixtures in yellow foxtail millet by terahertz time domain spectroscopy. *Food Chemistry*, *211*, 494–501. https://doi.org/10.1016/j.foodchem.2016.05.079

Luo, H., Zhu, J., Xu, W., & Cui, M. (2019). Identification of soybean varieties by terahertz spectroscopy and integrated learning method. *Optik*, *184*, 177–184.

Ma, X., Zhao, H., Dai, B., & Ge, M. (2008). Progress in application of THz-TDS to protein study. *Guang Pu Xue Yu Guang Pu Fen Xi*, *28*(10), 2237–2242.

Markl, D., Dong, R., Li, J., & Zeitler, J. A. (2018). In-situ monitoring of powder density using terahertz pulsed imaging, Paper presented at *2018 43rd International Conference on Infrared, Millimeter, and Terahertz Waves (IRMMW-THz)* (pp. 1–3). IEEE.

Markelz, A., Roitberg, A., & Heilweil, E. (2000). Pulsed terahertz spectroscopy of DNA, bovine serum albumin and collagen between 0.1 and 2.0 THz. *Chemical Physics Letters*, *320*(1–2), 42–48. https://doi.org/10.1016/S0009-2614(00)00227-X

Markelz, A., Knab, J., Chen, J.-Y., Cerne, J., & Cox, W. (2004). Tagless and universal biosensor for point detection of pathogens. Paper presented at *SPIE, Terahertz for Military and Security Applications* (pp. 182–186). https://doi.org/10.1117/12.563613

Massaouti, M., Daskalaki, C., Gorodetsky, A., Koulouklidis, A. D., & Tzortzakis, S. (2013). Detection of harmful residues in honey using terahertz time-domain spectroscopy. *Applied Spectroscopy*, *67*(11), 1264–1269. https://doi.org/10.1366/13-07111

Mathanker, S. K., Weckler, P. R., & Wang, N. (2013). Terahertz (THz) applications in food and agriculture: A review. *Transactions of the ASABE*, *56*(3), 1213–1226. https://doi.org/10.13031/trans.56.9390

May, R. K., Evans, M., Zhong, S. C., Clarkson, R., Shen, Y. C., & Gladden, L. F. . . . Ieee.(2009) Real-time in situ measurement of particle size in flowing powders by terahertz time-domain spectroscopy. Paper presented at *2009 34th International Conference on Infrared, Millimeter, and Terahertz Waves* (pp. 803–805).

May, R., & Taday, P. F. (2013). Crystallization of sucrose monitored by terahertz pulsed spectroscopy. Paper presented at *2013 38th International Conference on Infrared, Millimeter, and Terahertz Waves (IRMMW-THz)* (pp. 1-1). IEEE.

Mazhorova, A., Markov, A., Ng, A., Chinnappan, R., Skorobogata, O., Zourob, M., & Skorobogatiy, M. (2012). Label-free bacteria detection using evanescent mode of a suspended core terahertz fiber. *Optics Express*, *20*(5), 5344. https://doi.org/10.1364/OE.20.005344

Mcintosh, A. I., Yang, B., Goldup, S. M., & Donnan, R. S. (2012). Terahertz spectroscopy: A powerful new tool for the chemical sciences? *Chemical Society Reviews*, *41*(6), 2072–2082. https://doi.org/10.1039/c1cs15277g

Menikh, A., Mickan, S. P., Liu, H., MacColl, R., & Zhang, X. C. (2004). Label-free amplified bioaffinity detection using terahertz wave technology. *Biosensors and Bioelectronics*, *20*(3), 658–662. https://doi.org/10.1016/j.bios.2004.03.006

Mickan, S. P., Menikh, A., Liu, H., Mannella, C. A., MacColl, R., Abbott, D., . . . Zhang, X. C. (2002). Label-free bioaffinity detection using terahertz technology. *Physics in Medicine and Biology*, *47*(21), 3789–3795. https://doi.org/10.1088/0031-9155/47/21/317

Miotto, M., Júnior, A. A. F., Barretta, C., da Silva, H. S., Pellizzaro, T., Lindner, J. D. D., . . . Prudencio, E. S. (2019). Development and application of a real-time polymerase chain reaction method for quantification of Escherichia coli in oysters (*Crassostrea gigas*). *Food microbiology*, *77*, 85–92.

Mittleman, D. M., Gupta, M., Neelamani, R., Baraniuk, R. G., Rudd, J. V., & Koch, M. (1999). Recent advances in terahertz imaging. *Applied Physics B: Lasers and Optics*, *68*, 1085–1094. https://doi.org/10.1007/s003409900011

Møller, U., Folkenberg, J. R., & Jepsen, P. U. (2010). Dielectric properties of water in butter and water-AOT-heptane systems measured using terahertz time-domain spectroscopy. *Applied Spectroscopy*, *64*(9), 1028–1036. https://doi.org/10.1366/000370210792434422

Møller, U., Folkenberg, J. R., & Jepsen, P. U. H. D. (2010). Dielectric properties of water in butter and water-AOT-heptane systems measured using terahertz time- domain spectroscopy, *Applied spectroscopy*, *64*(9), 1028–1036.

Møller, U., Merbold, H., Folkenberg, J. R., & Jepsen, P. U. (2007). Determination of alcohol- and sugar concentration in aqueous solutions using reflection terahertz time-domain spectroscopy. Paper presented at *IEEE Xplore, International Conference on Terahertz Electronics* (pp. 1–2).

Morita, Y., Dobroiu, A., Otani, C., & Kawase, K. (2005). A real-time inspection system using a terahertz technique to detect microleak defects in the seal of flexible plastic packages. *Journal of Food Protection*, *68*(4), 833–837.

Naito, H., Ogawa, Y., Shiraga, K., Kondo, N., Hirai, T., Osaka, I., & Kubota, A. (2011). Inspection of milk components by terahertz attenuated total reflectance (THz-ATR) spectrometer equipped temperature controller. Paper presented at *IEEE/SICE International Symposium on System Integration* (pp. 192–196). https://doi.org/10.1109/SII.2011.6147444

Nakajima, S., Shiraga, K., Suzuki, T., Kondo, N., & Ogawa, Y. (2019). Quantification of starch content in germinating mung bean seedlings by terahertz spectroscopy. *Food Chemistry*, *294*, 203–208.

Nallappan, K., Dash, J., Ray, S., & Pesala, B. (2013). Identification of adulterants in turmeric powder using terahertz spectroscopy. Paper presented at *International Conference on Infrared, Millimeter, and Terahertz Waves* (pp. 1–2). https://doi.org/10.1109/IRMMW-THz.2013.6665688

Nie, P., Qu, F., Lin, L., Dong, T., & He, Y. (2017). Detection of water content in rapeseed leaves using terahertz spectroscopy. *Sensors*, *17*, 1–13. https://doi.org/10.3390/s17122830

Niehues, G., Heyden, M., Schmidt, D. A., & Havenith, M. (2011). Exploring hydrophobicity by THz absorption spectroscopy of solvated amino acids. *Faraday Discussions*, *150*, 193–207. https://doi.org/10.1039/c0fd00007h

O'Hara, J. F., Singh, R., Brener, I., Smirnova, E., Han, J., Taylor, A. J., & Zhang, W. (2008). Thin-film sensing with planar terahertz metamaterials: Sensitivity and limitations. *Optics Express*, *16*(3), 1786. https://doi.org/10.1364/OE.16.001786

Ogawa, Y., Cheng, L., Hayashi, S., & Fukunaga, K. (2009). Attenuated total reflection spectra of aqueous glycine in the terahertz region. *IEICE Electronics Express*, *6*(2), 117–121. https://doi.org/10.1587/elex.6.117

Ogawa, Y., Hayashi, S., Kondo, N., Ninomiya, K., Otani, C., & Kawase, K. (2006). Feasibility on the quality evaluation of agricultural products with terahertz electromagnetic wave. *ASABE Annual International Meeting*, *0300*(06), 1–13.

Ogawa, Y., Kondo, N., & House, G. (2011). Feasibility of using attenuated total reflectance terahertz (ATR-THz) spectroscopy for quantitative and qualitative study of vitamin C in aqueous solutions. Paper presented at *ASABE Annual International Meeting* (pp. 7–10).

Ok, G., Choi, S. W., Park, K. H., & Chun, H. S. (2013). Foreign object detection by sub-terahertz quasi-Bessel beam imaging. *Sensors (Switzerland)*, *13*(1), 71–85. https://doi.org/10.3390/s130100071

Ok, G., Kim, H. J., Chun, H. S., & Choi, S. W. (2014). Foreign-body detection in dry food using continuous sub-terahertz wave imaging. *Food Control*, *42*, 284–289. https://doi.org/10.1016/j.foodcont.2014.02.021

Ok, G., Park, K., Chun, H. S., Chang, H.-J., Lee, N., & Choi, S.-W. (2015). High-performance sub-terahertz transmission imaging system for food inspection. *Biomedical Optics Express*, *6*(5), 1929. https://doi.org/10.1364/BOE.6.001929

Ok, G., Park, K., Kim, H. J., Chun, H. S., & Choi, S. W. (2014). High-speed terahertz imaging toward food quality inspection. *Applied Optics*, *53*(7), 1406–1412. https://doi.org/10.1364/AO.53.001406.High

Ok, G., Park, K., Lim, M. C., Jang, H. J., & Choi, S. W. (2018). 140-GHz subwavelength transmission imaging for foreign body inspection in food products. *Journal of Food Engineering*, *221*, 124–131. https://doi.org/10.1016/j.jfoodeng.2017.10.011

Ouakhssase, A., Chahid, A., Choubbane, H., Aitmazirt, A., & Ait Addi, E. (2019). Optimization and validation of a liquid chromatography/tandem mass spectrometry (LC-MS/MS) method for the determination of aflatoxins in maize, *Heliyon*, *5*(5), e01565. https://doi.org/10.1016/j.heliyon.2019.e01565.

Pan, T., Li, S., Zou, T., Yu, Z., Zhang, B., Wang, C., . . . Zhao, H. (2017). Terahertz spectra of L-phenylalanine and its monohydrate. *Spectrochimica Acta - Part A: Molecular and Biomolecular Spectroscopy*, *178*, 19–23. https://doi.org/10.1016/j.saa.2017.01.050

Parasoglou, P., Parrott, E. P. J., Zeitler, J. A., Rasburn, J., Powell, H., Gladden, L. F., & Johns, M. L. (2009). Quantitative moisture content detection in food wafers. Paper presented at *34th International Conference on Infrared, Millimeter, and Terahertz Waves, IRMMW-THz 2009*. https://doi.org/10.1109/ICIMW.2009.5324623

Parasoglou, P., Parrott, E. P. J., Zeitler, J. A., Rasburn, J., Powell, H., Gladden, L. F., & Johns, M. L. (2010). Quantitative water content measurements in food wafers using terahertz radiation. *Terahertz Science and Technology*, *3*(4), 172–182. https://doi.org/10.11906/TST.172-182.2010.12.17

Park, S. J., Hong, J. T., Choi, S. J., Kim, H. S., Park, W. K., Han, S. T., . . . Ahn, Y. H. (2014). Detection of microorganisms using terahertz metamaterials. *Scientific reports*, *4*, 4988. https://doi.org/10.1038/srep04988

Park, S. J., Son, B. H., Choi, S. J., Kim, H. S., & Ahn, Y. H. (2014). Sensitive detection of yeast using terahertz slot antennas. *Optic Express*, *22*(25), 30467–30472. https://doi.org/10.1364/OE.22.030467

Pei, C., Lin, H., Markl, D., Shen, Y.-C., Zeitler, J. A., & Elliott, J. A. (2018). A quantitative comparison of in-line coating thickness distributions obtained from a pharmaceutical tablet mixing process using discrete element method and terahertz pulsed imaging. *Chemical Engineering Science*, *192*, 34–45. https://doi.org/10.1016/j.ces.2018.06.045

Pohl, A., Debmann, N., Dutzi, K., & Hübers, H.-W. (2014). Identification of substances by THz spectroscopy and multivariate analysis. Paper presented at *39th International Conference on Infrared, Millimeter, and Terahertz waves (IRMMW-THz)* (pp. 1–2). https://doi.org/10.1109/IRMMW-THz.2014.6956050

Probst, T., Scheller, M., & Koch, M. (2011). Nondestructive thickness determination of plastic pipes in a nearby industrial environment using terahertz time domain spectroscopy. Paper presented at *IEEE, International Conference on Infrared, Millimeter, Terahertz Waves* 1–2. https://doi.org/10.1109/irmmw-THz.2011.6105154

Qin, B., Li, Z., Chen, T., & Chen, Y. (2017). Identification of genetically modified cotton seeds by terahertz spectroscopy with MPGA-SVM. *Optik*, *142*, 576–582. https://doi.org/10.1016/j.ijleo.2017.06.030

Qin, J., Xie, L., & Ying, Y. (2014). Feasibility of terahertz time-domain spectroscopy to detect tetracyclines hydrochloride in infant milk powder. *Analytical Chemistry*, *86*(23), 11750–11757. https://doi.org/10.1021/ac503212q

Qin, J., Xie, L., & Ying, Y. (2015). Determination of tetracycline hydrochloride by terahertz spectroscopy with PLSR model. *Food Chemistry*, *170*, 415–422. https://doi.org/10.1016/j.foodchem.2014.08.050

Qin, J., Xie, L., & Ying, Y. (2016). A high-sensitivity terahertz spectroscopy technology for tetracycline hydrochloride detection using metamaterials. *Food Chemistry*, *211*, 300–305. https://doi.org/10.1016/j.foodchem.2016.05.059

Qin, J., Xie, L., & Ying, Y. (2017). Rapid analysis of tetracycline hydrochloride solution by attenuated total reflection terahertz time-domain spectroscopy. *Food Chemistry*, *224*, 262–269. https://doi.org/10.1016/j.foodchem.2016.12.064

Qin, J., Ying, Y., & Xie, L. (2013). The detection of agricultural products and food using terahertz spectroscopy: A review. *Applied Spectroscopy Reviews*, *48*(6), 439–457. https://doi.org/10.1080/05704928.2012.745418

Redo-Sanchez, A., Laman, N., Schulkin, B., & Tongue, T. (2013). Review of terahertz technology readiness assessment and applications. *Journal of Infrared, Millimeter, and Terahertz Waves*, *34*(9), 500–518. https://doi.org/10.1007/s10762-013-9998-y

Redo-Sanchez, A., Salvatella, G., Galceran, R., Rold, E., Castellari, M., & Tejada, J. (2011). Assessment of terahertz spectroscopy to detect antibiotic residues in food and feed matrices, *Analyst*, *136*(8), 1733–1738. https://doi.org/10.1039/c0an01016b

Ren, X., Zhang, Q., Wu, W., Yan, T., Tang, X., Zhang, W., . . . Li, P. (2019). Anti-idiotypic nanobody-phage display-mediated real-time immuno-PCR for sensitive, simultaneous and quantitative detection of total aflatoxins and zearalenone in grains, *Food Chemistry*. https://doi.org/10.1016/j.foodchem.2019.05.186

Ripoche, X., Reynard, D., Narcisse, P., & Roberts, G. (2018). *U.S. Patent Application No. 15/573,585*.

Rutz, F., Koch, M., Khare, S., & Moneke, M. (2006). Terahertz quality control of polymeric products. *International Journal of Infrared and Millimeter Waves*, *27*(4), 547–556. https://doi.org/10.1007/s10762-006-9106-7

Sarkar, S., Saha, D., Banerjee, S., Mukherjee, A., & Mandal, P. (2017). Broadband terahertz dielectric spectroscopy of alcohols. *Chemical Physics Letters*, *678*, 65–71. https://doi.org/10.1016/j.cplett.2017.04.026

Sirhan, A., Tan, G. H., & Wong, R. (2013). Determination of aflatoxins in food using liquid chromatography coupled with electrospray ionization quadrupole time of flight mass spectrometry (LC-ESI-QTOF-MS/MS). *Food Control*, *31*, 35–44.

Shin, H. J., Choi, S. W., & Ok, G. (2018). Qualitative identification of food materials by complex refractive index mapping in the terahertz range. *Food Chemistry*, *245*, 282–288. https://doi.org/10.1016/j.foodchem.2017.10.056

Shin, H. J., Kim, S. H., Park, K., Lim, M. C., Choi, S. W., & Ok, G. (2017). Free-standing guided-mode resonance humidity sensor in terahertz. *Sensors and Actuators, A: Physical*, *268*, 27–31. https://doi.org/10.1016/j.sna.2017.10.060

Shiraga, K., Ogawa, Y., Kondo, N., Irisawa, A., & Imamura, M. (2013). Evaluation of the hydration state of saccharides using terahertz time-domain attenuated total reflection spectroscopy. *Food Chemistry*, *140*(1–2), 315–320. https://doi.org/10.1016/j.foodchem.2013.02.066

Sibik, J., & Zeitler, J. A. (2015). Direct measurement of molecular mobility and crystallisation of amorphous pharmaceuticals using terahertz spectroscopy. *Advanced Drug Delivery Reviews*, *100*, 147–159.

Smith, G., Hussain, A., Bukhari, N. I., & Ermolina, I. (2015). Quantification of residual crystallinity of ball-milled, commercially available, anhydrous β-lactose by differential scanning calorimetry and terahertz spectroscopy. *Journal of Thermal Analysis and Calorimetry*, *121*(1), 327–333. https://doi.org/10.1007/s10973-015-4469-4

Smith, R. M., & Arnold, M. A. (2011). Terahertz time-domain spectroscopy of solid samples: Principles, applications, and challenges. *Applied Spectroscopy Reviews*, *46*(8), 636–679. https://doi.org/10.1080/05704928.2011.614305

Song, C., & Wang, P. (2009). A radio frequency device for measurement of minute dielectric property changes in microfluidic channels. *Applied Physics Letters*, *94*(2), 1–4. https://doi.org/10.1063/1.3072806

Staggs, C. G., Sealey, W. M., McCabe, B. J., Teague, A. M., & Mock, D. M. (2004). Determination of the biotin content of select foods using accurate and sensitive HPLC/avidin binding. *Journal of Food Composition and Analysis*, *17*(6), 767–776. https://doi.org/10.1021/nl061786n.Core-Shell

Su, R., Zheng, H., Dong, S., Sun, R., Qiao, S., Sun, H., . . . Sun, C. (2019). Facile detection of melamine by a FAM–aptamer–G-quadruplex construct. *Analytical and Bioanalytical Chemistry*, *411*, 2521–2530.

Suhandy, D., Suzuki, T., Ogawa, Y., Kondo, N., Naito, H., Ishihara, T., . . . Liu, W. (2012). A quantitative study for determination of glucose concentration using attenuated total reflectance terahertz (ATR-THz) spectroscopy. *Engineering in Agriculture, Environment and Food*, *3*, 90–95.

Suhandy, D., Yulia, M., Ogawa, Y., & Kondo, N. (2011). Prediction of vitamin C using FTIR-ATR terahertz spectroscopy combined with interval partial least squares (iPLS) regression. Paper presented at *2011 IEEE/SICE International Symposium on System Integration (SII)* (pp. 202–206) IEEE.

Sun, P., & Zou, Y. (2016). Complex dielectric properties of anhydrous polycrystalline glucose in the terahertz region. *Optical and Quantum Electronics*, *48*(1), 1–10. https://doi.org/10.1007/s11082-015-0273-4

Sun, Q., He, Y., Liu, K., Fan, S., Parrott, E. P. J., & Pickwell-MacPherson, E. (2017). Recent advances in terahertz technology for biomedical applications. *Quantitative imaging in medicine and surgery*, *7*(3), 345–355. https://doi.org/10.21037/qims.2017.06.02

Tajima, T., Nakamura, M., Shiraga, K., Ogawa, Y., & Ajito, K. (2016). Double-beam CW THz system with photonic phase modulator for sub-THz glucose hydration sensing. Paper presented at *2016 IEEE MTT-S International Microwave Symposium (IMS)* (pp. 1–4). IEEE.

Takahashi, M., Ishikawa, Y., Nishizawa, J. I., & Ito, H. (2005). Low-frequency vibrational modes of riboflavin and related compounds. *Chemical Physics Letters*, *401*(4–6), 475–482. https://doi.org/10.1016/j.cplett.2004.11.108

Tang, Z., Lin, H., Chen, X., & Zhang, Z. (2009). Detection of amino acids based on terahertz spectroscopy. *Guang Pu Xue Yu Guang Pu Fen Xi*, *29*(9), 2351–2356.

Tatebe, C., Zhong, X., Ohtsuki, T., Kubota, H., Sato, K., & Akiyama, H. (2014). A simple and rapid chromatographic method to determine unauthorized basic colorants (rhodamine B, auramine O, and pararosaniline) in processed foods. *Food Science & Nutrition*, *2*, 547–556.

Truong, B., Fitzgerald, A., Fan, S., & Wallace, V. (2018). Concentration analysis of breast tissue phantoms with terahertz spectroscopy. *Biomedical optics express*, *9*(3), 1334–1349.

Ueno, Y., Katsuhiro, A., Kukutsu, N., & Tamechika, E. (2011). Quantitative analysis of amino acids in dietary supplements using terahertz time-domain spectroscopy. *Analytical Science*, *27*, 351–356.

Ueno, Y., Rungsawang, R., Tomita, I., & Ajito, K. (2006). Quantitative measurements of amino acids by terahertz time-domain transmission spectroscopy. *Analytical Chemistry*, *78*(15), 5424–5428. https://doi.org/10.1021/ac060520y

Ung, B., Fischer, B. M., Ng, B. H., & Abbott, D. (2009). Comparative investigation of detection of melamine in food powders. Paper presented at *34th International Conference on Infrared, Milimeter and Terahertz Wave*, (pp. 1–3).

Ung, B., Fischer, B., Ng, B., & Abbott, D. (2007). Towards quality control of food using terahertz. *BioMEMS and Nanotechnology III*, *6799*, 67991E. https://doi.org/10.1117/12.759825

Ung, B., Ng, B., & Abbott, D. (2010). A preliminary study of hydrogenation of oils using terahertz time domain spectroscopy. Paper presented at *35th International Conference on Infrared, Millimeter, and Terahertz Waves*, *64*(2), 1–1. https://doi.org/10.1109/ICIMW.2010.5612480

Upadhya, P. C., Shen, Y. C., Davies, A. G., & Linfield, E. H. (2003). Terahertz time-domain spectroscopy of glucose and uric acid. *Journal of Biological Physics*, *29*(2–3), 117–121. https://doi.org/10.1023/A:1024476322147

Urbańczyk, M., Góra, J., Latajka, R., & Sewald, N. (2017). Antifreeze glycopeptides: From structure and activity studies to current approaches in chemical synthesis. *Amino Acids*, *49*(2), 209–222. https://doi.org/10.1007/s00726-016-2368-z

Wang, B., Zheng, J., Ding, A., Xu, L., Chen, J., & Li, C. (2019). Highly sensitive aflatoxin B1 sensor based on DNA-guided assembly of fluorescent probe and TdT-assisted DNA polymerization. *Food Chemistry*, *294*, 19–26.

Wang, C., Gong, J., Xing, Q., Li, Y., Liu, F., Zhao, X., . . . Zheltikov, A. M. (2010). Application of terahertz time-domain spectroscopy in intracellular metabolite detection. *Journal of Biophotonics*, *3*(10–11), 641–645. https://doi.org/10.1002/jbio.201000043

Wang, C., Qin, J. Y., Xu, W. D., Chen, M., Xie, L. J., & Ying, Y. B. (2018). Terahertz imaging applications in agriculture and food engineering: A review, *61*(2), 1–14.

Wang, K., Sun, D. W., & Pu, H. (2017). Emerging non-destructive terahertz spectroscopic imaging technique: Principle and applications in the agri-food industry. *Trends in Food Science and Technology*, *67*, 93–105. https://doi.org/10.1016/j.tifs.2017.06.001

Wang, S., Ferguson, B., Mannella, C., Abbott, D., & Zhang, X. (2002). Powder detection using THz imaging. Paper presented at *2002 Summaries of Papers Presented at the Quantum Electronics and Laser Science Conference* (p. 44). IEEE.

Wang, W. N., Li, H. Q., Zhang, Y., & Zhang, C. L. (2009). Correlations between terahertz spectra and molecular structures of 20 standard α-amino

acids. *Wuli Huaxue Xuebao/ Acta Physico - Chimica Sinica*, *25*(10), 2074–2079. https://doi.org/10.3866/PKU.WHXB20090931

Wang, Y., Wang, Q., Zhao, Z., Liu, A., Tian, Y., & Qin, J. (2018). Rapid qualitative and quantitative analysis of chlortetracycline hydrochloride and tetracycline hydrochloride in environmental samples based on terahertz frequency-domain spectroscopy. *Talanta*, *190*, 284–291.

Warnecke, S., Wu, J. X., Rinnan, Å., Allesø, M., van den Berg, F., Jepsen, P. U., & Engelsen, S. B. (2019). Quantifying crystalline α-lactose monohydrate in amorphous lactose using terahertz time domain spectroscopy and near infrared spectroscopy. *Vibrational Spectroscopy*, *102*, 39–46.

Wessel, J., Schmalz, K., Cahill, B. P., Gastrock, G., & Meliani, C. (2013). Contactless characterization of yeast cell cultivation at 7 GHz and 240 GHz. Paper presented at *BioWireleSS 2013 - Proceedings: 2013 IEEE Topical Conference on Biomedical Wireless Technologies, Networks, and Sensing Systems - 2013 IEEE Radio and Wireless Week, RWW 2013*, (May 2014), 70–72. https://doi.org/10.1109/BioWireleSS.2013.6613678

Wietzke, S., Jansen, C., Jördens, C., Krumbholz, N., Vieweg, N., Scheller, M., . . . Koch, M. (2009). Industrial applications of THz systems. Paper presented at *International Symposium on Photoelectronic Detection and Imaging 2009: Terahertz and High Energy Radiation Detection Technologies and Applications* (Vol. 7385, p. 738506). International Society for Optics and Photonics.

Xi-Ai, C., Guang-xin, Z., Ping-jie, H., Di-bo, H., Xu-sheng, K., & Ze-kui, Z. (2011). Classification of the green tea varieties based on support vector machines using terahertz spectroscopy. Paper presented at *2011 IEEE International Instrumentation and Measurement Technology Conference* (pp. 1–5). IEEE.

Xiao-li, Z., & Jiu-sheng, L. (2011). Diagnostic techniques of talc powder in flour based on the THz spectroscopy Diagnostic techniques of talc powder in flour based on the THz spectroscopy. *Journal of Physics: Conference Series, 276*, 012234. https://doi.org/10.1088/1742-6596/276/1/012234

Xie, L., Gao, W., Shu, J., Ying, Y., & Kono, J. (2015). Extraordinary sensitivity enhancement by metasurfaces in terahertz detection of antibiotics. *Scientific Reports*, *5*, 1–4. https://doi.org/10.1038/srep08671

Xie, L., Yang, Y., & Ying, Y. (2014). The application of terahertz spectroscopy to liquid petrochemicals detection: A review. *Applied Spectroscopy Reviews*, *49*(5), 448–461. https://doi.org/10.1080/05704928.2016.1141291

Xu, J., Plaxco, K. W., & Allen, S. J. (2006a). Collective dynamics of lysozyme in water: Terahertz absorption spectroscopy and comparison with theory. *Journal of Physical Chemistry B*, *110*, 24255–24259. https://doi.org/10.1021/jp064830w

Xu, J., Plaxco, K. W., & Allen, S. J. (2006b). Probing the collective vibrational dynamics of a protein in liquid water by terahertz absorption spectroscopy. *Protein Science*, *15*(5), 1175–1181. https://doi.org/10.1110/ps.062073506

Yan, L., Liu, C., Qu, H., & Liu, W. (2018). Discrimination and measurements of three flavonols with similar structure using terahertz spectroscopy and chemometrics. *Journal of Infrared Milli Terahz Waves*, *39*, 492–504.

Yan, Z.-K., Zhang, H.-J., & Ying, Y.-B. (2007). Research progress of terahertz wave technology in quality measurement of food and agricultural products. *Guang Pu Xue Yu Guang Pu Fen Xi*, *27*(11), 2228–2234.

Yan, Z., Hou, D., Huang, P., Cao, B., Zhang, G., & Zhou, Z. (2008). Terahertz spectroscopic investigation of L-glutamic acid and L-tyrosine. *Measurement Science and Technology*, *19*(1), 015602. https://doi.org/10.1088/0957-0233/19/1/015602

Yang, X., Shi, J., Yang, K., Xu, D., Yao, J., Wang, Y., & Fu, W. (2017). Label-free and reagentless bacterial detection and assessment by continous-wave terahertz imaging. Paper presented at *International Conference on Infrared, Millimeter, and Terahertz Waves, IRMMW-THz*, 2. https://doi.org/10.1109/IRMMW-THz.2017.8067149

Yang, X., Wei, D., Yan, S., Liu, Y., Yu, S., Zhang, M., . . . Fu, W. (2016). Rapid and label-free detection and assessment of bacteria by terahertz time-domain spectroscopy. *Journal of Biophotonics*, *9*(10), 1050–1058. https://doi.org/10.1002/jbio.201500270

Yang, X., Yang, K., Luo, Y., & Fu, W. (2016). Terahertz spectroscopy for bacterial detection: Opportunities and challenges. *Applied Microbiology and Biotechnology*, *100*(12), 5289–5299. https://doi.org/10.1007/s00253-016-7569-6

Yang, X., Zhao, X., Yang, K., Liu, Y., Liu, Y., Fu, W., & Luo, Y. (2016). Biomedical applications of terahertz spectroscopy and imaging. *Trends in Biotechnology*, *34*(10), 810–824. https://doi.org/10.1016/j.tibtech.2016.04.008

Yasui, T., & Araki, T. (2005). Sensitive measurement of water content in dry material based on low-frequency terahertz time-domain spectroscopy. Paper presented at *ICO20:OPtical Devices and Instruments* (p. 6024). https://doi.org/10.1117/12.666812

Yasui, T., & Araki, T. (2011). Sensitive measurement of water content in dry material using low-frequency terahertz time-domain spectroscopy system equipped with micro-structured photoconductive antennas. Paper presented at *European Optical Society: 1st EOS Topical Meeting on Micro and Nano-Optoeletronic Systems* (pp. 6–7).

Yin, M., Tang, S., & Tong, M. (2016). Identification of edible oils using terahertz spectroscopy combined with genetic algorithm and partial least squares discriminant analysis. *Analytical Methods*, *8*(13), 2794–2798. https://doi.org/10.1039/c6ay00259e

Yoneyama, H., Yamashita, M., Kasai, S., Ito, H., & Ouchi, T. (2007). Application of terahertz spectrum in the detection of harmful food additives. Paper presented at *Joint 32nd International Conference on Infrared and Millimeter Waves and the 15th International Conference on Terahertz Electronics*.

Yu, B., Alimova, A., Katz, A., & Alfano, R. R. (2005). THz absorption spectrum of Bacillus subtilis spores, Paper presented at Proceedings of the SPIE 5727, Terahertz and Gigahertz Electronics and Photonics IV. https://doi.org/10.1117/12.590951

Yu, B., Huang, Z., Wang, X., Zhao, G., & Zhang, C. (2009, February). Terahertz spectroscopic investigations of vitamin molecules. In *2008 International Conference on Optical Instruments and Technology: Microelectronic and Optoelectronic Devices and Integration* (Vol. 7158, p. 715815). International Society for Optics and Photonics.

Yu, B., Zeng, F., Yang, Y., Xing, Q., Chechin, A., Xin, X., . . . Alfano, R. R. (2004). Torsional vibrational modes of tryptophan studied by terahertz time-somain spectroscopy. *Biophysical Journal*, *86*(3), 1649–1654. https://doi.org/10.1016/S0006-3495(04)74233-2

Zhan, H., Xi, J., Zhao, K., Bao, R., & Xiao, L. (2016). A spectral-mathematical strategy for the identification of edible and swill-cooked dirty oils using terahertz spectroscopy. *Food Control*, *67*, 114–118. https://doi.org/10.1016/j.foodcont.2016.02.043

Zhang, H., & Li, Z. (2018). Terahertz spectroscopy applied to quantitative determination of harmful additives in medicinal herbs. *Optik*, *156*, 834–840.

Zhang, H., Li, Z., Chen, T., & Qin, B. (2017). Quantitative determination of Auramine O by terahertz spectroscopy with 2DCOS-PLSR model. *Spectrochimica Acta - Part A: Molecular and Biomolecular Spectroscopy*, *184*, 335–341. https://doi.org/10.1016/j.saa.2017.05.017

Zhang, M., Cai, H., & Shen, J. L. (2011). Terahertz spectroscopic testing of food additive tert-butylhydroquinone. *Guang Pu Xue Yu Guang Pu Fen Xi*, *31*(7), 1809–1813. https://doi.org/10.3964/j.issn.1000-0593(2011)07-1809-05

Zhang, X., Lu, S., Liao, Y., & Zhang, Z. (2017). Simultaneous determination of amino acid mixtures in cereal by using terahertz time domain spectroscopy and chemometrics. *Chemometrics and Intelligent Laboratory Systems*, *164*, 8–15. https://doi.org/10.1016/j.chemolab.2017.03.001

Zhao, Z., Lian, F., & Zhang, Y. (2015). Aflatoxin B1 detected by terahertz time-domain spectroscopy. Paper presented at *8th I nternational Congress on Image and Signal Processing (CISP 2015)* (pp. 1225–1230).

Zheng, Z. P., Fan, W. H., Li, H., & Tang, J. (2014). Terahertz spectral investigation of anhydrous and monohydrated glucose using terahertz spectroscopy and solid-state theory. *Journal of Molecular Spectroscopy*, *296*, 9–13. https://doi.org/10.1016/j.jms.2013.12.002

Zheng, Z. P., Fan, W. H., Liang, Y. Q., & Yan, H. (2012). Application of terahertz spectroscopy and molecular modeling in isomers investigation: Glucose and fructose. *Optics Communications*, *285*(7), 1868–1871. https://doi.org/10.1016/j.optcom.2011.12.016

Zong, S., Ren, G. H., Li, S., Zhang, B., Zhang, J., Qi, W., . . . Zhao, H. (2018). Terahertz time-domain spectroscopy of L-histidine hydrochloride monohydrate. *Journal of Molecular Structure*, *1157*, 486–491. https://doi.org/10.1016/j.molstruc.2017.12.088